UNIVERSIDADE FEDERAL DE SANTA MARIA
CENTRO DE TECNOLOGIA
DEPARTAMENTO DE ENGENHARIA QUÍMICA
PROGRAMA DE PÓS-GRADUAÇÃO EM ENGENHARIA QUÍMICA

Dison Stracke Pfingsten Franco

AVALIAÇÃO DA ADSORÇÃO DE INDIO (III) ATRAVÉS DE REDES NEURONAIS ARTIFICIAIS E MODELOS DIFUSIVOS DE TRANSFERÊNCIA DE MASSA

Santa Maria, RS
2021

Dison Stracke Pfingsten Franco

AVALIAÇÃO DA ADSORÇÃO DE INDIO (III) ATRAVÉS DE REDES NEURONAIS ARTIFICIAIS E MODELOS DIFUSIVOS DE TRANSFERÊNCIA DE MASSA

Tese de Doutorado apresentada ao Programa de Pós-Graduação em Engenharia Química da Universidade Federal de Santa Maria (UFSM, RS), como requisito parcial para obtenção do grau de **Doutor em Engenharia Química.**

Orientador: Prof. Dr. Guilherme Luiz Dotto
Coorientador: Profª. Drª. Nina Paula Gonçalves Salau

Santa Maria, RS
2021

Franco, Dison Stracke Pfingsten
AVALIAÇÃO DA ADSORÇÃO DE INDIO (III) ATRAVÉS DE REDES NEURONAIS ARTIFICIAIS E MODELOS DIFUSIVOS DE TRANSFERÊNCIA DE MASSA / Dison Stracke Pfingsten Franco.- 2021.
144 p.; 30 cm

Orientador: Guilherme Luiz Dotto
Coorientadora: Nina Paula Gonçalves Salau
Tese (doutorado) - Universidade Federal de Santa Maria, Centro de Tecnologia, Programa de Pós-Graduação em Engenharia Química, RS, 2021

1. Adsorção 2. Índio 3. ANN 4. PVSDM 5. EMTM I. Dotto, Guilherme Luiz II. Salau, Nina Paula Gonçalves III. Título.

Sistema de geração automática de ficha catalográfica da UFSM. Dados fornecidos pelo autor(a). Sob supervisão da Direção da Divisão de Processos Técnicos da Biblioteca Central. Bibliotecária responsável Paula Schoenfeldt Patta CRB 10/1728.

Declaro, DISON STRACKE PFINGSTEN FRANCO, para os devidos fins e sob as penas da lei, que a pesquisa constante neste trabalho de conclusão de curso (Tese) foi por mim elaborada e que as informações necessárias objeto de consulta em literatura e outras fontes estão devidamente referenciadas. Declaro, ainda, que este trabalho ou parte dele não foi apresentado anteriormente para obtenção de qualquer outro grau acadêmico, estando ciente de que a inveracidade da presente declaração poderá resultar na anulação da titulação pela Universidade, entre outras consequências legais.

Dison Stracke Pfingsten Franco

AVALIAÇÃO DA ADSORÇÃO DE INDIO (III) ATRAVÉS DE REDES NEURONAIS ARTIFICIAIS E MODELOS DIFUSIVOS DE TRANSFERÊNCIA DE MASSA

Tese de Doutorado apresentada ao Programa de Pós-Graduação em Engenharia Química da Universidade Federal de Santa Maria (UFSM, RS), como requisito parcial para obtenção do grau de **Doutor em Engenharia Química.**

Aprovado 11 junho de 2021:

Guilherme Luiz Dotto, Dr. (UFSM)
(Presidente, Orientador)

Evandro Stoffels Mallmann, Dr (UFSM)
(Examinador)

Edson Luiz Foletto, Dr (UFSM)
(Examinador)

Jivago Schumacher de Oliveira , Dr (UFSM)
(Examinador).

Tito Roberto Sant'anna Cadaval Junior, Dr (FURG)
(Examinador).

Santa Maria, RS
2021

AGRADECIMENTOS

Primeiro gostaria de agradecer pela oportunidade que ganhei para desenvolver e trabalhar na minha tese e no desenvolvimento da ciência.

Gostaria de agradecer a minha mãe (Anna Elisabeth Pfingsten), meu pai (Gilberto S. Franco) e minha vó (Silvia S. Franco) pelo apoio durante está jornada.

Meus amigos Pedro Balen e Henrique Fich, estes sempre me apoiando. E conversando diariamente nos últimos anos;

Aos meus outros amigos Jean Fagundez, Estevan Cruz e Pedro Limberger pela amizade, suporte e pelos mesões de Magic;

Gostaria de agradecer especialmente a companhia e esforço da minha companheira Jordana Georgin. Que me ajudou a me dedicar e a expandir a minha vida acadêmica.

A oportunidade que recebi do EBW+ e a orientação do professor Julien Vieillard durante meu período na França.

Ao secretário da pós-graduação Marcos Mello! Por me ajudar em diversas etapas desta jornada.

As orientações e ensinos que meu orientador (Guilherme L. Dotto) e minha coorientadora (Nina P. G. Salau) que me passaram durante o período do doutorado.

Por fim, gostaria de dedicar este trabalho e esforço ao meu avô (João Altair G. Franco).

“Então, vamos tentar escalar a montanha,
não pisando no que está abaixo de nós, mas
nos puxando para o que está acima de nós”

M.C. Escher

RESUMO

AVALIAÇÃO DA ADSORÇÃO DE INDIO (III) ATRAVÉS DE REDES NEURONAIS ARTIFICIAIS E MODELOS DIFUSIVOS DE TRANSFERÊNCIA DE MASSA

AUTOR: Dison Stracke Pfingsten Franco
ORIENTADOR: Guilherme Luiz Dotto
COORIENTADORA: Nina Paula Gonçalves Salau

O desenvolvimento tecnológico aumentou o consumo de índio na última década, sendo atualmente classificado como material crítico, devido sua escassez. Sua principal aplicação está relacionada a produção de display de cristal líquido. Devido a este contexto, o reciclo do índio é necessário. Uma rota é a obtenção do mesmo após a lixiviação de display de cristal líquido, este podendo ser feito através da operação unitária de adsorção. Este trabalho teve como objetivo investigar a adsorção de In (III) utilizando os modelos de redes neuronais e de transferência de massa. A adsorção de In (III) foi avaliada utilizando dez adsorventes diferentes, carvão ativado, nanotubos de carbono de múltiplas paredes funcionalizados com OH, nanotubos de carbono funcionalizados com COOH, quitina, quitosana, palha de milho, bagaço de cana, casca de laranja e casca de arroz. Os modelos de redes neuronais conseguiram prever a capacidade de adsorção para todos os adsorventes com R^2 de 0,9998 e MSE $8{,}423 \times 10^{-5}$ utilizando o ANFIS e R^2 de 0.9913 e MSE 0.1721 utilizando o ANN. Dentre todos os dez adsorventes os nanotubos de carbono de múltiplas paredes funcionalizado com OH e outro COOH, quitina e quitosana foram os que apresentaram melhor capacidade de adsorção. Foi encontrado que a quitosana apresenta uma capacidade de adsorção de In (III) de 1000 mg g^{-1}. A microscopia eletrônica de varredura da quitina e quitosana confirmaram que ambas apresentam uma superfície rígida sem a presença de poros. As isotermas de equilíbrio mostraram que capacidade de adsorção aumenta com a temperatura. A partir do modelo de transferência de massa externo e dos valores do número de Biot ($8{,}82 \times 10^{-4}$ e 2,71) modificado foi encontrado que a transferência de massa externa é o fenômeno dominante na adsorção do In (III) sobre a quitina e quitosana. Em resumo, os átomos de In (III) se deslocam do seio da solução e são instantemente adsorvidos na superfície através de precipitação ou ligações de coordenação.

Palavras-chave: Adsorção, índio, ANN, PVSDM, EMTM, resíduos, quitina, quitosana.

ABSTRACT

EVALUATION OF INDIO (III) ADSORPTION THROUGH ARTIFICIAL NEURONAL NETWORKS AND DIFFUSIVE MASS TRANSFER MODEL

AUTHOR: Dison Stracke Pfingsten Franco
ORIENTADOR: Guilherme Luiz Dotto
COORIENTADORA: Nina Paula Gonçalves Salau

Technological development has increased the consumption of indium in the last decade and is currently classified as a critical material due to its scarcity. Its main application is related to the production of liquid crystal display. Due to this context, the recycling of indium is necessary. One route is to obtain it after leaching from a liquid crystal display, which can be done through the unitary adsorption operation. This work aimed to investigate the adsorption of In(III) using the neural network and mass transfer models. The adsorption of In (III) was evaluated using ten different adsorbents, activated carbon, multi-walled carbon nanotubes functionalized with OH, carbon nanotubes functionalized with COOH, chitin, chitosan, corn straw, sugarcane bagasse, orange peel and rice husks. The neural network models were able to predict the adsorption capacity for all adsorbents with R2 of 0.9998 and MSE 8.423x10-5 using ANFIS and R2 of 0.9913 and MSE 0.1721 using ANN. Among all ten adsorbents, the multiwalled carbon nanotubes functionalized with OH and another COOH, chitin and chitosan were the ones with the best adsorption capacity. It was found that chitosan has an In(III) adsorption capacity of 1000 mg g-1. Scanning electron microscopy of chitin and chitosan confirmed that both have a rigid surface without the presence of pores. Equilibrium isotherms showed that adsorption capacity increases with temperature. From the external mass transfer model and the modified Biot number values (8.82×10–4 and 2.71) it was found that the external mass transfer is the dominant phenomenon in the adsorption of In(III) onto chitin and chitosan. In summary, the In(III) atoms move out of solution and are instantly adsorbed to the surface through precipitation or coordination bonds.

Keywords: Adsorption, Indium, ANN, PVSDM, EMTM, Residues, Chitin, Chitosan.

LISTA DE FIGURAS

3. REVISÃO BIBLIOGRÁFICA

4.1 ARTIGO I

4.2 ARTIGO II

4.3 ARTIGO III

LISTA DE TABELAS

3. REVISÃO BIBLIOGRÁFICA

4.1 ARTIGO I

4.2 ARTIGO II

4.3 ARTIGO III

LISTA DE ABREVIATURAS E SIGLAS

$1/n_f$	Fator de heterogeneidade	(-)
C	Concentração do adsorbato na fase líquida	(mg L^{-1})
c	Parâmetro da equação de Gauss	(-)
C_0	Concentração inicial do adsorbato na fase líquida	(mg L^{-1})
C_A	Concentração do adsorbato na fase líquida	(mg L^{-1})
C_{A0}	Concentração inicial do adsorbato A na fase líquida	(mg L^{-1})
C_{Ar}	Concentração do adsorbato A na entrada da região poroso	(mg L^{-1})
C_e	Concentração do adsorbato no equilíbrio	(mg L^{-1})
D_0	Dosagem do adsorvente	(g L^{-1})
D_{AB}	Difusividade molecular em diluição infinita	(cm^2 s^{-1})
D_p	Difusividade efetiva do poro	(cm^2 s^{-1})
D_s	Difusividade efetiva de superfície	(cm^2 s^{-1})
EMQ	Erro por mínimos quadrados	(-)
EQM	Erro dos quadrados médios	(-)
k_L	Coeficiente de transferência de massa externa	(cm s^{-1})
K_F	Constante de Freundlich	(mg g^{-1})(mg L^{-1})$^{-1/n_F}$
K_L	Constante de Langmuir	(L mg^{-1})
m	Massa do adsorvente	(g)
N	Número de pontos experimentais	(-)
N_A	Fluxo molar de A	(mg cm s^{-1} L^{-1})
$N_{A,p}$	Fluxo molar do soluto no poro da partícula	(mg cm g^{-1} L^{-1})
$N_{A,S}$	Fluxo molar do soluto na superfície da partícula	(mg cm g^{-1} L^{-1})
p_i	Parâmetro de regra fuzzy	(-)
q	Capacidade de adsorção	(mg g^{-1})
q_e	Capacidade de adsorção no equilíbrio	(mg g^{-1})
q_i	Parâmetro de regra fuzzy	(-)
q_m	Capacidade máxima de adsorção	(mg g^{-1})
R	Raio	(cm)
R_G	Constante universal dos gases	(8,31x10^{-3} kJ mol^{-1} K^{-1})
R	Coeficiente de correlação	(-)
REQM	Raiz do erro dos quadrados médios	(-)
r_i	Parâmetro de regra fuzzy	(-)
R_p	Raio da partícula	(cm)
S	Área superficial específica	(cm^2 g^{-1})
SEA	Soma dos erros absolutos	(-)
SQS	Soma dos quadrados dos resíduos	(-)
t	Tempo	(min)
T	Temperatura	(K)
V	Volume do fluido	(mL)
w_{ij}	Peso de entrada j para o neurônio i	(-)
x_{ij}	Vetor de entrada da entrada j para o neurônio i	(-)
y_j	Vetor de saída da saída j	(-)
z_i	Vetor de saída do neurônio i da camada oculta	(i)
y_{exp}	Valores experimentais	(-)
y_m	Média dos valores preditos pelas redes neurais	(-)
W_I	Peso da rede fuzzy	(-)
y_{prd}	Valores preditos pelas rede neurais	(-)

Letras gregas

ε_p	Porosidade do adsorvente	(-)
ρ_p	Massa específica da partícula	(g cm^{-3})
ξ_i	Potencial do neurônio i	(-)
θ_i	Bias do neurônio i	(-)
σ	Parâmetro da função de Gauss	(-)
τ	Tortuosidade da partícula	(-)
υ_{ij}	Peso de saída j do neurônio i	(-)
$\partial E/\partial w_{ij}$	Derivada parcial dos mínimos quadrados em função do peso de entrada.	(-)
$\partial E/\partial \upsilon_{ij}$	Derivada parcial dos mínimos quadrados em função do peso de entrada.	(-)
ΔG^0	Variação da energia livre de Gibbs padrão	(kJ mol^{-1})
ΔH^0	Variação da entalpia padrão	(kJ mol^{-1})
ΔS^0	Variação da entropia padrão	(kJ mol^{-1} K^{-1})

SUMÁRIO

1 INTRODUÇÃO

Índio (In) é um metal pertencente ao grupo das terras raras e possui uma grande aplicação na indústria tecnológica. Recentemente foi classificado, pela União Europeia como um material crítico (European Comission, 2017)**.** É esperado que as reservas se esgotem em até 14 anos, em função da demanda que tende a crescer a cada ano. Em comparação ao ano de 2015, a demanda de In aumentou em 100 tons (U.S geological survey,2016 e 2017). Uma das principais aplicações do In está relacionada à produção de display de cristal líquido (em inglês: liquid crystal display LCD), onde o mesmo se encontra na forma de filmes de óxido de estanho de In (em inglês: índium tin oxide, ITO), sendo, os resíduos de LCD podem ser uma possível fonte secundária para a obtenção do metal. Dependendo da fonte original do LCD é possível encontrar de 100 até 600 mg de In por kg de LCD. O LCD pode ser desmantelado manualmente, sendo obtido o ITO, onde a etapa final de separação se faz através de um processo de extração ácida (Silveira et al, 2015). Entretanto, quando extraído, o In acaba se encontrando em baixas concentrações em fase líquida, sendo que sua posterior precipitação através de aplicação de base, resulta em mais um problema ambiental (Grimes et al, 2017). Ambos os problemas podem ser resolvidos com a aplicação da adsorção.

A adsorção é uma operação unitária, caracterizada pela transferência de massa de uma fase fluida (líquida ou gás) para a superfície de um sólido (McCabe, 1993). Esta, se destaca por sua facilidade de aplicação e operação, sustentabilidade, baixo custo de operação e baixo consumo energético (Dotto et al, 2015, Franco et al, 2017). Um dos principais fatores da adsorção, está no material a ser escolhido como adsorvente, pois este está ligado diretamente o quanto é possível adsorver. Atualmente, diferentes grupos de materiais são aplicados, entre eles tem se: o grupo dos carbonáceos, constituídos pelo carvão ativado (CA); e mais recentemente os nanotubos de carbono, com múltiplas paredes funcionalizados; e os biopolímeros, onde se tem a presença das quitosana e da quitina. Outro grupo que recebe destaque devido aos custos, é o dos rejeitos agroindustriais. Estes, compostos por materiais oriundos de processos de beneficiação, como por exemplo: casca de arroz, bagaço de cana, bagaço de laranja, sementes de uva, palha de milho. (Dotto et al, 2012, Escudero et al, 2018, Dotto et al, 2016, Franco et al, 2017, Lima et al, 2017).

A fim de predizer a capacidade de adsorção e classificar o melhor adsorvente entre os mencionados, é possível aplicar técnicas matemáticas baseadas em redes. Entre elas, temos as redes neuronais artificiais (em inglês: artificial neural network, ANN) e sistema de interferência

adaptativo neuro-fuzzy (em inglês: adaptative interference neural fuzzy system, ANFIS). A ANN consegue relacionar problemas não lineares em soluções lineares, entre variáveis independes e dependentes. Enquanto o ANFIS, pode ser utilizado para relacionar propriedades qualitativas e quantitativas, sendo assim possível determinar qual o melhor material a ser aplicado para adsorção de In (Ghaedi et al 2017). A partir do momento que o melhor material é escolhido, para ser utilizado como adsorvente, é possível aplicar modelos de transferência de massa difusivos para compreender melhor o processo fenomenológico da adsorção (Souza, 2016). Os modelos de transferência de massa externa e de difusão na superfície e no volume de poro foram aplicados para elucidar o fenômeno de adsorção do In na quitina e quitosana. Neste contexto, estudos aplicando redes neuronais artificiais e modelos de transferência de massa no estudo da adsorção de In em diferentes materiais não foram encontrados na literatura, desta forma se tornando uma temática ainda mais relevante.

2 JUSTIFICATIVA

Os resíduos provenientes de equipamentos eletrônicos constituem um grande problema para a humidade atual e para gerações futuras. A poluição causada pelos resíduos é uma realidade mundial, que pode ser atenuada pelo meio de reciclagem, a qual se tornou necessária, inclusive na cidade de Santa Maria- RS (Reis,2013). Visando a necessidade de reaproveitamento destes resíduos eletrônicos, foram desenvolvidos trabalhos de pesquisa na Universidade Federal de Santa Maria (UFSM), como por exemplo: A obtenção do In através de extração utilizando diferentes solventes (Pereira et al., 2018). A Adsorção de metais originários de componentes descartados (Zaycki et al., 2017). Silveira et al (2015) extraiu e precipitou In de LCD. Por fim, o estudo da extração supercrítica com ácidos orgânicos foi feito utilizando LCD. Dentre os resíduos provenientes de equipamentos eletrônicos, o In se destaca devido suas fontes naturais estarem se esgotando e, processos que visem a sua obtenção a partir de fontes secundárias são necessários a fim de abastecer o mercado de eletroeletrônicos. Nesse contexto, o In pode ser recuperado de telas de LCD. Durante este processo, o In é lixiviado das telas de LCD e uma solução diluída do metal é obtida. Para recuperar o In desta solução, geralmente utiliza-se precipitação, a qual gera problemas de poluição secundários. Assim a adsorção é uma alternativa para a recuperação de In.

A recuperação do In através da adsorção é pouco estudada e compreendida. Tendo isso em vista que é necessário conhecer qual o melhor adsorvente em relação as suas características e do fenômeno de transporte para o material escolhido. As redes neuronais são uma poderosa ferramenta capaz de auxiliar na escolha do adsorvente em relação as suas características. Em paralelo, os modelos difusivos de transferência de massa são adequados para compreender corretamente o fenômeno de transferência de massa. Assim, o presente estudo visa entender e propor uma operação de adsorção adequada para a recuperação de In a partir de soluções aquosas, tema este que é muito pouco investigado na literatura, devido a ampla complexidade do sistema.

2.1 OBJETIVO GERAL

O objetivo deste trabalho é avaliar a adsorção de In através de redes neuronais artificiais e modelos difusivos de transferência de massa.

2.2 OBJETIVOS ESPECÍFICOS

i. Extrair In das telas de LCD, utilizando água régia

ii. Obter dados experimentais de adsorção de In para diferentes condições e diferentes materiais;

iii. Construir modelos ANN e ANFIS, a fim de determinar a melhor condição de operação e provável adsorvente

iv. Avaliar o mecanismo de transferência de massa de In utilizando os modelos difusivos, utilizando a quitina e quitosana como adsorventes.

3 REVISÃO BIBLIOGRÁFICA

Neste capítulo serão abordados os seguintes aspectos: problemática em relação ao In; adsorventes, fundamentos de adsorção, incluindo os modelos de transferência de massa e fundamentos das redes neurais artificiais. Estes serão os conceitos necessários para o embasamento teórico das atividades que foram desenvolvidas nesse trabalho.

3.1 PROBLEMÁTICA EM RELAÇÃO AO IN

Embora o In esteja associado a minérios de estanho, chumbo, cobre e ferro, é mais comumente encontrado em associação com materiais contendo zinco, como em solução sólida em esfarelita. O mineral mais comum contendo zinco é a esfarelita (ZnS), que é frequentemente associada à Galena (ou seja, um sulfeto de chumbo). A esfarelita é estável abaixo de 1020 ° C, enquanto a segunda forma de sulfeto de zinco (Wurtzita) é estável em temperaturas elevadas. Os sulfuretos de zinco são encontrados em corpos de minério em associação com calcário ou rochas dolomíticas. O zinco contendo enxofre é frequentemente combinado com ferro e manganês com inclusão ocasional de cádmio e mercúrio, enquanto o chumbo e o estanho raramente são misturados com os sulfetos. Traços de In, gálio e tálio são encontrados no ZnS, enquanto o mineral pode ser argentífero ou aurífero (Alfantazi e Moskalyk, 2003). Os minérios de sulfeto normalmente são o resultado de alguma intrusão ígnea e substituição de rochas do tipo sedimentar típicas de depósitos metamórficos. Os sulfuretos de zinco são frequentemente encontrados em associação com pirita, galena, tetraédrica, calcopirita, minérios de prata, calcita, barita, fluorita e outros tipos sedimentares. As maiores concentrações conhecidas de índio são encontradas em veios e corpos de minério de sulfureto associados a minerais contendo estanho. Uma fonte de Inde alto teor é o depósito de zinco Huari Huari dentro de um corpo de minério de esfalerita na Bolívia. Os principais minerais de zinco incluem Sphalerite como encontrado na Espanha e Romênia, Zincite e Franklinite como encontrado nos EUA, Skare Ofe no Peru e Smithsonite na Namíbia (Alfantazi e Moskalyk, 2003).

Nos últimos anos, o consumo de In tem aumentado devido suas aplicações tecnológicas na forma de ITO, a qual é geralmente aplicada em LCD e outros materiais como: painéis *touchscreeen*, eletrodos transparentes e células solares. Devido a este fato, e em conjunto com a raridade do material, é esperado que as reservas terrestres do mesmo se acabem em torno de 14 anos (U.S geological survey, 2016 e 2017). Baseado neste fato, é necessária a aplicação de um processo de recuperação de In, para que seja possível manter a demanda tecnológica. É

possível recuperar o In a partir do desmantelamento de telas de LCD, seguindo de uma extração ácida. Após este processo o In se encontra diluído em fase líquida (conforme a Figura 1 que mostra o diagrama de especiação para ao In), para isso se pode utilizar processo de precipitação (Silveira et al, 2017), extração por solvente (Gupta et al, 2004, Swain et al, 2015) ou adsorção (Lee e Lee, 2016, Alguacil et al, 2016).

Figura 1–Especiação do In na presença de íons H^+.

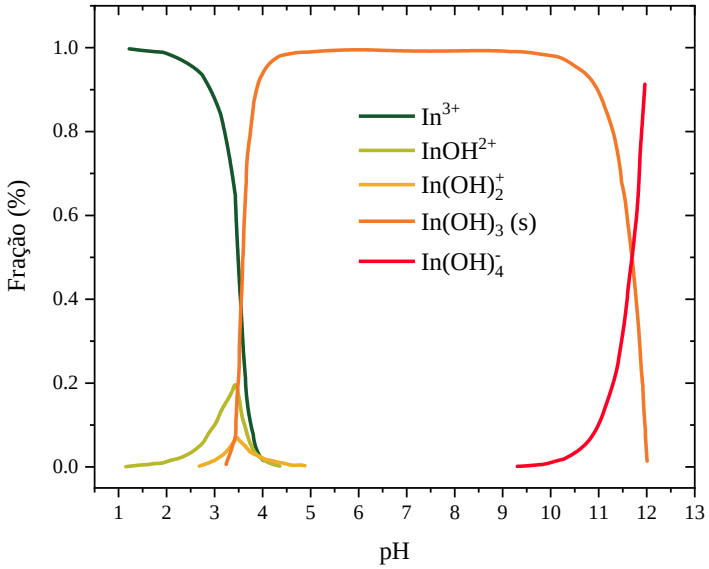

Fonte: O Autor.

Embora as técnicas de precipitação e extração por solvente acabam gerando um novo problema ambiental, relacionados aos produtos químicos e solventes utilizados, o In também, geralmente é encontrado em baixa concentração em fase líquida (Grimes et al, 2017), sendo assim, a operação unitária de adsorção é a mais indicada, devido sua facilidade de aplicação e operação, sustentabilidade, baixo custo de operação e de consumo energético (Dotto et al, 2015, Franco et al, 2017).

3.2 ADSORVENTES

Um dos pontos mais importantes da adsorção está vinculado a escolha do adsorvente. Existem inúmeros materiais empregados como adsorventes, sendo possível separar em duas categorias, os carbonáceos, biopolímeros e resíduos agroindustriais. Os materiais carbonáceos são aqueles que sua composição é quase toda constituída por carbono. Dentro desta

classificação se enquadra o carvão ativado, os nanotubo de carbono, e grafeno. Embora altamente eficientes o custo de produção dos materiais carbonáceos se torna um problema econômico e de natureza ambiental (Turan e Mesci, 2011).

Segundo se tem os biopolímeros, este são compostos que possuem a natureza polimérica sendo como por exemplo a quitina e a quitosana. Estas são geralmente encontradas em micro-organismos, insetos e animais marítimos. A quitosana e a quitina são obtidas do processamento do exoesqueleto de camarões ou caranguejos. A quitina é possui uma estrutura similar a celulose, entretanto formado por cadeias de acetilglucosamina. Enquanto a quitosana é a forma desacetilação quitina (podendo ter vários graus de desacetilação). Além disso a quitina e quitosana possuem geralmente uma alta porcentagem de nitrogênio, em torno de 6.89 %. A estrutura da quitina e quitosana em conjunto com a alta porcentagem de nitrogênio a tornam um excelente adsorvente para remoção de diversas moléculas (Elieh-Ali-Komi and Hamblin, et al 2016).

Por fim, temos os rejeitos agroindústrias, este são materiais de origem vegetal constituídos de lignina, celulose e hemicelulose. Este são explorados especialmente afim de diminuir o custo dos adsorventes e de dar finalidade aos rejeitos sólidos da agroindústria. Dentro desta categoria se tem materiais como: como resíduos de chá, cascas de amendoim e amêndoas, bagaço de cana-de-açúcar, casca de arroz, sabugo de milho, folhas de cacto, casca de melancia, casca de laranja entro outros. Embora de custo de aquisição destes resíduos seja negligente, a área superficial tende de ser baixa e muitas vezes é necessária uma modificação da superfície (Ahmed e Ahmaruzzaman, 2016; Bhattacharjee et al., 2020). No geral cada grupo apresentado possuí seus pontos positivos e negativos, sendo é necessário considerar tanto os aspectos econômicos quanto os de eficiência de adsorção (Sigh et al., 2018).

3.3 ADSORÇÃO

A adsorção é uma operação unitária baseada no fenômeno de transferência de massa, que pode ser descrito como o aumento da concentração de uma substância dissolvida na interface do sólido-líquido, sendo um fenômeno dependente das forças de superfície (Rolando, 2018, McCabe, 1993). O fenômeno de adsorção (apresentado na Figura 1) pode ser separado de acordo com a interação molecular com a superfície, havendo dois tipos de adsorção que podem ser classificados: a fissiossorção e quimiosorção (Rouquerol, 2014).

Figura 2 – Representação do fenômeno de adsorção.

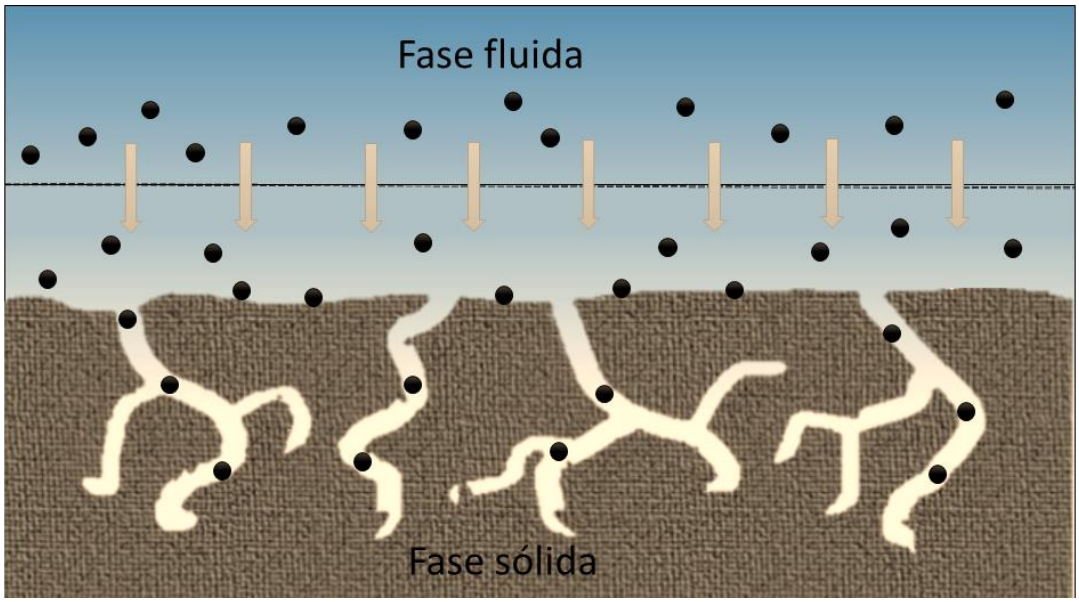

Fonte: Franco (2016).

A fisiosorção consiste nas de forças de repulsão-dispersão (Van de Waals) e forças eletrostáticas (campo dipolo-dipolo, polarização), enquanto a quimiosorção está relacionada com a transferência de elétrons, nas quais formam reações química (Ruthven, 1994). Em resumo, a Tabela 1 mostra as principais diferenças entre os tipos de adsorção.

Tabela 1– Propriedades da fisissorção e quimisorção.

Adsorção física	**Adsorção Química**
Baixo calor de adsorção (1 a 1,5 vezes o calor latente de evaporação)	Alto calor de adsorção (maior que 1,5 vezes o calor latente de evaporação)
Monocamada e multicamadas	Monocamada somente
Sem dissociação das espécies adsorvidas	Pode acontecer dissociação do adsorbato
De caráter rápido, não ativado e reversível	De caráter rápido, podendo ser devagar e irreversível
Sem a presença de transferência de elétrons, embora possa ocorrer polarização do adsorbato	Com a presença de transferência de elétrons, a qual resultada em ligação química entre o adsorbato e a superfície do adsorvente

Fonte: Karge, 2008, p.4.

Quando adsorção se dá em batelada, a capacidade de adsorção (em qualquer tempo e no equilíbrio) pode ser estimada, através do balanço de massa macroscópico no tanque agitado (Franco, 2016), conforme a equação 1 e 2:

$$q=\frac{(C_0-C)}{D_o} \quad (1)$$

$$q_e=\frac{(C_0-C_e)}{D_o} \quad (2)$$

onde C_0 é a concentração inicial do adsorbato na fase líquida (mg L^{-1}), C é a concentração de adsorbato (mg L^{-1}) na fase líquida, D_o é a dosagem de adsorvente (g L^{-1}) e q é capacidade de adsorção (mg g^{-1}).

3.3.1 Isotermas de adsorção

As isotermas de adsorção podem ser descritas como: o equilíbrio termodinâmico entre as moléculas do adsorbato, presente na fase líquida e sólida (Suzuki, 1990), ou seja, quando adsorbato não está mais mudando de fase. Com objetivo de estimar a capacidade de adsorção no equilíbrio e no fenômeno de adsorção, os dados experimentais da isoterma de adsorção são aplicados a modelos matemáticos, podendo estes serem físicos, empíricos ou semi-impíricos.

Um dos modelos mais empregados é o de Langmuir, que foi derivado a partir da cinética de adsorção considerando o mecanismo da equação 3:

$$A+S\leftrightarrow AS \quad (3)$$

onde, A é o adsorbato, S é a superfície do adsorvente e AS é a molécula do adsorvida.
Considerando que não existe variação no tempo, quando a adsorção acontece somente em monocamada, e os sítios de adsorção são homogêneos e energeticamente iguais, se obtém o modelo de Langmuir, aqui representado pela equação 4 (Langmuir, 1918):

$$q_e=\frac{q_m K_L C_e}{1+K_L C_e} \quad (4)$$

onde C_e é a concentração do adsorbato no equilíbrio. K_L é a constante de Langmuir (L mg^{-1}), q_m é a capacidade máxima de adsorção (mg g^{-1}).

Outro modelo aplicado comumente na adsorção é o modelo semi-empírico de Freundlich, este por sua vez assume que a adsorção ocorre em uma superfície heterogênea, e que a quantia de adsorbato por crescer infinitamente com a concentração, apresentado pela equação 5 (Freundlich, 1907):

$$q_e = K_F C_e^{1/n_F} \quad (5)$$

onde $1/n_F$ é o fator de heterogeneidade (-) e K_F é a constante de Freundlich (mg g^{-1})(mg L^{-1})$^{-1/n_f}$. Há, ainda, outros modelos de isotermas que também são amplamente aplicados, como por exemplo: Redlich-Peterson, Temkin, Dubinin-Radushkevich, Toth, entre outros modelos.

3.3.2 Termodinâmica de adsorção

A termodinâmica de adsorção é fundamental para entender se ocorre espontaneamente e qual o tipo de adsorção é preferencial (fissisorção ou quimisorção). Para isto, é necessário determinar a variação na energia livre de Gibbs padrão (ΔG^0, kJ mol^{-1}), mudança na entalpia padrão (ΔH^0, kJ mol^{-1}) e mudança na entropia padrão (ΔS^0, kJ mol^{-1} K^{-1}). Este pode ser feito conforme proposta por Lima (2019), onde a constante de equilíbrio (K_e, adimensional) é calculada utilizando a constante de isoterma que melhor se ajustou aos dados experimentais, e os outros parâmetros termodinâmicos são estimados, conforme as equações 6 a 9:

$$K_e = \frac{K M_a \gamma^{In(III)}}{\gamma} \quad (6)$$

$$\Delta G^0 = -R_G T \ln(K_e) \quad (7)$$

$$\Delta G^0 = \Delta H^0 - T\Delta S^0 \quad (8)$$

$$\ln(K_e) = \frac{\Delta S^0}{R} - \frac{\Delta H^0}{RT} \quad (9)$$

onde K é o parâmetro da isoterma que melhor se ajustou (L mg^{-1}), M_a é a massa atômica do In (III) (mg mol^{-1}), R_G é a constante universal dos gases ($8{,}31 \times 10^{-3}$ kJ mol^{-1} K^{-1}), T é a temperatura da solução (K).

3.3.3 Modelos de transferência de massa

Dentro do estudo da adsorção é importante conhecer a cinética de transferência de massa, que pode ser feita através dos modelos difusivos. Os modelos difusivos são a maneira mais realista de interpretar a cinética de adsorção, pois eles consideram o fenômeno de transferência de massa nos poros (Souza, 2016). Neste caso foram escolhidos utilizar dois modelos de

transferência de massa: o modelo de transferência de massa externa (em inglês: *External Mass Transfer Model*, EMTM) e o modelo de difusão na superfície e no volume do poro (em inglês: *Pore Volume and Surface Diffusion Model*, PVSDM).

O EMTM assume que a transferência de massa externa controla a taxa global de adsorção. Em outras palavras, a difusão intraparticula é instantânea, sem a presença de gradiente de concentração dentro da partícula (Leyva-Ramos et al., 2012). A expressão do EMTM pode ser expressa conforme as seguintes equações 10 a 13:

$$V\frac{dC_A}{dt} = -mSk_L(C_A - C_{Ar}|_{r=R}) \tag{10}$$

$$t=0,\ C_A = C_{A0} \tag{11}$$

$$\frac{m\varepsilon_p}{\rho_p}\frac{dC_{Ar}|_{r=R}}{dt} + m\frac{dq}{dt} = mSk_L(C_A - C_{Ar}|_{r=R}) \tag{12}$$

$$t=0,\ C_{Ar}=0,\ q=0 \tag{13}$$

onde V é o volume da solução (L), C_A é a concentração do adsorbato A (mg L^{-1}), C_{Ar} é a concentração do adsorbato A dentro da partícula na distância r (mg L^{-1}), $C_{Ar|r=R}$ é a concentração do adsorbato A na superfície externa do adsorvente (mg L^{-1}), C_{A0} é a concentração inicial do adsorbato (mg L^{-1}), m é a massa de adsorvente (g), ε_p é a porosidade do adsorvente (adimensional), ρ_p é a densidade aparente (g cm^{-3}), S é a área superficial especifica (cm^2 g^{-1}), k_L é o coeficiente de transferência de massa externa (cm s^{-1}). Para equação 12 o primeiro termo a esquerda corresponde ao acumulo do adsorbato no volume do poro, o segundo termo é devido ao acumulo na superfície do material. Por fim, o termo a direita está relacionado a taxa de transferência de massa externa onde o adsorbato é transferido do seio da solução até a superfície externa do adsorvente.

O PVSDM assume que ocorre 4 etapas de transferência de massa conforme a Figura 2. A primeira etapa (1) acontece a transferência de massa geral devido a convecção, onde o adsorbato A se desloca do seio da fase líquida, até a região de entrada dos poros (Levya-Ramos e Geankoplis, 1984). Este é expresso pela Lei de Fick, conforme a equação 14

$$N_A = k_L(C_A - C_{Ar}|_{r=R}) \tag{14}$$

onde N_A é o fluxo molar do adsorbato A no poro da partícula (mg cm s^{-1} L^{-1}).

Na segunda etapa (2), ocorre a difusão molecular no líquido no volume do poro, conforme a equação 15

$$N_{A,p}=-D_{AB}\left(\frac{\varepsilon_p}{\tau}\right)\frac{\partial C_{Ar}}{\partial r}=-D_p\frac{\partial C_{Ar}}{\partial r} \quad (15)$$

onde $N_{A,p}$ é o fluxo molar do soluto no poro da partícula (mg cm s^{-1} L^{-1}), D_{AB} é o coeficiente de difusividade molecular em diluição infinita (cm^2 s^{-1}), ε_p é a porosidade da partícula, τ é a tortuosidade, D_p é a difusividade efetiva do poro (cm^2 s^{-1}).

Figura 3 – Representação esquemática do fenômeno de adsorção em uma partícula esférica.

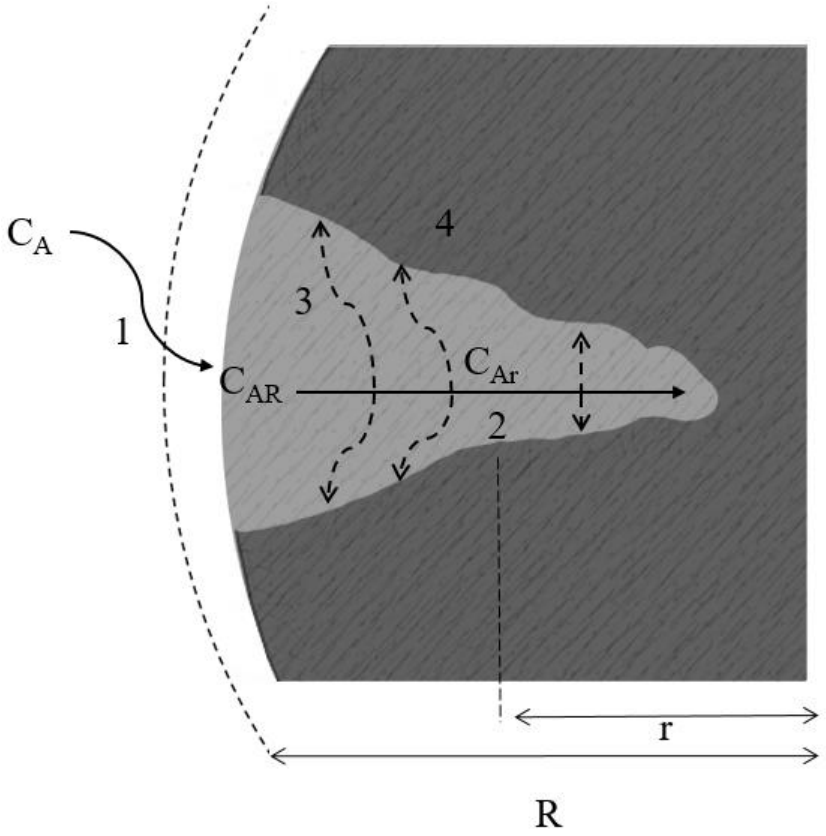

Fonte: Autor.

Na terceira etapa (3) o soluto é adsorvido na superfície do poro. Se assume que a concentração C_{Ar} está em equilíbrio local com a fase adsorvida (q), de acordo com a posição (r). Em adição, taxa de adsorção na terceira etapa é considerada muito rápida e reversível. A relação entre o C_{Ar} pode ser estimada através de modelos isotérmicos, conforme a equação 16:

$$q=f(C_{Ar}) \quad (16)$$

Por fim, a quarta etapa (4) é a difusão na superfície do soluto adsorvido na superfície do poro. Esta ocorre em paralelo com a segunda etapa (2). A difusão de superfície pode expressa pela equação 17:

$$N_{A,s}=-D_s\rho_p\frac{\partial q}{\partial r} \tag{17}$$

Onde$N_{A,s}$ D_s é a difusividade efetiva na superfície ($cm^2\ s^{-1}$), ρ_p é a massa específica da partícula ($g\ cm^{-3}$).

Levando em consideração as seguintes hipóteses simplificadoras: convecção dos poros internos é desprezível, difusão total é dependente da difusão superficial e do volume de poros. O balanço no interior da partícula, é representado pela equação 18 e sua condição inicial e condições de contorno respectivamente as equações (19 até 21), estas correspondem ao PVSDM:

$$\varepsilon_p\frac{\partial C_{Ar}}{\partial r}+\rho_p\frac{\partial q}{\partial t}=\frac{1}{r^2}\frac{\partial}{\partial r}\left[r^2\left(D_p\frac{\partial C_{Ar}}{\partial r}+\rho_p D_s\frac{\partial q}{\partial r}\right)\right] \tag{18}$$

$$C_A(0\leq r\leq R,0)=0 \tag{19}$$

$$\left.\frac{\partial C_{Ar}}{\partial r}\right|_{r=0}=0 \tag{20}$$

$$D_p\left.\frac{\partial C_{Ar}}{\partial r}\right|_{r=R}+\rho_p D_s\left.\frac{\partial q}{\partial r}\right|_{r=R}=k_F(C_A-C_{Ar}|_{r=R}) \tag{21}$$

3.4 MODELAGEM UTILIZANDO REDES NEURONAIS ARTIFICAIS

As redes neuronais artificiais (em inglês *Artificial neural network, ANN*) são modelos computacionais inspirados no sistema biológico do cérebro humano (Agatonovic-Kustrin e Beresford, 2000). Embora um neurônio biológico seja capaz de processar a informação, no caso das ANN, este processamento vem das conexões entre os neurônios que se dão através de coeficientes. Nesta seção é abordado os fundamentos matemáticos das redes neuronais artificias de múltiplas camadas retroalimentadas (em inglês: *Multilayer Feedforward Neural Network*, MLFNN) e sistema de interferência fuzzy neuro adaptável (em inglês: *Adaptative Neuro Fuzzy Interference System*, ANFIS).

3.4.1 MLFNN

Na adsorção a modelagem de redes mais aplicada é MLFNN. Esta é a combinação da ANN tradicional com o diferencial no seu treinamento que ocorre através do algoritmo de retroalimentação. As principais características relacionadas a rede é a sua estrutura que engloba o número de entradas, saídas, camadas ocultas, neurônios e a função de transferência (Ghaedi, 2017). Considerando um exemplo de rede onde constituída de camadas de entrada saída e oculta, conforme a Figura 3. Na camada de entrada sem as variáveis de entradas, estas são parâmetros experimentais, operacionais ou qualquer variável que possa afetar a performance do processo, como por exemplo a concentração inicial do adsorbato, ou a área superficial especifica do adsorvente. Os valores de saída da rede são as variáveis a serem preditas, como por exemplo: a capacidade de adsorção, percentual de remoção e concentração final. As camadas de neurônios que conectam as entradas e saídas da rede são chamadas de camadas ocultas.

Figura 4 – Exemplo de estrutura de ANN.

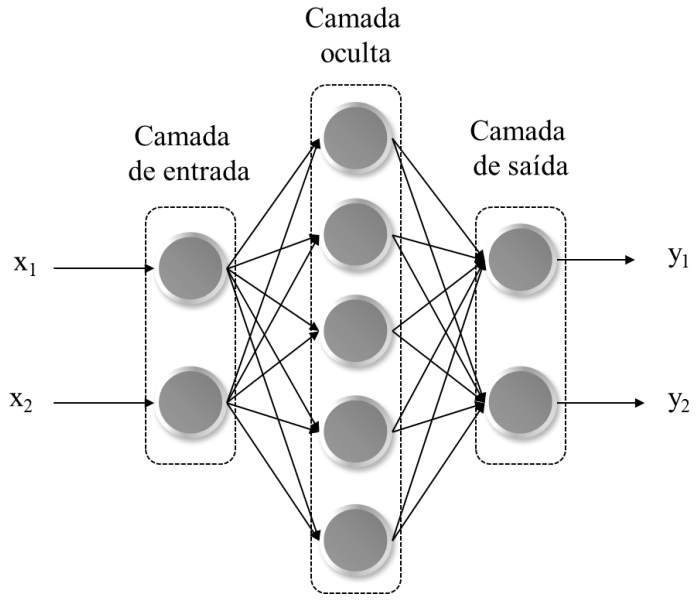

Fonte: Autor.

Primeiramente os valores de entrada são atribuídos a um peso (w_{ij}), podendo existir a presença de bias/limite (θ_i =1). Este são utilizados para calcular o potencial do neurônio i (ξ_i), conforme a equação 22 (Svozil et al., 1997):

$$\xi_i=\theta_i+\sum_{i=0}^{h} w_{ij}x_j \tag{22}$$

onde x_{ij} é o peso associado ao neurônio i com a entra j, x_j é o valor de entrada j, θ_i é o bias/limite do neurônio i.

Logo após o valor do potencial do neurônio é aplicado a função de transferência, para calcular o valor de saída do neurônio da camada oculta (z_i). No caso da MLFNN está é dada pela função sigmoide, conforme a equação 23:

$$z_i=f(\xi_i)=\frac{1}{1+\exp(-\xi_i)} \tag{23}$$

Por fim, o valor predito de saída é feito uma reversão linear baseada em peso (υ_{ij}), conforme a equação 24:

$$y_j=\sum_{i=0}^{h} \upsilon_{ij}z_i \tag{24}$$

onde y_j é o valor predito pela rede.

O algoritmo de treinamento através da retroalimentação pode ser conduzido de diferentes formas. No geral os valores dos pesos w_{ij} e υ_{ij} são estimados utilizando as equações 25 e 26:

$$w_{ij}^{k+1}=w_{ij}^{k}-\lambda\left(\frac{\partial E}{\partial w_{ij}}\right)^{k} \tag{25}$$

$$\upsilon_{ij}^{k+1}=\upsilon_{ij}^{k}-\lambda\left(\frac{\partial E}{\partial \upsilon_{ij}}\right)^{k} \tag{26}$$

onde sobrescrito k indica a iteração do pesos, λ é a taxa de aprendizado ($\lambda>0$), $\partial E/\partial w_{ij}$ e $\partial E/\partial \upsilon_{ij}$ são as derivadas do mínimos quadrados em relação ao peso da camada de entrada e da camada de saída.

3.4.2 ANFIS

Inicialmente sugerido por Jang (1993) o ANFIS é uma modelagem que combina o MLFFN com o sistema de interferência difusa (em inglês: *Fuzzy interference system* FIS), sendo a principal vantagem do sistema, a habilidade de raciocínio em conjunto com as capacidades de aprendizados da MLFFN (Ghaedi, 2017). A estrutura básica do FIS é constituída de três componentes conceituais, conforme a Tabela 2:

Tabela 2– Estrutura conceitual do FIS

Componente	Conceito
Regra de base	Contém as regras fuzzy.
Base de dados	Contém as funções de associação
Mecanismo de raciocínio	Causa interferência no sistema baseado na regras afim de estimar uma conclusão

Fonte: Shamshirband et al 2014

As regras fuzzy são feitas de todas as possíveis relações e regras entre as variáveis de entrada e saída, estas são dados por conjuntos de "se-então" (em inglês: *if-then*), por exemplo: "se x é A então y é B", onde x ϵ X (valores de entrada) e y ϵ Y(valores saída). As funções de associação são funções distributivas que variam de 0 até 1, como por exemplo a função de distribuição de Gauss, representada pela equação 27:

$$f(x;\sigma,c)=\exp\left(\frac{-(x-c)^2}{2\sigma^2}\right) \tag{27}$$

onde c e σ são parâmetros da distribuição de Gauss. Por fim o mecanismo de raciocínio faz uma busca de qual é a melhor condição ideal em base das regras fuzzy (Shamshirband et al 2014).

No caso do ANFIS, é considerado por exemplo, um FIS na qual possui apenas duas entradas X_1 e X_2 e uma saída Y, e seguem a seguinte regra presente na equação 28:

$$y=f(X_1, X_2) := \begin{cases} X_1=A \\ X_2=B \end{cases} \tag{28}$$

Este conjunto Fuzzy é chamado de função pura (em inglês: *Crisp function*), embora qualquer função possa ser aplicada como uma função pura, para definir as relações de entrada e saída (Jang,1993).

Se a função é especificada como uma constante, então é chamado de modelo Fuzzy de ordem zero do tipo Sugeno. Geralmente o modelo de primeira ordem de Sugeno é aplicado, este correlaciona as variáveis de entrada linearmente mais uma constante, equação 29:

$$\begin{aligned} &\text{Regra 1:Se}[X_1=A_1, X_2=B_1\ ] \text{ então } f_1=p_1X_1+q_1X_2+r_1 \\ &\text{Regra 2:Se}[X_1=A_2, X_2=B_2\ ] \text{ então } f_2=p_2X_1+q_2X_2+r_2 \end{aligned} \tag{29}$$

onde p_1,q_1, r_1, p_2,q_2,r_2, são parâmetros das funções do modelo. Este modelo é o mais aplicado, em conjunto com o ANFIS (Baghban et al,2017).

Para resolver o sistema gerado de regras, é utilizado o método de pesos médio para cada regra relacionada com a saída. A estrutura é apresentada na Figura 4, sendo que a metodologia consiste em camadas:

Figura 5 – Exemplo de estrutura do ANFIS.

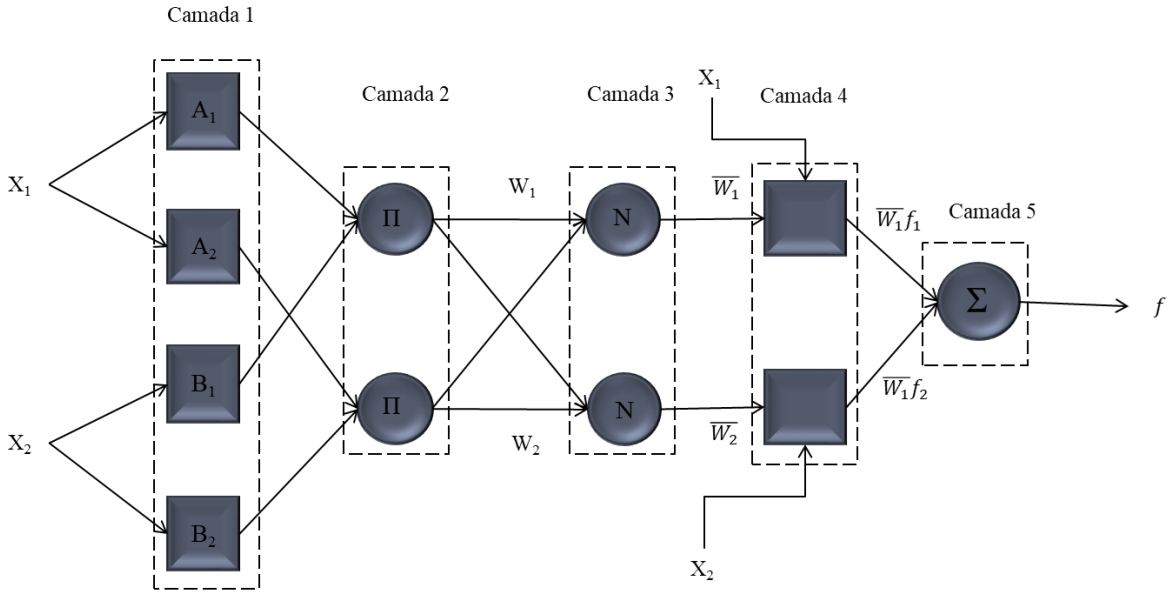

Fonte: O autor

A primeira camada inicializa a função de associação (equação 27) e conecta os nós afim de representar as condições da lógica fuzzy. A segunda camada faz uma avalição da consistência e confiabilidade da função de associação, utilizando a equação 30:

$$W_i=\beta_{Ai}(X)\beta_{Bi}(X) \tag{30}$$

A terceira camada é a normalização dos pesos dado pela equação 31:

$$\overline{W}_i=\frac{W_i}{\sum_i W_i} \tag{31}$$

A quarta camada relaciona os modelos FIS com a normalização, conforme equação 32:

$$\bar{W}_i f_i = \bar{W}_i \left(p_i X_1 + q_i X_2 + r_i \right) \tag{32}$$

Por fim a última camada faz a estimativa da saída através do somatório de cada e função pura, apresentado pela equação 33:

$$Y = \sum_i \bar{W}_i \, f_i = \frac{\sum_i w_i f_i}{\sum_i w_i} \tag{33}$$

3.4.3 Avaliação da performance das redes neuronais

Para determinar a performance da rede neuronal é feita utilizando parâmetros estatísticos, estes sendo: erro do quadrado médio (EQM), raiz do erro quadrado médio (REQM), coeficiente de correlação (R), soma dos quadrados dos resíduos (SQS), soma dos erros absolutos (SEA), números de épocas (quantia de vezes que os valores experimentais são expostos aos dados experimentais), sendo todos representados nas equações de 34 até 38:

$$R = \sqrt{1 - \frac{\sum_{i=1}^{N} \left(y_{prd,i} - y_{exp,i} \right)^2}{\sum_{i=1}^{N} \left(y_{prd,i} - y_m \right)^2}} \tag{34}$$

$$EQM = \frac{1}{N} \sum_{i=1}^{N} \left(y_{prd,i} - y_{exp,i} \right)^2 \tag{35}$$

$$REQM = \sqrt{\frac{1}{N} \sum_{i=1}^{N} \left(y_{prd,i} - y_{exp,i} \right)^2} \tag{36}$$

$$SQS = \sqrt{\frac{1}{N} \sum_{i=1}^{N} \left(y_{exp,i} - y_{prd,i} \right)^2} \tag{37}$$

$$SEA = \sum_{i=1}^{N} \left| y_{pred,i} - y_{exp,i} \right| \tag{38}$$

onde N é o número de pontos experimentais, y_{prd} é o valor predito pela rede, y_{exp} é o valor experimental, y_m é a média do predito pela rede.

4 RESULTADOS

Neste capítulo são apresentados os trabalhos publicados, cada um contendo sua respectiva metodologia. Os trabalhos desenvolvidos no tema desta Tese foram escritos na forma de três artigos, onde os mesmos se encontram conforme o molde das revistas onde foram publicados. Sendo eles:

- ✓ Primeiro artigo, intitulado: Adaptive neuro–fuzzy interference system (ANIFS) and artificial neural network (ANN) applied for indium (III) adsorption on carbonaceous materials, foi publicado na Chemical Engineering Communications, com fator de impacto de 1.431 e Qualis A1 para as engenharias II;
- ✓ Segundo artigo, intitulado: Analysis of indium (III) adsorption from leachates of LCD screens using artificial neural networks (ANN) and adaptive neuro–fuzzy interference systems (ANIFS), foi publicado no Journal of Hazardous Materials, com factor de impacto de 7.650 e Qualis A1 para as engenharias II;
- ✓ Terceiro artigo, intitulado: Interpretations on the mechanism of In(III) adsorption onto chitosan and chitin: a mass transfer model approach, foi publicado no Journal of Molecular Liquids com fator de impacto de 4.561 e Qualis B1 para as engenharias II.

4.1 ARTIGO I: Adaptive neuro–fuzzy interference system (ANIFS) and artificial neural network (ANN) applied for indium (III) adsorption on carbonaceous materials

DISON S. P. FRANCO[1], FÁBIO A. DUARTE[2], NINA PAULA G. SALAU[1], GUILHERME L. DOTTO[1]*

[1]Chemical Engineering Department, Federal University of Santa Maria–UFSM, 1000 Roraima Avenue, 97105–900 Santa Maria, RS, Brazil.

[2]Department of Chemistry, Federal University of Santa Maria–UFSM, 1000 Roraima Avenue, 97105–900 Santa Maria, RS, Brazil.

Dison S. P. Franco (E–mail address: francodison@gmail.com); Fábio A. Duarte (E–mail address: fabioand@gmail.com); Nina Paula G. Salau (E–mail address: ninasalau@ufsm.br); Guilherme Luiz Dotto* (E–mail address: guilherme_dotto@yahoo.com.br)

***Corresponding author:** UFSM, 1000 Roraima Avenue, 97105–900, Santa Maria, RS, Brazil. Tel: +55 55 3220 8448; Fax: +55 55 3220 8448. E–mail address: guilherme_dotto@yahoo.com.br

4.1.1 Abstract:

In this paper, we present an initial study relating the adsorption of indium (III) onto carbonaceous materials, namely the activated carbon (AC), multi–walled carbon nanotubes functionalized with OH (MWCNT–OH), and the multi–walled carbon nanotubes functionalized with COOH (MWCNT–COOH). The main objective of this study is the development of the adaptive neuro–fuzzy interference system (ANFIS) and an artificial neural network (ANN) for predicting the adsorption capacity in different operating conditions for different materials. Both models take into account the adsorbent type, adsorbent dosage (0.05, 0.25, 0.5, 1.0, 1.5 and 2.0 g L^{-1}), and the contact time (5, 20, 60 and 120 min) for predicting the adsorption capacity, which varied from 12.896 to 981.000 mg g^{-1}, a total record of 72 were used. Both modeling methodologies applied can represent the experimental data, taking into account the statistical values obtained. The ANFIS achieved the best performance when the hybrid method was selected, this leads into R of 0.9998, RMSE of 4,8373 with 250 epochs. On the other hand, the ANN can represent the best performance when using the Levenberg–Marquardt algorithm, reaching an R of 0.9831, MSE of 0.0180 and 9 epochs. Considering the modeling and experimental aspects indicates that the increase of the adsorbent dosage diminished the adsorbent capacity. The increase of the contact time, causes the effect to increase the adsorption capacity until its equilibrium. Lastly, it is possible to conclude that the MWCNT–COOH it is the most suitable adsorbent to be used between the selected materials.

Keywords adaptive neuro–fuzzy interference system; adsorption; artificial neural network; carbon nanotubes; indium; modeling

4.1.2 Introduction

In recent years' indium has been classified as critical raw material, indicating that this metal will start to run low in the supply market until 2020 (European–Union, 2015). Usually, indium is applied in electronic products, such as liquid–crystal displays (LCD), semiconductors and infrared photodetectors (Li et al., 2011; Jeon et al., 2015,). Indium is generally obtained as a by–product of zinc mining, with a concentration of around 20 mg kg^{-1} (Argenta et al., 2015; Li et al., 2015). On the other side of the spectrum, it is possible to find around 100 mg kg^{-1} of indium from discarded LCD screens, where, the metal is in the form of indium tin oxide (ITO) (Zhang et al., 2017). In this sense, LCD screens have gained attention as a possible source of indium. Silveira et al. (2015) demonstrated that indium can be recovered from the LCD screens trough dismantling followed by acid leaching. After leaching, a solution with low indium concentration is generated. The precipitation process is normally used for the recovery. However, precipitation can lead to more environmental problems (Grimes et al., 2017). The problematic recycling process can be mitigated by the application of the adsorption operation (Franco et al., 2017).

The adsorption process is commonly studied and applied for the removal or recovery of different species, such as dyes, metal ions and emerging contaminants (Vakili et al., 2014; Cadaval Jr. et al., 2016; Haro et al., 2017; Zare et al., 2018). The main advantages of adsorption are the low–cost, low energy consumption, and simple operation. This operation is especially efficient for recovering metal ions at low concentrations in the liquid phase (Dotto et al., 2015; Franco et al., 2017). The process efficiency also depends on the adsorbent material. Activated carbon is the most commonly used adsorbent since can be obtained from different materials and presents high values of surface area (Carmalin and Lima, 2018). Recently, the application of carbon nanotubes for metal ions adsorption has gained attention since these materials present high surface area, scalable production, tunable surface chemistry, non–corrosive properties and surface oxygen–containing functional groups (Xu et al., 2018).

For an effective application of adsorption operation, the adsorption capacity of a determined adsorbent need to be maximized as a function of the process variables, like pH, contact time, adsorbent dosage, initial concentration, temperature, stirring rate and others (Peres et al., 2018). Mendoza–Castillo et al. (2018) have highlighted the need for selecting the proper output variables for adsorption data modeling with an ANNs approach. In particular, the application of intensive variables such as adsorption capacities is a better choice than using equilibrium adsorbate concentrations or removal percentages, which are extensive variables. In

recent times, the application of adaptive neuro–fuzzy interference system (ANFIS) and artificial neural networks (ANN) in adsorption systems has become an important tool for forecasting the adsorption capacity for different systems (Singha et al., 2015, Bhowmik et al., 2017, Pooralhossini et al., 2018), since both methods can include the adsorbent type onto the modeling when compared with traditional models. This paper presents for the first time in the literature, the development of an adaptive neuro–fuzzy interference system (ANIFS) and an artificial neural network (ANN) applied for indium (III) adsorption on activated carbon (AC), multi–walled carbon nanotubes functionalized with OH groups (MWCNT–OH) and multi–walled carbon nanotubes functionalized with COOH groups (MWCNT–COOH), using the adsorption capacity (q) as the output variable. With the objective of predicting the adsorption capacity for distinct process conditions and different materials.

4.1.3 Experimental setup

4.1.3.1 Adsorbent materials

Three carbon–based adsorbents were used in this work. Multi–walled carbon nanotubes (MWCNT) were purchased from Nanostructure & Amorphous Materials, Inc. (USA). Two types of carbon nanotubes were utilized: multi–walled carbon nanotubes functionalized with OH groups (MWCNT–OH) (industrial grade, purity higher than 90%, OH content of 2.36–2.60 wt%, outer diameter of 10–30 nm, inner diameter of 5–10 nm, specific surface area of 200 m^2 g^{-1}, bulk density of 0.14 g cm^{-3} and true density of 2.10 g cm^{-3}), and multi–walled carbon nanotubes functionalized with COOH groups (MWCNT–COOH) (industrial grade, purity higher than 90%, COOH content of 1.47–1.63wt%, outer diameter of 10–30 nm, inner diameter of 5–10 nm, specific surface area of 200 m^2 g^{-1}, bulk density of 0.14 g cm^{-3} and true density of 2.10 g cm^{-3}). Commercial activated carbon (AC) produced from the babassu coconut husk was obtained from Peixe Bello Company (Brazil) (specific surface area of 639.9 m^2 g^{-1}, the bulk density of 0.21 g cm^{-3}).

4.1.3.2 Indium (III) adsorption assays

A stock solution of indium (III) (1.00 g L^{-1}) was prepared using indium (III) nitrate hydrate (Sigma Aldrich) and deionized water. The pH of the stock solution was adjusted to 2.5 using HNO_3. The solution was stored in an amber glass, which was previously cleaned with

HNO_3 and H_2SO_4. All the experiments were carried out by diluting the stock solution until the desired concentrations. All the chemical compounds used were of analytical grade, and the experiments were performed in triplicate.

Adsorption experiments were performed in an orbital agitator (Incubator shaker, SL222, Brazil) at 298 K and 150 rpm, with initial indium concentration of 50.0 mg L^{-1}. Different dosages (0.05, 0.25, 0.5, 1.0, 1.5, 2.0 g L^{-1}) of the adsorbents (AC, MWCNT–OH and MWCNT–COOH) were put in contact with indium solutions, and these solutions were stirred at predetermined time intervals (5, 20, 60 and 120 min). After the assays, the remaining indium (III) concentration in the liquid phase was determined by inductively coupled plasma analysis (ICP) (Spectra Ciros CCD, Spectra Analytical Instruments, Germany). The adsorption capacity (q, mg g^{-1}) was estimated by Equation 1:

$$q = \frac{(C_0 - C_t)}{D_o} \quad (1)$$

where, C_0 is the initial indium (III) concentration in the liquid phase (mg L^{-1}), C_t is the final indium (III) concentration in the liquid phase (mg L^{-1}) and D_o is the adsorbent dosage (g L^{-1}).

4.1.3.3 Development of ANFIS and ANN

The ANFIS and ANN were developed to take into account the type of adsorbent (AC, MWCNT–OH or MWCNT–COOH), adsorbent dosage (0.05, 0.25, 0.5, 1.0, 1.5 and 2.0 g L^{-1}) and contact time (5, 20, 60 and 120 min) as input variables. The main reasons for choosing these input variables are correlated to the classic adsorption studies, such as the time that is a foremost concern in the kinetics studies; the mass effect, here presented as dosage, affects directly the adsorption process; lastly, the evaluation of materials to be used as the adsorbent is a major concern in the field. Regarding output variables, it was chosen the adsorption capacity (q) for being an intensive variable, and for being the classical variable related to the adsorption process. The training of both networks was run in MatLab scripts using 288 points. All the values were normalized between –1 and 1, using Equation 2 (Oladipo et al., 2018, Oladipo et al., 2017):

$$Y_{nom} = \frac{Y - Y_{\min}}{Y_{\max} - Y_{\min}} \quad (2)$$

where, Y_{nom} is the normalized value, Y is the vector of values, Y_{min} is the minimum value of the vector Y, Y_{max} is the maximum value for the vector Y.

The fuzzy interference system (FIS) applied to ANFIS was generated through MatLab built–in function *genfis1* using two membership functions (to avoid overfitting) for each input. Gaussian (*gaussmf*) was chosen as the membership function (Equation 3). The developed ANFIS was of Sugeno type, which consists of four hidden layers: the fuzzification layer with two membership functions; the interference layer with eight rules; the defuzzification layer; and the output layer. The architecture is displayed in Figure 1. All the data were randomly split into 2 sets, 70% for training and 30% for the check using the "*randperm*" function. Two different optimization methods were tested: hybrid method (combination of least–squares estimation and backpropagation) and back–propagation in steepest descent method (BPSDM), cf. Equation3.

$$f(x;\sigma,c) = e^{-\frac{(x-c)^2}{2\sigma^2}} \tag{3}$$

where, x is the input value, c and σ are parameters of the function.

The ANN created uses the backpropagation feedforward neural network, which consists of two layers: one neuron in the output and 10 neurons in the hidden layer, as presented in Figure 2. To obtain a better suitable ANN, 5 different backpropagation training functions were tested and compared: Levenberg–Marquardt (*trainlm*), resilient (*trainrp*), scaled conjugate gradient (*trainscg*), Polak–Ribiére conjugate gradient (*traincpg*) and variable learning rate gradient (*traingdx*). All data were randomly split into 70% for training, 15% for checking and the remaining for validation. This separation was made by the "*diverand*" function. Further information and deductions about ANFIS and ANN can be found elsewhere (Jang, 1991; Caudil and Butler, 1992; Jang, 1993; Hagan and Menhaj, 1999, Gazi et al., 2017).

Figure 1: ANFIS architecture: I=2 (number of membership) and n=8 (number of rules).

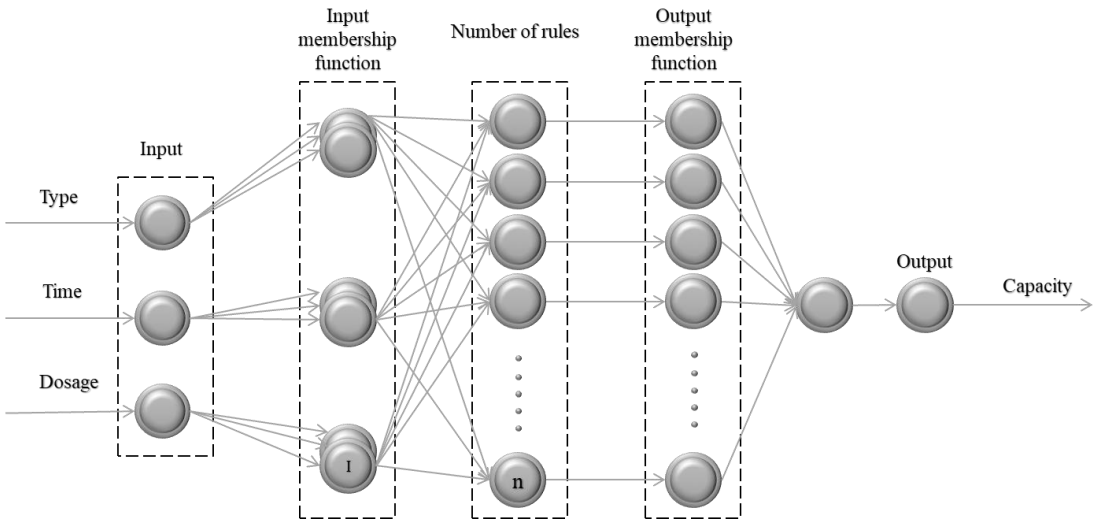

Figure 2: ANN architecture.

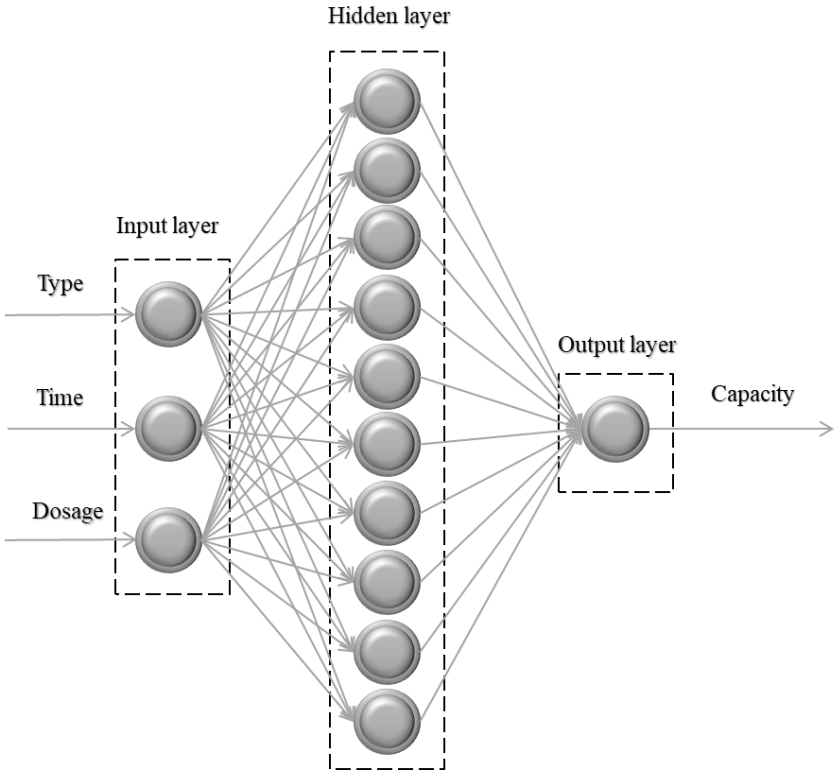

4.1.3.4 Performance evaluation

The performance of ANFIS and ANN was evaluated by the following statistical parameters: correlation coefficient (*R*), epochs (number of times presented in the training data), mean–squared error (*MSE*), root–mean–squared error (*RMSE*), sum of squared errors (*SSE*) and sum of the absolute error (*SAE*), as follows (Bhowmik et al., 2018, Debnath et al., 2016):

$$R = \sqrt{1 - \frac{\sum_{i=1}^{N} (y_{prd,i} - y_{\exp,i})^2}{\sum_{i=1}^{N} (y_{prd,i} - y_m)^2}} \quad (4)$$

$$MSE = \frac{1}{N} \sum_{i=1}^{N} (y_{prd,i} - y_{\exp,i})^2 \quad (5)$$

$$RMSE = \sqrt{\frac{1}{N} \sum_{i=1}^{N} (y_{prd,i} - y_{\exp,i})^2} \quad (6)$$

$$SSE = \sqrt{\frac{\sum_{i=1}^{N} (y_{\exp,i} - y_{pred,i})^2}{N}} \quad (7)$$

$$SAE = \sum_{i=1}^{N} \left| y_{prd,i} - y_{\exp,i} \right| \quad (8)$$

where, N is the number of experimental points, $y_{prd,I}$ is the predicted response, $y_{exp,I}$ is the experimental value and y_m is the mean value of the response. These statistical parameters are commonly applied for evaluating the overall performance (Jang, 1991; Ghaedi and Vafaei, 2017).

4.1.4 Results and discussion

4.1.4.1 Experimental inferences

The Table I, II and II show the indium (III) adsorption capacity values for each adsorbent: AC, MWCNT–OH, and MWCNT–COOH for each dosage and contact time.

From the tables, it is possible to observe that the q values ranged from 12.896 to 981.000 mg g^{-1}, is extremely dependent on the input variables. Table IV presents the comparison with other reports the materials tested in this work presented a higher adsorption capacity. In this way, AC, MWCNT–OH and MWCNT–COOH can be potential candidates to adsorb indium (III) from aqueous media.

Table 1: Experimental values of the indium (III) adsorption capacity on activated carbon (AC).

D_o (g L^{-1})	Time (min)	q (mg g^{-1})
0.05	5	512.38
	20	594.30
	60	604.44
	120	656.00
0.25	5	117.424
	20	131.100
	60	165.192
	120	187.180
0.5	5	73.324
	20	78.334
	60	80.656
	120	90.436
1.0	5	19.898
	20	35.373
	60	35.369
	120	46.550
1.5	5	15.102
	20	24.893
	60	27.282
	120	33.233
2.0	5	12.896
	20	24.897
	60	24.857
	120	25.000

Table 2: Experimental values of the indium (III) adsorption capacity on multi–walled carbon nanotubes functionalized with OH (MWCNT–OH).

D_o (g L^{-1})	Time (min)	q (mg g^{-1})
0.05	5	534.080
	20	544.720
	60	664.360
	120	973.320
0.25	5	127.772
	20	128.784
	60	134.200
	120	142.756
0.5	5	66.970
	20	68.156
	60	69.400
	120	71.730
1.0	5	40.097
	20	41.413
	60	42.208
	120	42.514
1.5	5	31.014
	20	31.302
	60	33.074
	120	33.196
2.0	5	22.893
	20	24.809
	60	25.000
	120	25.000

Table 3: Experimental values of the indium (III) adsorption capacity on multi–walled carbon nanotubes functionalized with COOH (MWCNT–COOH).

D_o (g L^{-1})	Time (min)	q (mg g^{-1})
0.05	5	560.460
	20	654.820
	60	627.040
	120	981.000
0.25	5	114.300
	20	121.328
	60	157.180
	120	172.700
0.5	5	65.022
	20	67.924
	60	73.904
	120	74.026
1.0	5	32.839
	20	33.053
	60	33.466
	120	34.507
1.5	5	23.500
	20	24.487
	60	23.883
	120	32.996
2.0	5	18.589
	20	19.239
	60	20.202
	120	24.967

Table 4: Comparison of the adsorption capacity for indium (III) onto different materials.

Material	pH (-)	q_{exp}(mg g^{-1})	Reference
Resin	3	35	Li et al. (2012)
Chelating resin	3.5	0.15	Akama (2016)
Resin Lewatit Tp207	-	55	Lee and Lee (2016)
AC	2.5	656.00	This work
MWCNT-OH	2.5	973.320	This work
MWCNT-COOH	2.5	981.000	This work

Regarding the physicochemical influence of the input variables on the indium adsorption capacity, it is possible to infer three main trends: firstly, it was verified that the adsorbent dosage increase caused a decrease in the adsorption capacity values. From a molecular viewpoint, the adsorbent dosage increase leads to an increase in the total number of adsorption sites. However, the number of available sites per gram of adsorbent decreases, leading to lower adsorption capacity values (Georgin et al., 2018). Secondly, the contact time increase led to an increase in adsorption capacity. In general, at 5 min, adsorption capacity reached 50% of the maximum value. This is a result of the progressive blocking of the adsorption sites. Lastly, it was verified that MWCNT–COOH presented higher adsorption capacity values than the other adsorbents, indicating a higher affinity with indium (III). The best performance of MWCNT–COOH in relation to AC can be attributed to the nanometric size. On the other hand, when comparing MWCNT–COOH in relation to MWCNT–OH the best performance can be attributed to the acid character of the COOH group. These inferences will be corroborated in the subsequent sections, by the ANFIS and ANN evaluation.

3.3. ANFIS evaluation

The ANFIS precision was evaluated using two optimization methods; i. e. the hybrid and BPSDM. The statistical parameters relative to this comparison are displayed in Table V. The higher values of R and the lower values of *RMSE*, *SAE*, and *SSE* were found using the hybrid method. Then this method presented better performance in comparison with BPSDM. The low performance of BPSDM (R=0.7922) can be related with the high step size value, which leads to low sensitivity. Thus, using BPSDM, ANFIS have difficulties to represent real data (Salomon and Hemmen, 1996).

Table 5: Error analysis for the two methods tested in the ANFIS development.

Algorithm	*R*	epochs	*RMSE*	*SAE*	*SSE*
Hybrid	0.9998	250	4.83	179.4	23.4
BPSDM	0.7922	250	154.82	3983.2	23970.0

Figure 3 shows the ANFIS performance (using the hybrid method) for the training and checking data. It can be verified that using 250 epochs the *MSE* value is minimized for both, training and checking data. Thus, it is possible to conclude that ANFIS presented a good performance to forecast the indium (III) adsorption capacity values as a function of the input variables. The values of indium (III) adsorption capacity as a function of adsorbent type, contact time and adsorbent dosage, which were predicted by ANFIS are presented in Figures 4, 5 and 6, respectively. The 3D prediction for the adsorption capacity as a function of contact time and adsorbent dosage is depicted in Figure 7. The 3D prediction for the adsorption capacity as a function of contact time and adsorbent type is presented in Figure 8.

Figure 3: ANFIS performance.

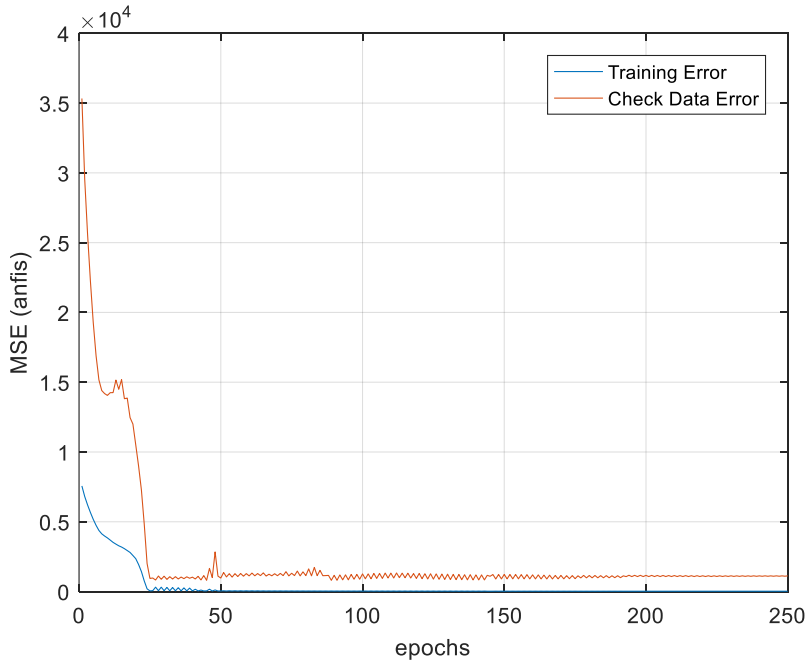

It can be proved that ANFIS was able to predict different behaviors, as the dependence on indium (III) adsorption capacity with the adsorbent dosage, contact time and adsorbent type. The ANFIS results clearly indicated that the adsorbent dosage increase caused a decrease in the adsorption capacity; that the contact time increase led to an increase in adsorption capacity, and that MWCNT–COOH presented higher adsorption capacity values than the other adsorbents. In this way, ANFIS is in agreement with the experimental inferences. Ghaedi et al. (2013, 2014) successfully applied ANFIS with the hybrid method in different solid–liquid adsorption systems. They found interesting results using contact time, adsorbent mass and initial concentration as input variables, and removal percentage as the output variable. Aghajani and Tayebi (2017) also demonstrated that ANFIS was able to predict the adsorption capacity of Reactive Red 198 on SBA–15/CTAB composite.

Figure 4: Prediction of the adsorption capacity as a function of adsorbent type (ANFIS).

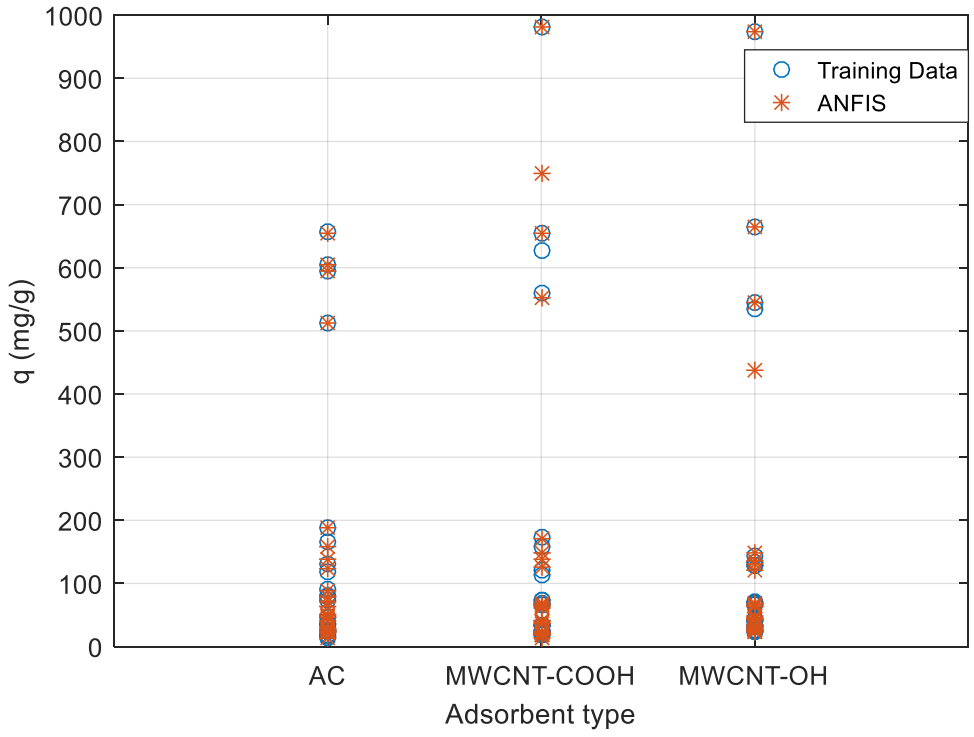

Figure 5: Prediction of the adsorption capacity as a function of contact time (ANFIS).

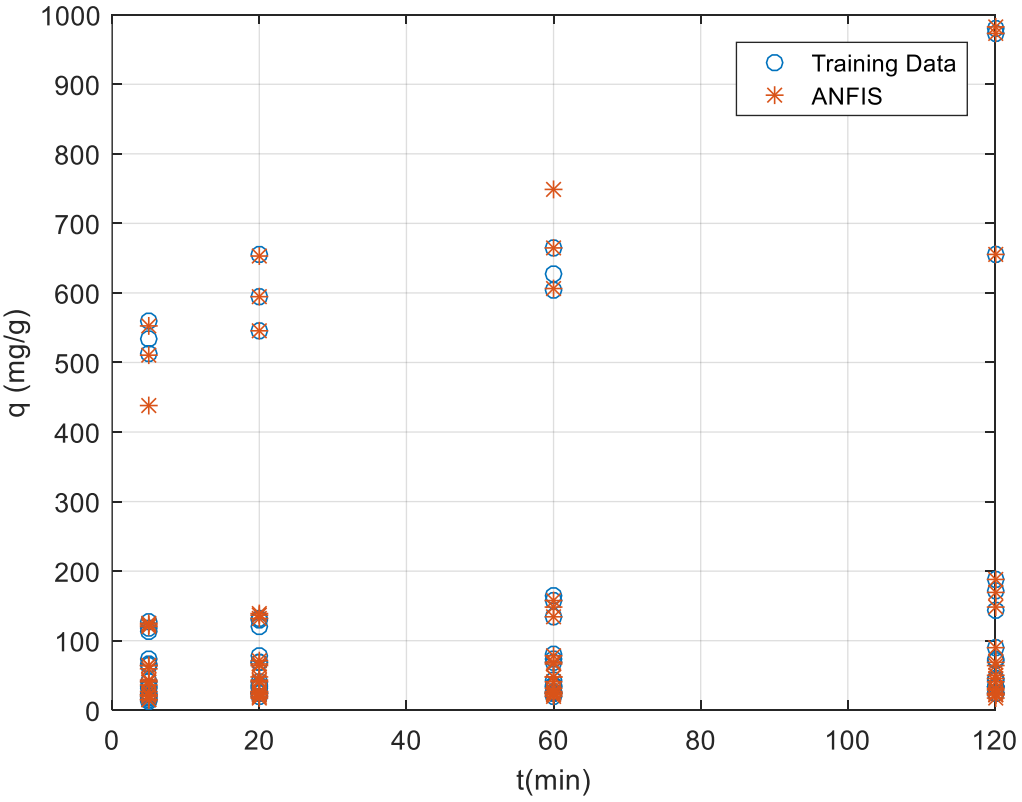

Figure 6: Prediction of the adsorption capacity as function of adsorbent dosage (ANFIS).

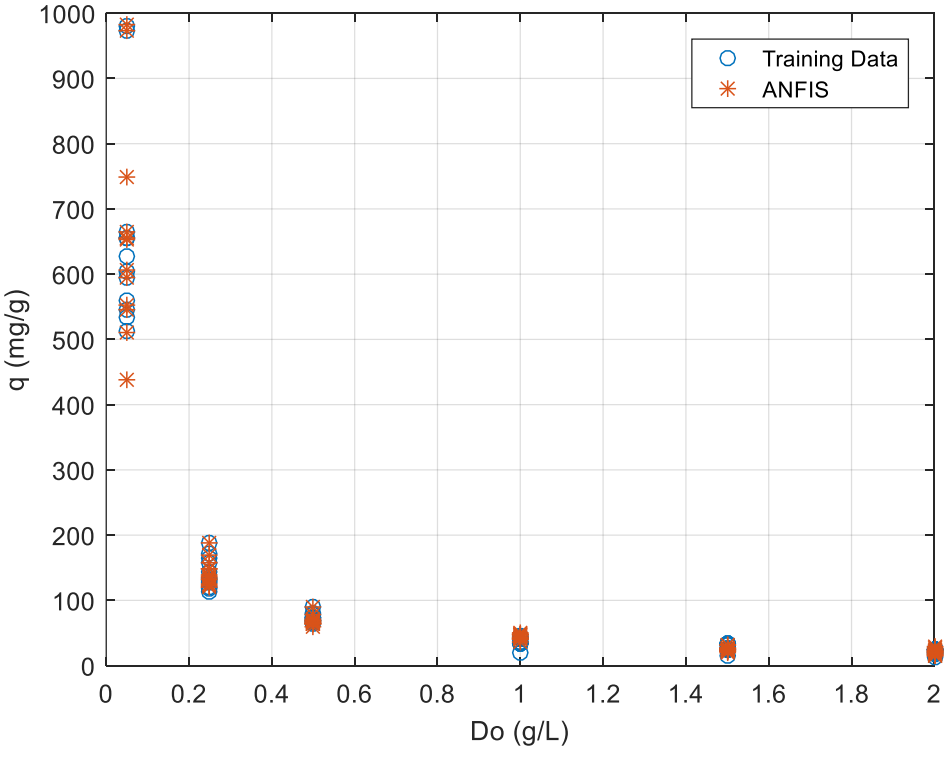

Figure 7: Surface prediction for the adsorption capacity as a function of contact time and adsorbent dosage.

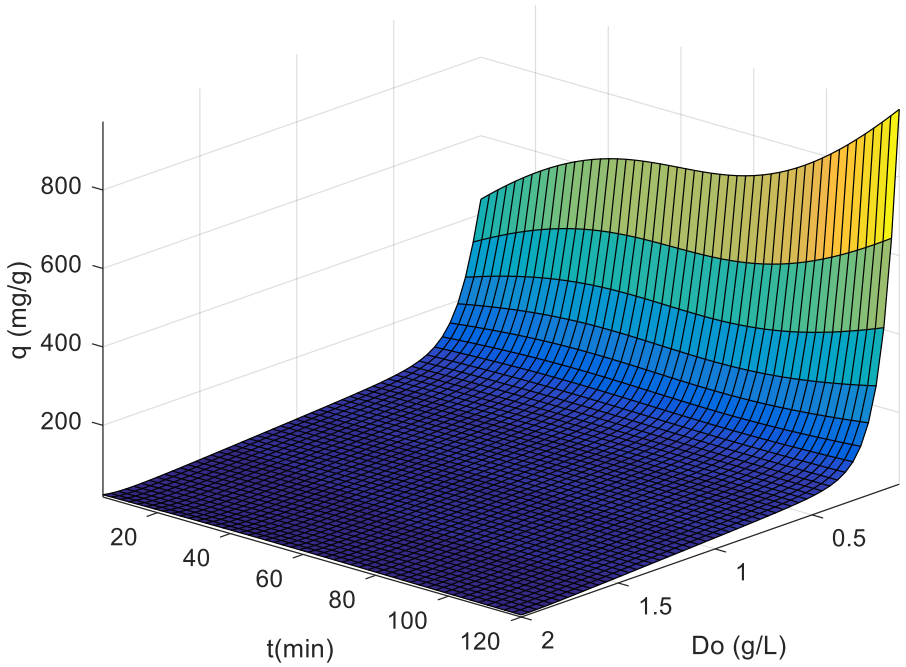

Figure 8: Surface prediction for the adsorption capacity as a function of contact time and adsorbent type.

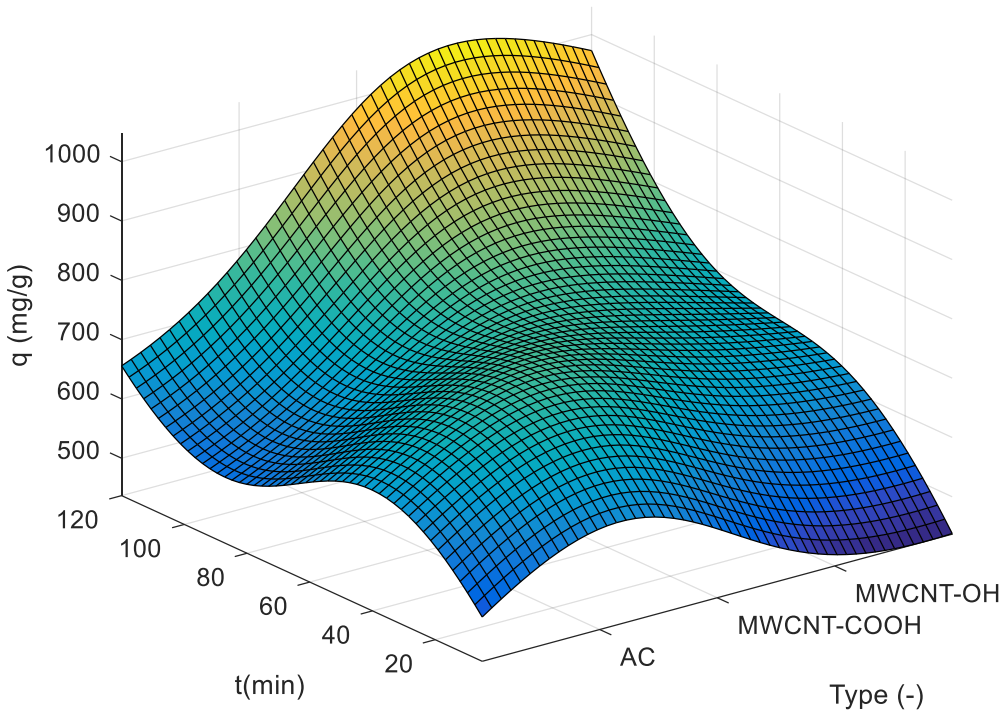

4.1.4.2 ANN results

The ANN accuracy was tested with five different back–propagation training functions: Levenberg–Marquardt (*trainlm*), resilient (*trainrp*), scaled conjugate gradient (*trainscg*), Polak–Ribiére conjugate gradient (*traincpg*) and variable learning rate gradient (*traingdx*). From the statistical parameters presented in Table VI, it can be verified that the Levenberg–Marquardt (*trainlm*) algorithm was the most suitable function for training the ANN. Ghaedi and Vafaei (2017) also verified that Levenberg–Marquardt was the most adequate algorithm to be used in ANN for adsorption systems. Figure 9 represents the ANN performance for the *trainlm* algorithm. It was found that the *MSE* values were minimized with 9 epochs for the validation data. Figure 10 is the comparison between the experimental and ANN predicted data for the indium (III) adsorption. In general, the ANN predicted data agreed with the experimental data, demonstrating that ANN can be used to predict the indium (III) adsorption capacity as a function of contact time, adsorbent dosage and adsorbent type.

Table 6: Error analysis for the five tested algorithms in the ANN model development.

Algorithm	*R*	epochs	*MSE*	*SAE*	*SSE*
Trainlm	0.9831	9	0.0180	2.8190	0.6464
Trainrp	0.9655	38	0.0139	0.9319	0.1533
Trainscg	0.9284	15	0.0476	0.5234	0.5234
Traincpg	0.9880	41	0.0029	0.4749	0.0315
Traingdx	0.9857	145	0.0252	1.0405	0.2767

Figure 9: ANN performance.

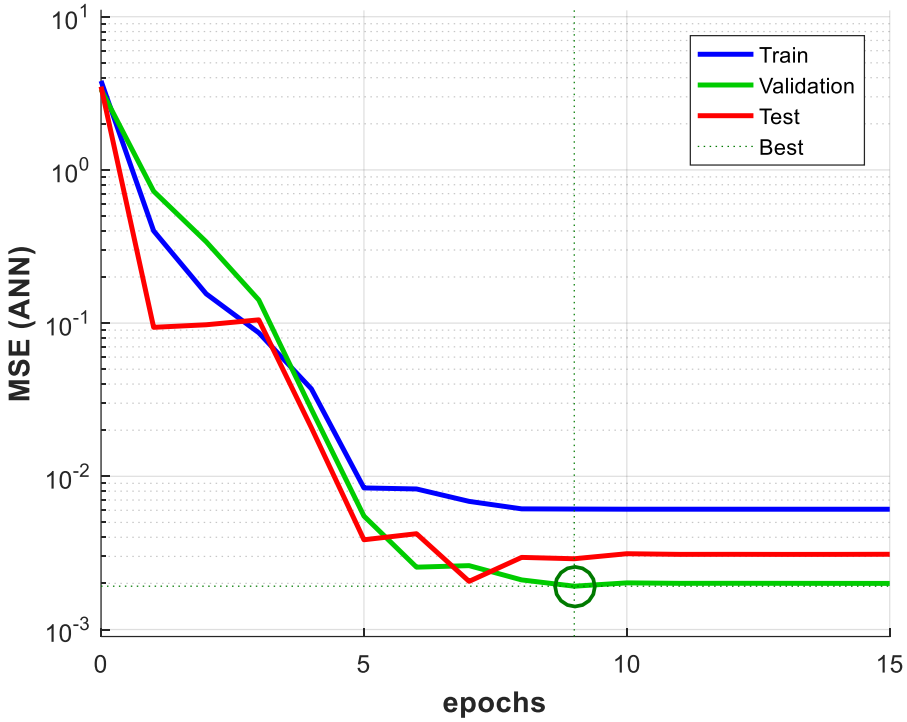

Figure 10: Comparison between the experimental data and predicted values by the ANN.

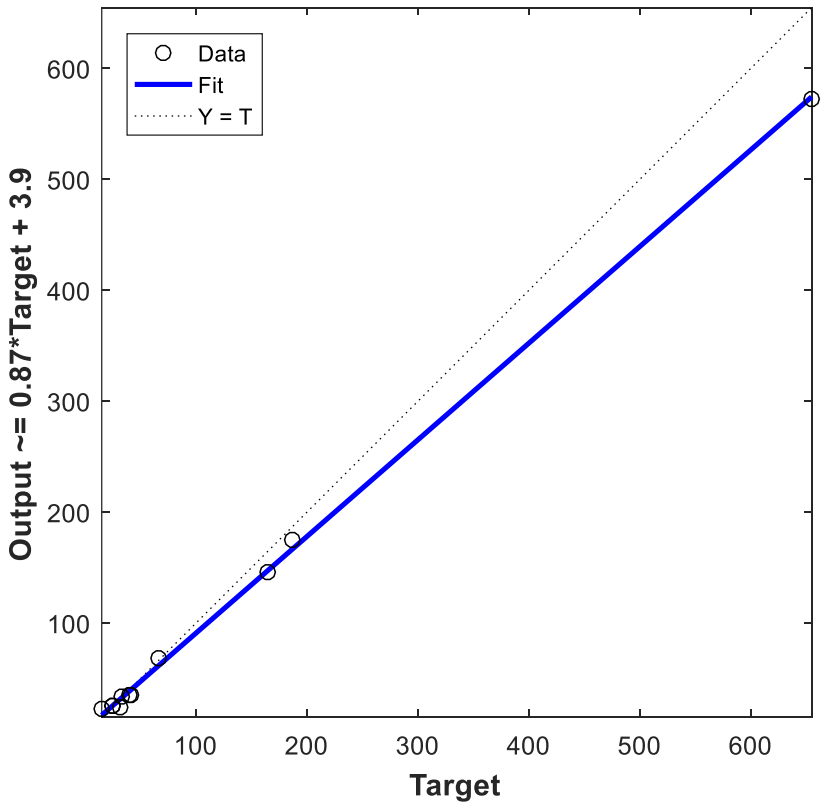

4.1.5 Conclusion

In this research, an adaptive neuro–fuzzy interference system (ANIFS) and an artificial neural network (ANN) were applied to predict the indium (III) adsorption capacity (*q*) onto three carbonaceous materials (AC, MWCNT–OH and MWCNT–COOH) as a function of the adsorbent dosage, contact time and adsorbent type. The experimental results indicated that the *q* values increased with the contact time; decreased with the adsorbent dosage and were higher when MWCNT–COOH was used. It was possible to develop an ANFIS model using the hybrid method, with 250 epochs, *R* of 0.9998, *RMSE* of 4.83, *SAE* of 179.4 and *SSE* of 23.4. The developed ANFIS can be successfully used for forecasting the adsorption capacity as a function of the adsorbent dosage, contact time and adsorbent type. In parallel, the ANN model was applied to the experimental data, and in this case, the Levenberg–Marquardt (*trainlm)* was the most suitable algorithm, attaining *R* of 0.9831, 9 epochs, *MSE* of 0.0180, *SAE* of 2.8190 and *SSE* of 0.6464. The choice of this algorithm was based on the low epochs value. The comparison between the experimental and ANN predicted data confirmed that ANN can be also used to forecast the indium (III) adsorption capacity as a function of the input variables.

4.1.6 References

Aghajani, K. and Tayebi, H. A. (2017). Adaptive Neuro–Fuzzy Inference system analysis on adsorption studies of Reactive Red 198 from aqueous solution by SBA–15/CTAB composite, *Spectrochim. Acta Part A Mol. Biomol. Spectrosc.* 171, 439–448.

Alguacil, F. J., Lopez, F. A., Rodriguez, O., Martinez–Ramirez, S. and Garcia–Diaz, I. (2016). Sorption of indium (III) onto carbon nanotubes, *Ecotoxicol. Environ. Saf.* 130, 81–86.

Argenta, A. B., Reis, C. M., Mello, G. P., Dotto, G. L., Tanabe, E. H. and Bertuol, D. A. (2017). Supercritical CO_2 extraction of indium present in liquid crystal displays from discarded cell phones using organic acids, *J. Supercrit. Fluids.* 120, 95–101.

Bhowmik, K., Debnath, A.; Ranendu K. N. and Biswajit, S. (2017). Synthesis of MnFe2O4and

Mn3O4magnetic Nano–Composites with Enhanced Properties for Adsorption of Cr(VI): Artificial Neural Network Modeling, *Water Sci. Technol.* 76, 3368–3378.

Bhowmik, M., Deb, K., Debnath, A., Saha, B. (2018). Mixed–phase Fe2O3/Mn3O4magnetic nanocomposite for enhanced adsorption of methyl orange dye: Neural network modeling and response surface methodology optimization, *Appl. Organomet. Chem.* 32, 1–17.

Cadaval Jr., T. R. S., Dotto, G. L., Seus, E. R., Mirlean, N. and Pinto, L. A. A. (2016). Vanadium removal from aqueous solutions by adsorption onto chitosan films, *Desalin. Water Treat.* 57, 16583–16591.

Carmalin, S. A. and Lima, E. C. (2018). Removal of emerging contaminants from the environment by adsorption, *Ecotoxicol. Environ. Saf.* 150, 1–17.

Caudill, M. and Butler, C. (1992). *Understanding Neural Networks: Computer Explorations*, Cambridge, MA. The MIT Press.

Debnath, A., Majumder, M., Pal, M., Das, N. S., Chattopadhyay, K. K. and Saha, B. (2016). Enhanced Adsorption of Hexavalent Chromium onto Magnetic Calcium Ferrite Nanoparticles: Kinetic, Isotherm, and Neural Network Modeling, *J. Dispers. Sci. Technol*. 37, 1806–1818.

Dotto, G. L., dos Santos, J. M. N., Rosa, R., Pinto, L. A. A., Pavan, F. A. and Lima, E. C. (2015). Fixed bed adsorption of Methylene Blue by ultrasonic surface modified chitin supported on sand, *Chem. Eng. Res. Des.* 100, 302–310.

European Commision (2015). Report on critical raw materials for EU. European Commision. 1–205.

Franco, D. S. P., Tanabe, E. H. and Dotto, G. L. (2017). Continuous Adsorption of a Cationic Dye on Surface Modified Rice Husk: Statistical Optimization and Dynamic Models, *Chem. Eng. Commun.* 204, 625–634.

Franco, D. S. P., Piccin, J. S., Lima, E. C. and Dotto, G. L. (2015). Interpretations about

methylene blue adsorption by surface modified chitin using the statistical physics treatment, *Adsorption*. 21, 557–564.

Gazi, M., Oladipo, A. A., Ojoro, Z. E. and Gulcan, H. O. (2017). High–Performance Nanocatalyst for Adsorptive and Photo–Assisted Fenton–Like Degradation of Phenol: Modeling Using Artificial Neural Networks. *Chem. Eng. Commun*. 204, 729–738.

Georgin, J., da Silva Marques, D. Silveira Salla, J., Foletto, E. L., Allasia, D. and Dotto, G. L. (2018). Removal of Procion Red dye from colored effluents using H_2SO_4/HNO_3–treated avocado shells (*Persea americana*) as adsorbent, *Environ. Sci. Pollut. Res.* 25, 6429–6442.

Ghaedi, A. M. and Vafaei, A. (2017). Applications of artificial neural networks for adsorption removal of dyes from aqueous solution: A review, *Adv. Colloid Interface Sci.* 245, 20–39.

Ghaedi, M., Ghaedi, A. M., Abdi, F., Roosta, M., Vafaei, A. and Asghari, A. (2013). Principal component analysis–adaptive neuro–fuzzy inference system modeling and genetic algorithm optimization of adsorption of methylene blue by activated carbon derived from Pistacia khinjuk, *Ecotoxicol. Environ. Saf.* 96, 110–117.

Ghaedi, M., Hosaininia, R., Ghaedi, A. M., Vafaei, A. and Taghizadeh, F. (2014). Adaptive neuro–fuzzy inference system model for adsorption of 1,3,4–thiadiazole–2,5–dithiol onto gold nanoparticales–activated carbon, *Spectrochim. Acta Part A Mol. Biomol. Spectrosc.* 131, 606–614.

Grimes, S. M., Yasri, N. G. and Chaudhary, A. J. (2017). Recovery of critical metals from dilute leach solutions – Separation of indium from tin and lead, *Inorganic. Chim. Acta.* 461, 161–166.

Hagan, M. T. and Menhaj, M. (1999). Training feed–forward networks with the Marquardt algorithm, *IEEE Trans. Neural Networks*. 5, 989–993.

Haro, N. K., Del Vecchio, P., Marcilio, N. R. and Féris, L. A. (2017). Removal of atenolol by adsorption – Study of kinetics and equilibrium, *J. Clean. Prod.* 154, 214–219.

Jang, J. S. R. (1991). Fuzzy Modeling Using Generalized Neural Networks and Kalman Filter Algorithm, *Proc. of the 9th National Conf. on Artificial Intelligence (AAAI–91)*. 762–767.

Jang, J. S. R. (1993). ANFIS: Adaptive–Network–based Fuzzy Inference Systems, *IEEE Trans. Syst. Man. Cybernetics*. 23, 665–685.

Jeon, C., Cha, J. and Choi, J. (2015). Adsorption and recovery characteristics of phosphorylated sawdust bead for indium (III) in industrial wastewater, *J. Ind. Eng. Chem.* 27, 201–206.

Lee, S. and Lee, U. (2016). Adsorption and desorption property of iminodiacetate resin (Lewatit 1 TP207) for indium recovery, *J. Ind. Eng. Chem.* 40, 23–25.

Li, F., Bai, L., He, W., Li, G. and Huang, J. (2015). Resource recovery from waste LCD panel by hydrothermal transformation of polarizer into organic acids, *J. Hazard. Mater.* 299, 103–111.

Li, Y., Liu, Z., Li, Q., Liu, Z. and Zeng, L. (2011). Recovery of indium from used indium–tin–oxide (ITO) targets, *Hydrometallurgy.* 105, 207–212.

Mendoza–Castillo, D. I., Reynel–Ávila, H. E., Sánchez–Ruiz, F. J., Trejo–Valencia, R., Jaime–Leal, J. E. and Bonilla–Petriciolet A. (2018). Insights and pitfalls of artificial neural network modeling of competitive multi–metallic adsorption data, *J. Mol. Liq.* 251, 15–27.

Oladipo, A. A., Vaziri, R. and Abureesh, M. A. (2018). Highly robust AgIO3/MIL–53 (Fe) nanohybrid composites for degradation of organophosphorus pesticides in single and binary systems: Application of artificial neural networks modelling, *J. Taiwan Inst. Chem. Eng*. 83, 133–142.

Oladipo, A. S., Ajayi, O. A., Oladipo, A. A., Azarmi, S. L., Nurudeen, Y., Atta, A. Y. and Ogunyemi, S. S. (2018). Magnetic recyclable eggshell–based mesoporous catalyst for biodiesel production from crude neem oil: Process optimization by central composite design and artificial neural network, *Comp. Rend. Chim*. 21, 684–695.

Peres, E. C., Cunha, J. M., Dortzbacher, G. F., Pavan, F., Lima, E. C., Foletto, E. L. and Dotto,

G. L. (2018). Treatment of leachates containing cobalt by adsorption on Spirulina sp. and activated charcoal, *J. Environ. Chem. Eng.* 6, 677–685.

Pooralhossini, J., Zanjanchi, M. A., Ghaedi, M., Asfaram, A. and Azqhandi, M. H. A. (2018). Statistical optimization and modeling approach for azo dye decolorization: Combined effects of ultrasound waves and nanomaterial–based adsorbent, *Appl. Organomet. Chem*. 32, 1–14.

Salomon, R. and Van Hemmen, J. L. (1996). Accelerating Backpropagation through Dynamic Self–Adaptation, *Neural Networks*. 9, 589–601.

Silveira, A. V. M., Fuchs, M. S., Pinheiro, D. K., Tanabe, E. H. and Bertuol, D. A. (2015). Recovery of indium from LCD screens of discarded cell phones, *Waste Manag.* 45, 334–342.

Singha, B., Bar, N., and Das, S. K. (2015). The use of the artificial neural network (ANN) for modeling of Pb(II) adsorption in a batch process, *J. Mol. Liq.* 211, 228–232.

Vakili, M., Rafatullah, M., Salamatinia, B., Abdullah, A. Z., Ibrahim, M. H., Gholami, Z. and Amouzgar, P. (2014). Application of chitosan and its derivatives as adsorbents for dye removal from water and wastewater: A review, *Carbohydr. Polym.* 113, 115–130.

Xu, J., Cao, Z., Zhang, Y., Yuan, Z., Lou, Z., Xu, X. and Wang, X. (2018). A review of functionalized carbon nanotubes and graphene for heavy metal adsorption from water: Preparation, application, and mechanism, *Chemosphere*. 195, 351–364.

Zare, E. N., Motahari, A. and Sillanpää, M. (2018). Nanoadsorbents based on conducting polymer nanocomposites with main focus on polyaniline and its derivatives for removal of heavy metal ions/dyes: A review, *Environ. Res.* 162, 173–195.

Zhang, K., Li, B., Wu, Y., Wang, W., Li, R., Zhang, Y. N. and Zuo, T. (2017). Recycling of indium from waste LCD: A promising non–crushing leaching with the aid of ultrasonic wave, *Waste Manag.* 64, 236–243.

4.2 ARTIGO II: Analysis of indium (III) adsorption from leachates of LCD screens using artificial neural networks (ANN) and adaptive neuro–fuzzy interference systems (ANIFS)

Dison S. P. Franco[1], Fábio A. Duarte[2], Nina Paula G. Salau[1], Guilherme L. Dotto[1*]

[1]Chemical Engineering Department, Federal University of Santa Maria–UFSM, Santa Maria, RS, Brazil.

[2]Department of Chemistry, Federal University of Santa Maria–UFSM, Santa Maria, RS, Brazil.

Dison S. P. Franco E–mail address: francodison@gmail.com

Fábio A. Duarte E–mail address: fabioand@gmail.com

Nina Paula G. Salau E–mail address: ninasalau@ufsm.br

Guilherme Luiz Dotto* E–mail address: guilherme_dotto@yahoo.com.br

[*]Corresponding author: UFSM, 1000, Roraima Avenue, 97105-900, Santa Maria, RS, Brazil.
E-mail address: guilherme_dotto@yahoo.com.br

4.2.1 Abstract

Ten different adsorbent materials were tested to adsorb indium (III) from leachates of LCD screens, aiming to concentrate this valuable material. Artificial neural network (ANN) and adaptive neuro–fuzzy interference system (ANIFS) were applied to analyze the indium (III) adsorption. The input variables for the network models were: specific surface area, point of zero charge, adsorbent dosage and contact time. Adsorption capacity (q) was used as output variable. The adsorption capacity values ranged from 8.203 to 1000 mg g^{-1}. The ANN modeling presented the best fit when the Levenberg–Marquardt algorithm was used. The ANFIS modeling presented the optimum performance when the hybrid method was used. Among the tested adsorbents, chitosan presented the best performance; attaining adsorption capacity of 1000 mg g^{-1} within 20 min. This is an excellent value since the maximum indium concentration in LCD screens is 0.613 mg g^{-1}. This high capacity was attributed to the coordination ligation between chitosan and indium (III).

Keywords: adaptive neuro–fuzzy interference system; artificial neural network; indium concentration; leachates from LCD screens; coordination ligation.

4.2.2 Introduction

The consumption of electronic products increases every year, requiring more quantities of raw materials and generating more quantities of wastes [1]. Several valuable raw materials, including indium, are then become scarce. In general, indium is only obtained as a by–product of zinc ores refinement, where it concentrations reach only 20 mg kg^{-1} [2]. This shortage of indium in natural resources is pointed out by the European Union, where they classified the metal as a critical raw material and the possible shortfall for 2020. These data are in agreement

with the data provided by the U.S. Geological Survey, where, it was shown that the indium production has decreased at 100 tons per year [3, 4].

In order to avoid the indium scarcity, it is possible to obtain this metal from secondary sources. Liquid crystal displays (LCD) uses about 70% of the indium produced worldwide, in the of form indium tin oxide (ITO, In_2O_3) [5]. The ITO films can be separated manually, and indium can be recycled. For this purpose, hydrometallurgical and pyrometallurgical routes can be used. The hydrometallurgical processes include acid leaching, cementation and solvent extraction [6]. It was reported that the quantities of indium vary according to the original source (televisions, cell phones, and computers), from 102 to 613 mg kg^{-1} [7]. However, after the acid leaching process, the high concentrations of indium presented on the ITO films become low on the liquid phase, and thus a precipitation process is required, leading to another environmental problem [8, 9]. These aspects can be mitigated by applying the adsorption, which is known as a low–cost and easy unit operation [10]. Applying adsorption, indium becomes concentrated in the solid surface, while the leached liquor is purified [11, 12].

Concerning the liquid phase adsorption, around 85% of the studies are focused on the removal of a target molecule or ion from a single synthetic solution. The data are normally evaluated in terms of isotherms, kinetics, and thermodynamics [13–16]. Lee and Lee [9] studied In(III) adsorption using a commercial resin. They used a synthetic solution prepared by dissolving $InCl_34H_2O$ in water, and found adsorption capacity of 55 mg g^{-1}. Calagui et al. [17] studied the In(III) adsorption using chitosan–coated bentonite. An indium standard solution ($In(NO_3)_3$ in HNO_3) with purity of at least 99% and deionized water was used for the tests. Isotherms, kinetics and thermodynamics were analyzed, being obtained adsorption capacity of 17.89 mg g^{-1}. Others studies evaluated the In(III) adsorption employing different adsorbents [18–20] and also used synthetic solutions. The above studies used synthetic solutions, and aimed the In(III) removal from aqueous solutions, to avoid environmental impacts caused by

this metal. In opposite, this work evaluated adsorption as a unit operation to concentrate indium (III) from real leachate found in the LCD recycling process. Furthermore, differently of the conventional literature, the data were evaluated using artificial neural networks (ANN) and adaptive neuro–fuzzy interference systems (ANFIS). ANN and ANFIS are two types of neural network models. ANN can learn from experimental data to solve the complex non–linear, multi–dimensional functional relationship without prioritization, while ANFIS can mix the learning effect of the ANN and the reasoning effect, thus leading to a more realistic result [21]. ANN and ANFIS were already applied for some adsorption systems [22–25]. However, in the great majority of the works, the input variables were not related to the adsorbent characteristics. In this work, surface area and point of zero charge were considered as input variables, which is another innovative point.

This work aimed the construction of ANN and ANFIS models as tools to predict the indium(III) adsorption capacity (q) in a real leachate found in the LCD recycling process, using ten different adsorbents. Activated carbon (AC), multi–walled carbon nanotubes functionalized with OH (M–OH), multi–walled carbon nanotubes functionalized with COOH (M–COOH), chitin (CIN), chitosan(CAN), corn straw (CS), grape seeds (GS), sugarcane bagasse (SB), orange peel (OP) and rice husk (RH) were tested as adsorbents. The input variables for the network models were composed of adsorbent characteristics (specific surface area and point of zero charge) and process conditions (adsorbent dosage and contact time).

4.2.3 Experimental

4.2.3.1 Obtainment and characterization of the adsorbents

Ten materials of different origins were tested to concentrate indium(III) from LCD leachates by adsorption, as follows: activated carbon made from coconut shells (AC) was purchased from Peixe Bello Company (Brazil); multi–walled carbon nanotubes functionalized with OH (M–OH) and multi–walled carbon nanotubes functionalized with COOH (M–COOH) were purchased from Nanostructure & Amorphous Materials (USA); chitin (CIN) and chitosan (CAN) were prepared from shrimp wastes according to the literature [26]; corn straw (CS) was obtained from a local farm (Santa Maria, RS, Brazil) and processed according to a previous work [27]; grape seeds (GS) were donated from a wine industry (Mendoza, Argentina) [28]; sugarcane bagasse (SB) and orange peel (OP) were obtained from local food industries [29]; rice husk (RH) was obtained from a local processing industry [30]. Activated carbon was used because is the most common commercial used adsorbent; multi–walled carbon nanotubes were tested as advanced adsorbents due its interesting textural (surface area, pore volume and particle size) and chemical characteristics (functional groups); chitin and chitosan were employed due its cost benefit, availability and reactive functional groups in the surface like acetamide, hydroxyl and mainly amine; corn straw, grape seeds, sugarcane bagasse, orange peel and rice husk were tested since are agro industrial wastes generated in large quantities.

The specific surface area (A_s) and point of zero charge (pH_{pzc}) were estimated for each adsorbent studied. N_2 adsorption/desorption isotherms (Micrometrics, ASAP 2020, USA) were used to obtain the specific surface area of the adsorbents, by application of the Brunauer, Emmett and Teller (BET) method [31]. The point of zero charge was found by the 11 points experiment [32]. These results are presented in Table 1. In addition, the adsorbents were characterized by Fourier transform infrared spectroscopy (FT–IR) (Shimadzu, Prestige

21210045, Japan) using KBr pellets, in the range of 4500 to 500 cm^{-1} [33]. Other characteristics of these adsorbents can be found in the literature [26–30].

Table 1: Specific surface area (As) and point of zero charge (pHpzc) of the adsorbents used to concentrate indium(III) from the LCD leachates.

Adsorbent	Abbreviation	A_s (m^2 g^{-1})*	pH_{pzc}*
Activated carbon	AC	65.20 ± 1.23	5.6 ± 0.2
Carbon nanotube functionalized with OH	M–OH	200.40 ± 2.49	7.0 ± 0.1
Carbon nanotube functionalized with COOH	M–COOH	200.40 ± 2.31	7.0 ± 0.1
Chitin	CIN	4.00 ± 0.12	5.4 ± 0.2
Chitosan	CAN	4.52 ± 0.15	6.3 ± 0.2
Corn straw	CS	0.85 ± 0.05	2.3 ± 0.1
Grape seeds	GS	1.35 ± 0.03	4.5 ± 0.1
Sugarcane bagasse	SB	1.85 ± 0.10	4.6 ± 0.1
Orange peel	OP	1.73 ± 0.15	4.9 ± 0.1
Rice husk	RH	3.21 ± 0.20	6.0 ± 0.1

4.2.3.2 Process for indium (III) leaching from LCD screens

Indium (III) was selectively extracted from LCD screens of discarded cell phones according to Silveira et al. [6]. In brief, the LCD screens were separated from the discarded cell phones, being the adhesives and polymers manually removed. The resulting material was ground. Leaching was then performed with 1.0 mol L^{-1} H_2SO_4 solution at 90 °C. The leachate solution containing around 600 mg L^{-1} of In(III) had the pH regulated to 2.5. It is important highlight that indium was selectively extracted using H_2SO_4. Consequently, the real leachate is a solution containing few co–existing substances (H+, OH^-, $SO4^{-2}$ and In, mainly in the form of In^{+3}).

4.2.3.3 Adsorption of Indium (III) from leachates

Ten adsorbents (AC, M–OH, M–COOH, CIN, CAN, CS, GS, SB, OP and RH) were tested to concentrate indium (III) from the real leachate of LCD screens. All the adsorption

experiments were carried out in a thermostated agitator (Solab, SL222, Brazil) at temperature of 298 K and stirring rate of 150 rpm. Different adsorbent dosages (0.05, 0.25, 0.5, 1.0, 1.5 and 2.0 g L^{-1}) were inserted in Erlenmeyer flasks containing the leachate (indium (III) concentration of 50 mg L^{-1}). The Erlenmeyer flasks were stirred and samples were collected at 5, 20, 60 and 120 min. All these experimental conditions were previously screened on the basis in preliminary experiments, real process conditions (section 2.2) and literature [9, 13–20]. The indium (III) concentration in the liquid phase was measured using inductively coupled plasma (ICP) analysis (Spectra Ciros CCD, spectra Analytical Instruments, Germany). Indium (III) adsorption capacity (q, mg g^{-1}) was determined by Eq. (1):

$$q = \frac{(C_0 - C_t)}{D_0} \tag{1}$$

where C_0 is the initial In(III) concentration in the liquid phase (mg L^{-1}), C_t is the In(III) concentration in a determined time in the liquid phase (mg L^{-1}) and D_0 is the adsorbent dosage (g L^{-1}).

4.2.3.4 Analysis by ANN and ANFIS

The ANN and ANFIS were developed taking into account specific surface area (A_S), point of zero charge (pH_{pzc}), adsorption time (t) and adsorbent dosage (D_0) as input variables. These input variables were selected because are related with the adsorbent characteristics (specific surface area and point of zero charge) and process conditions (adsorbent dosage and contact time). Regarding the output, adsorption capacity (q) was used because is the most common value estimated in the adsorption studies. The development and training of the networks were

performed in MatLab scripts using a total data of 1200 points. The values were normalized between 0.1 and 0.9, using Eq. (2):

$$Y_{nom} = \frac{Y - Y_{\min}}{Y_{\max} - Y_{\min}} \tag{2}$$

where Y_{nom} is the normalized value, Y is the vector of values, Y_{min} is the minimum value of the vector Y and Y_{max} is the maximum value for the vector Y.

For the ANN development, it was performed an architecture investigation to determinate the minimum number of neurons in relation to the minimum squared error (*MSE*) and the running time. The data in the ANN were randomly split into three groups, training (70%), checking (15%), and validation (15%). The separation was made by the "diverand" function. All the ANN developed in this work have used the Levenberg–Marquardt algorithm [21, 34].

The fuzzy interference system (FIS) applied to ANFIS was developed in MatLab built–in function *genfis1* using the Gaussian form (*gaussmf*, Eq. 3). The developed ANFIS was of Sugeno type, which is built in four hidden layers as follows: the fuzzification layer with two membership functions; the interference layer with weight rules; the de–fuzzification layer; and the output layer.

$$f(x;\sigma,c) = \exp\left(-\frac{(x-c)^2}{2\sigma^2}\right) \tag{3}$$

where x is the input value, c and σ are parameters of the function.

The ANFIS architecture was investigated do determinate de minimum number of membership functions in relation to *MSE* and running time. The data were randomly split into 2 sets, 70% for training and 30% for the check using the "randperm" function. The optimization

method used was the hybrid method (a combination of least–squares estimation and backpropagation)

The performances of ANN and ANFIS were evaluated by the coefficient of determination (R^2) Eq. (4), epochs (number of times presented in the training data), mean–squared error (*MSE*) (Eq. (5)), the sum of squared errors (*SSE*) (Eq. (6)) and average relative error (*ARE*) (Eq. (7)), as follows:

$$R^2 = 1 - \frac{\sum_{i=1}^{N} (y_{prd,i} - y_{\exp,i})^2}{\sum_{i=1}^{N} (y_{prd,i} - y_m)^2} \tag{4}$$

$$MSE = \frac{1}{N} \sum_{i=1}^{N} (y_{prd,i} - y_{\exp,i})^2 \tag{5}$$

$$SSE = \sqrt{\frac{\sum_{i=1}^{N} (y_{\exp,i} - y_{pred,i})^2}{N}} \tag{6}$$

$$ARE = \frac{100\%}{N} \sum_{i=1}^{N} \left| \frac{y_{prd,i} - y_{\exp,i}}{y_{\exp,i}} \right| \tag{7}$$

where, N is the number of experimental points, $y_{prd,I}$ is the predicted response, $y_{exp,I}$ is the experimental value and y_m is the mean value of the response. In addition, the behavior of *MSE* as a function of epochs was used for architecture selection and performance.

R^2 (Eq. (4)) is the conventional statistical metric to determine the proportion of variance between the experimental and model predictions. The value of R^2 is between 0 and 1. A value of R^2 near to 1 indicates that most of the variation between the experimental and model predictions is explained, whereas a value of R^2 near to 0 indicates that little of such variation is explained. *MSE* (Eq. (5)) is a widely used error function, which is employed as an objective

function in most of the optimization techniques. This function is also sometimes referred as the mean squared deviation (*MSD*), which aggregates the magnitudes of the errors and is a good measure of accuracy. *SSE* (Eq. (6)) is also a frequently used error function, and it increases as the deviation in error between the experimental and model predictions increases. If the error deviation is high, then the magnitude of *SSE* increases much fold which is the major drawback of this function. *ARE* (Eq. (7)) is a function which minimizes the fractional error distribution across the entire range [21, 34].

4.2.4 Results and Discussion

4.2.4.1 Adsorption interpretations and characterizations

The results of In(III) adsorption using all adsorbents in all experimental conditions are presented in Tables 1S to 10S (supplementary material). It was evident that the adsorption capacities were dependent of all experimental parameters. The values ranged from 8.203 to 1000 mg g^{-1}, depending of the adsorbent type, contact time and adsorbent dosage. The adsorption capacities found in this work were, in general, high when compared with the literature [17–20, 35, 36]. All adsorbents tend to surpass 60% of the maximum experimental adsorption capacity within 5 min of contact time. This indicates a fast covering of the adsorbent surface. This is interesting since In(III) can be fast concentrated in the solid matrix. Concerning the adsorbent dosage, this effect was inversely proportional with the adsorption capacity. This occurred because, at lower dosages, more adsorption sites are available to interact with In(III), while, at higher dosages, there are more sites, but, fewer sites are available due to the aggregation.

Analyzing Tables 1S to 10S it can be stated that CIN, CAN, M–OH, and M–COOH achieved higher adsorption capacities or faster adsorption rate when compared to the other

materials. Thus, these adsorbents were selected for FT–IR analysis, before and after the adsorption process. The FT–IR spectra of CIN, CAN, M–OH, and M–COOH before and after In(III) adsorption are presented, respectively, in Figures 1, 2, 3 and 4.

Figure 1: FT–IR vibrational spectra of chitin before and after In(III) adsorption.

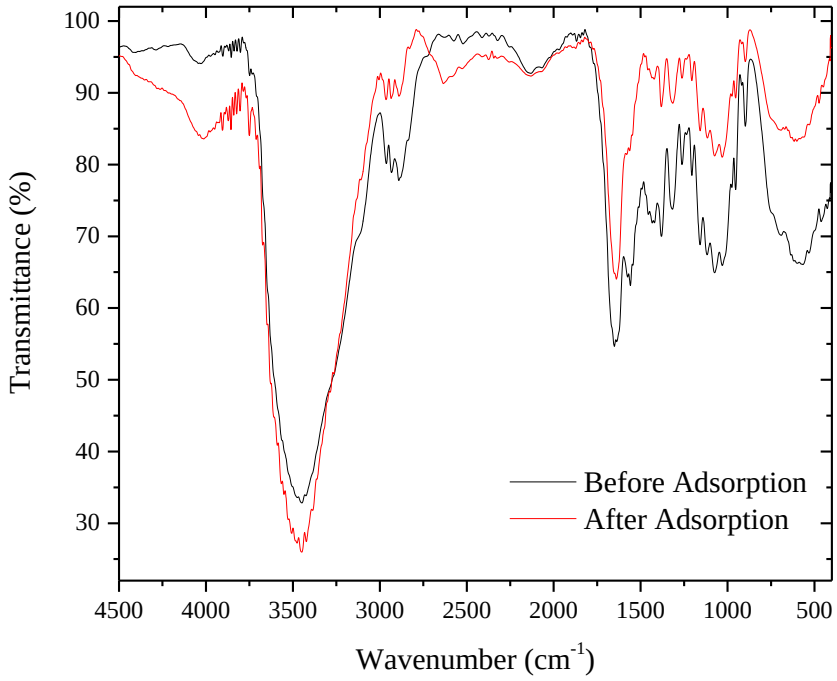

Figure 2: FT–IR vibrational spectra of chitosan before and after In(III) adsorption.

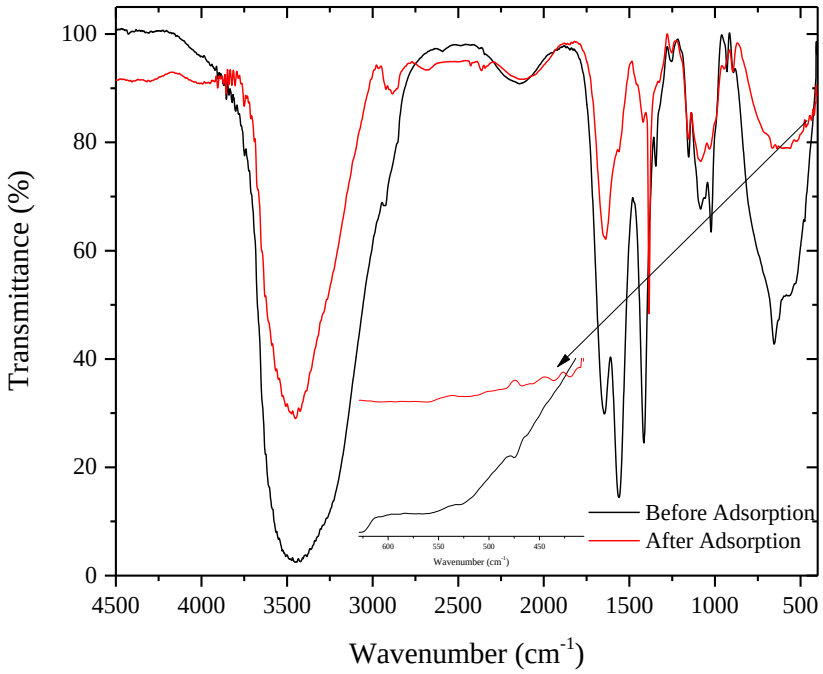

Figure 3: FT–IR vibrational spectra of multi–walled carbon nanotubes functionalized with OH before and after In(III) adsorption.

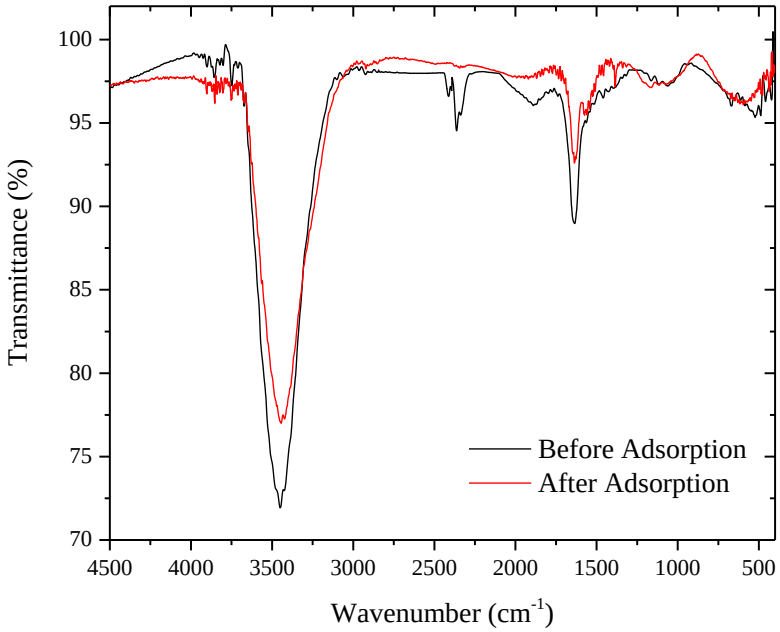

Figure 4: FT–IR vibrational spectra of multi–walled carbon nanotubes functionalized with COOH before and after In(III) adsorption

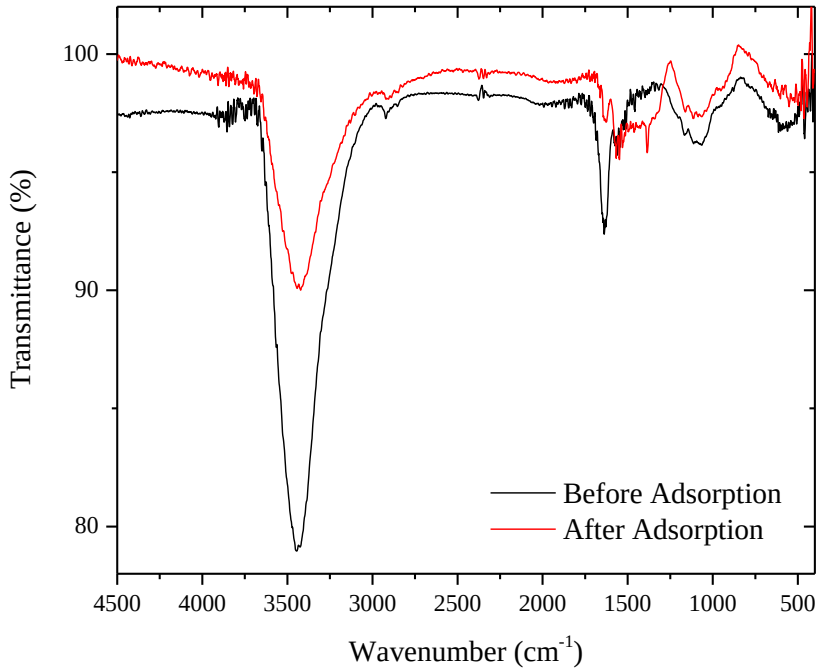

Typical bounds for chitin (CIN, Figure 1) were observed at 3330, 3000, 2800, 1650, 1550, 1450, 1020, 820 and 750 cm^{-1} [37]. The band at 3330 cm^{-1} is related to O–H and N–H stretches. The vibrations at 3000 and 2800 cm^{-1} can be attributed to CH_2 and CH_3 stretches [38, 39]. Secondary amide stretch can be observed at 1650 cm^{-1}. The N–H and C–N bonds for the amide II are presented at 1550 cm^{-1}. Asymmetric elongation for the C–O ring is found at 1020 cm^{-1}. Single bounds for C–O at 820 cm^{-1} and N–H at 750 cm^{-1} were observed [40]. The main shifts after In(III) adsorption (red spectrum in Figure 1) were in the bands 1550 cm^{-1} and 1650 cm^{-1}, which were coupled. This is an indicative that the amide II group was involved in the indium adsorption.

For chitosan (CAN, Figure 2), the following bands were encountered: 3400, 3000–2900, 1650, 1550, 1400 and 650 cm^{-1}. The band at 3400 cm^{-1} is correspondent to the O–H and N–H links. From 2900 to 3000 cm^{-1} it can be found a C–H asymmetric stretch. The bands at 1650,

1550, 1400 and 650 cm^{-1} are related to the secondary amide, C–N, C–H and N–H stretch, respectively [39, 40]. After adsorption (red spectrum in Figure 2), the bands at 1650, 1550 cm^{-1} were coupled and, the band at 650 cm^{-1} disappeared. This is a strong indicative that In(III) was anchored in the chitosan amino groups. Furthermore, the highlighted region (spectrum after adsorption) contains bands from 400 to 600 cm^{-1}. This indicates a possible In–O bond [41].

For M–OH, and M–COOH (Figures 3 and 4), typical bands of carbon nanotubes can be verified before adsorption. Around 3420 cm^{-1} O–H groups are observed. The band at 1550 cm^{-1} can be attributed to C=O or C=C. For both nanotubes after adsorption, a new band appeared around 1300 cm^{-1}. This signal can be attributed to In–O–H bond [42], confirming the interaction with the nanotubes.

From the FT–IR spectra of CIN, CAN, M–OH, and M–COOH before and after In(III) adsorption, it was possible to verify that In(III) was interacted with the functional groups of these adsorbents. These interactions were sufficient to attain high adsorption capacities.

4.2. ANN and ANFIS results

The ANN architecture was selected on the basis of the minimum *MSE* and run time (see Figure 1S). The structure is presented in Figure 5. It contains 4 hidden neurons. The ANN achieved 0.9913 for R^2, 0.0010 for *MSE*, 0.1721 for *SSE*, 5.451 % for *ARE* and number of epochs of 27. It was obtained weights for the neurons of 4.2135, –0.9732, –7.5992 and 7.6718 with neuron bias of –0.5022.

Figure 5: Artificial neural network architecture.

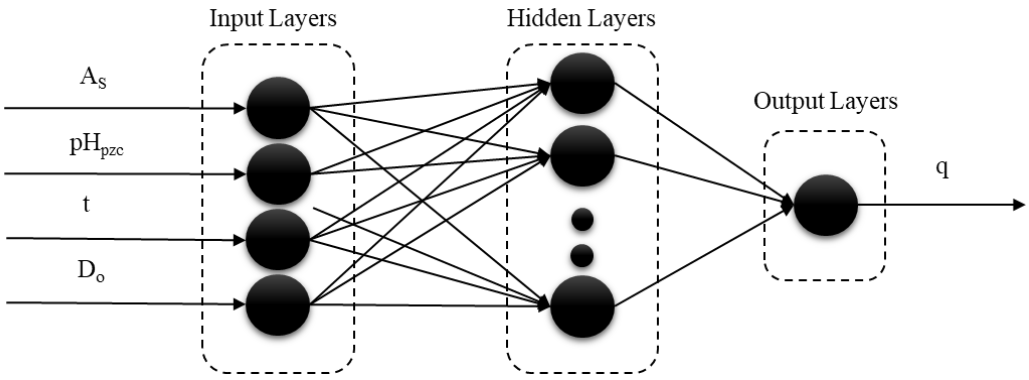

It was verified that the *MSE* values were minimized with 21 epochs for the validation data (Figure 2S). Figure 6 represents the comparison between the experimental and predicted (ANN) data for In(III) adsorption. The data predicted by ANN were in good concordance with the experimental values (see experimental data and ANN predicted values in Tables 1S–10S), indicating that ANN can be used to predict the In(III) adsorption capacity as a function of the specific surface area, point of zero charge, adsorbent dosage and contact time.

Figure 6: Difference between the experimental data with the predicted by the ANN.

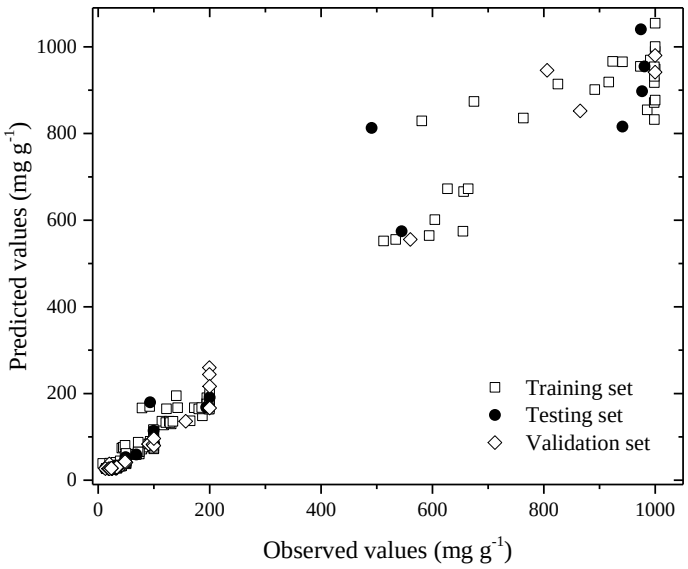

The ANFIS architecture was selected by evaluating the minimum *MSE* for validation and run time (see Figure 3S). The structure is presented in Figure 7, and it contains 3 membership functions for A_S, 2 for pH_{pzc}, 2 for t and 3 for D_0, generating a number of rules 36.

Figure 7: Simplified version of the ANFIS architecture.

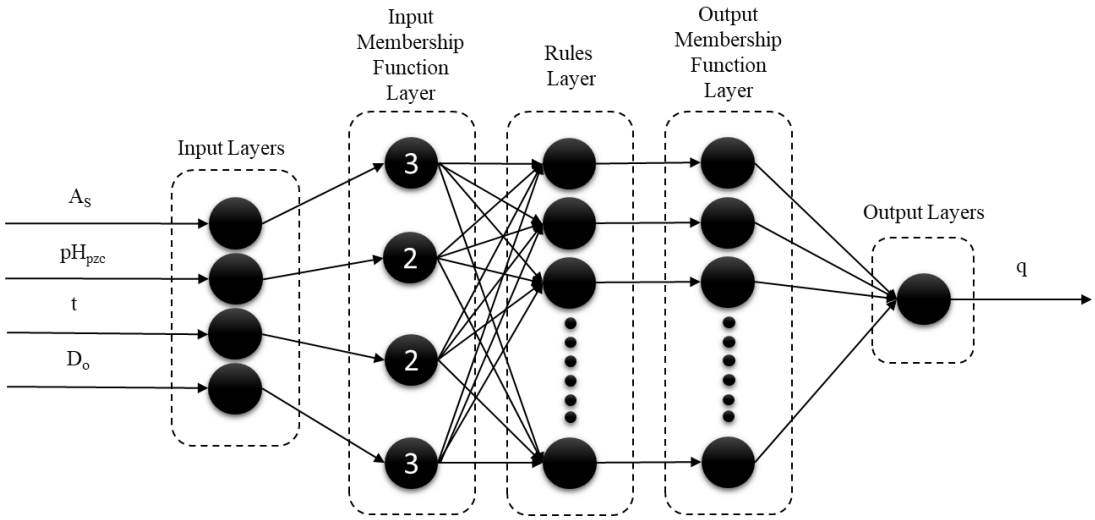

The statistical values for this architecture were: 0.9998 for R^2, 8.4239×10^{-5} for *MSE* (trained data), 9.34×10^{-3} for *MSE* (checked data), 1.86% for *ARE* (trained), and 10.1% for *ARE* (checked data) for 300 epochs. Figure 4S presents the ANFIS performance. Take into account the statistical values and Figure 4S, it can be stated that the ANFIS achieved good performance and is capable of forecasting the indium(III) adsorption.

Figure 8 shows the trained and checked data of In(III) adsorption capacity as a function of the specific surface area (A_S), point of zero charge (pH_{pzc}), adsorption time (t) and adsorbent dosage (D_0). Analyzing Figure 8 it possible to conclude that the ANFIS was successfully trained and can be used for forecasting the In(III) adsorption capacity as a function of the desired inputs. Furthermore, the ANFIS can be used for describing the adsorption of indium (III) onto various materials.

Figure 8: Trained and checked data of In(III) adsorption capacity as a function of the specific surface area (A_S), point of zero charge (pH_{pzc}), adsorption time (t) and adsorbent dosage (D_0).

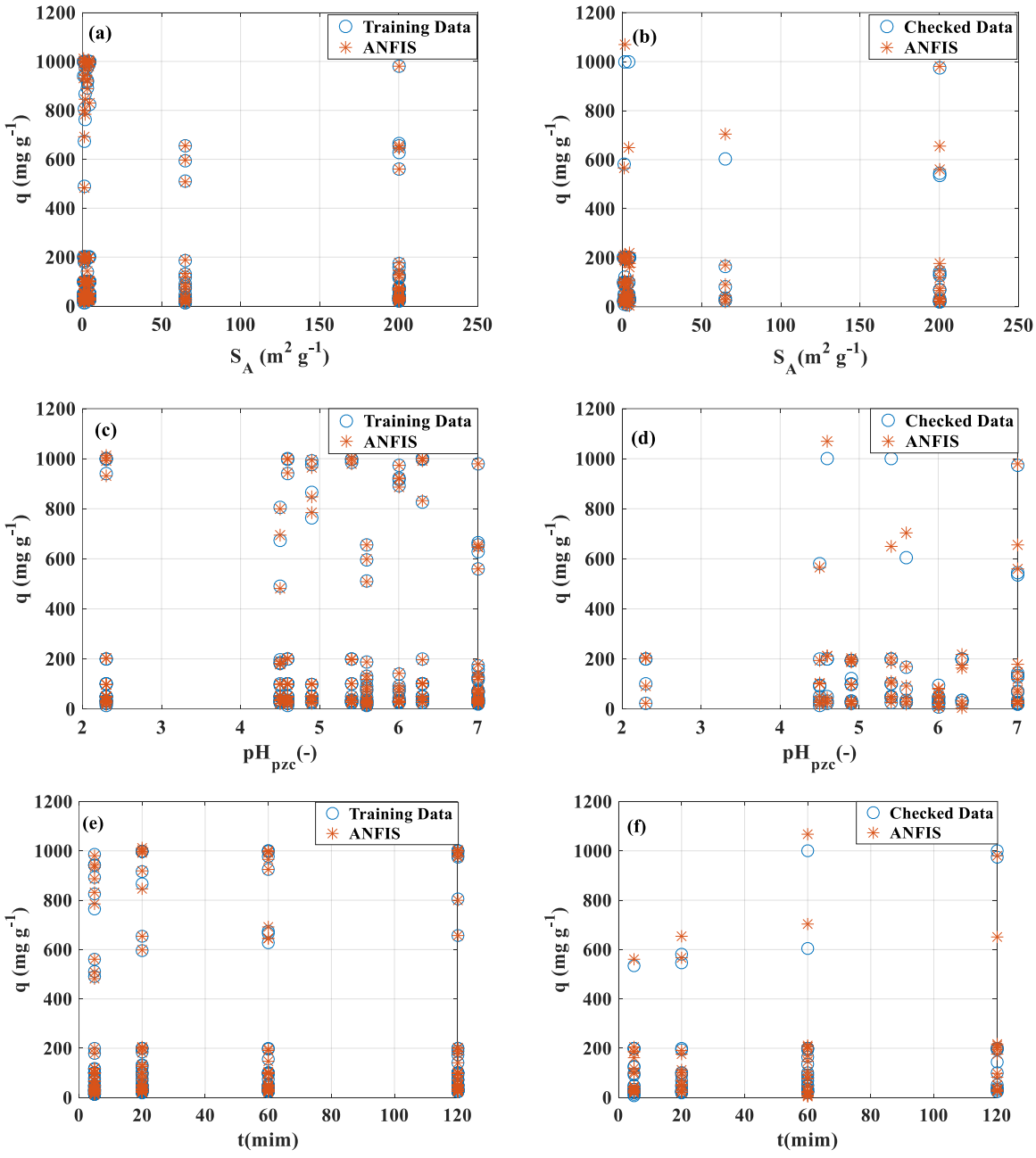

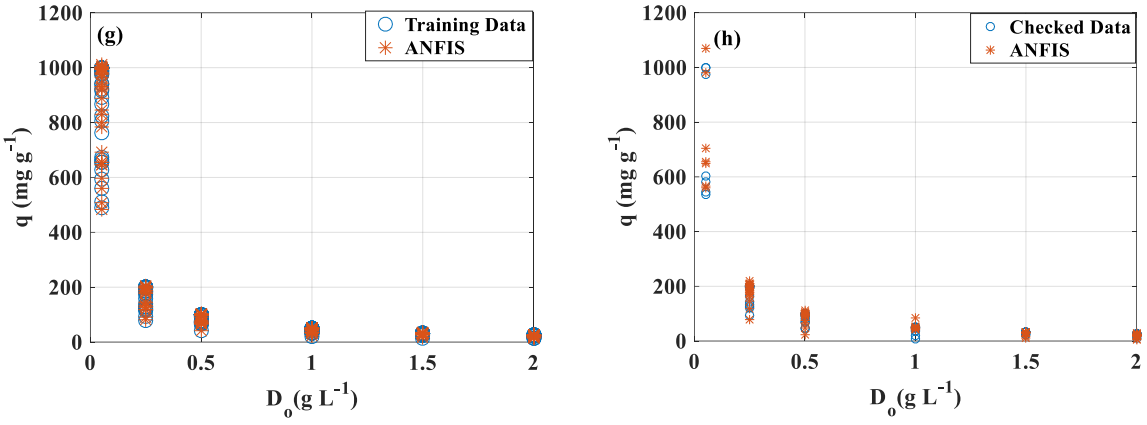

ANN and ANFIS were able to predict the In(III) adsorption capacity from the LCD leachates, as a function of the specific surface area (A_S), point of zero charge (pH_{pzc}), adsorption time (t) and adsorbent dosage (D_0). Concerning the specific surface area (A_S), ANN and ANFIS revealed that high values of adsorption capacity were found for materials with high and low A_S (Figures 8 (a) and (b)). This is in accordance with the experimental observations, where CAN, CIN (low surface area) M–OH and M–COOH (high surface area) were the best adsorbents. In relation to the point of zero charge (Figures 8 (c) and (d)), it was verified that the materials with pH_{pzc}>5 presented the higher adsorption capacities. This trend is also in agreement with the experimental observations since CAN, CIN, M–OH, and M–COOH has pH_{pzc}>5. Figures 8 (e) and (f) show that higher values of In(III) adsorption capacities were found in short time intervals. This is relevant for the In(III) concentration in the solid matrix since a fast process can be designed. Finally, higher adsorption capacities were encountered at lower values of adsorbent dosage (Figures 8 (g) and (h)). This occurred because, at lower dosages, more adsorption sites are available, while, at higher dosages, there are more sites, but, fewer sites are available due to the aggregation.

4.2.4.2 In(III) adsorption onto chitosan

The experimental evidence coupled with the ANN and ANFIS results revealed that chitosan (CAN) was the material that presented the best performance to uptake In(III) from the LCD leachate. So, a more detailed analysis was carried out for this system. Figure 9 shows the kinetic profile of In(III) adsorption onto chitosan (CAN) for all the dosages utilized. It was possible to verify that the In(III) adsorption capacity attained 1000 mg g^{-1} within only 20 min of operation. This shows that chitosan has a high affinity for In(III), confirming the FT–IR, ANN and ANFIS evaluations. This is an excellent result from the technological viewpoint. Primary sources of indium contain around 20 mg kg^{-1} [2]. Secondary sources like televisions, cell phones, and computers contain from 102 to 613 mg kg^{-1} [7]. The LCD screens used in this work contain around 600 mg kg^{-1}. The adsorption onto chitosan proposed in this work was able to generate a solid matrix with 1000 mg of In per gram of material. This represents a concentration of more than 1500 times in relation to the original LCD.

Figure 9: Kinetic profile of In(III) adsorption onto chitosan.

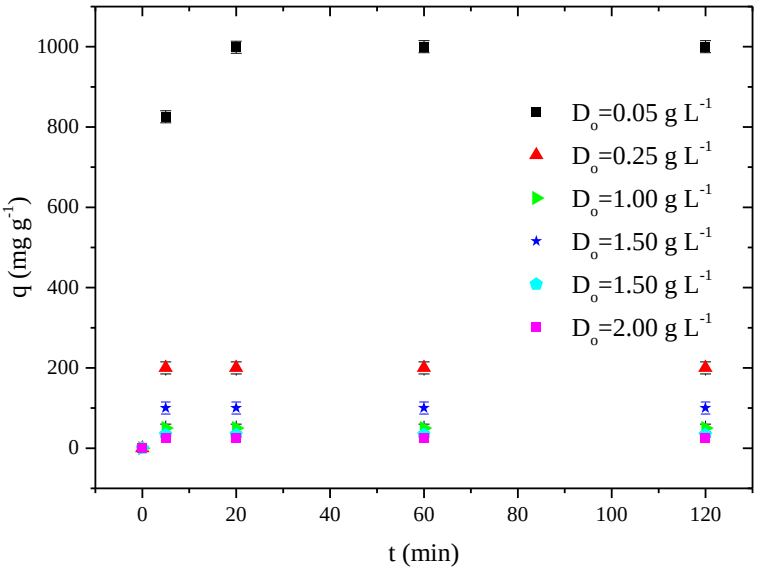

A possible interaction mechanism between In and chitosan was proposed on the basis in the experimental results, speciation diagram of the leachate, FT–IR, and literature [43, 44]. The leachate has a pH of 2.5. In this condition, indium is the form of In^{3+}. Also, SO_4^{2-} anions are present in the solution. In parallel, chitosan, a polycationic biopolymer, is positively charged due its NH_2 groups. FT–IR revealed that chitosan amino groups participate in the interaction and also In–O links were formed. So, a coordination ligation between In(III) and chitosan was proposed according to Figure 10. According to this mechanism, each chitosan glucosamine unit can adsorb one In^{3+} with help of SO_4^{2-} to form the coordination complex. This suggestion could explain the reason why chitosan have high affinity with In(III) ions, presenting high adsorption capacity in short times.

Figure 10: Proposed interaction mechanism between In(III) and chitosan.

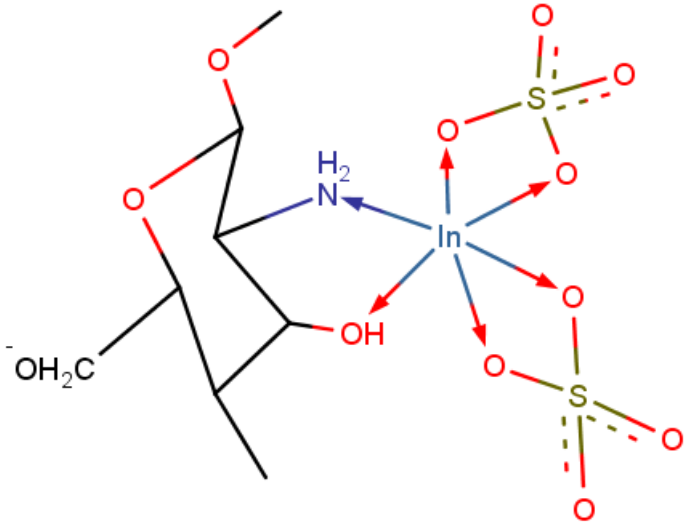

4.2.4.3 Thermodynamic approach of In(III) adsorption onto chitosan

In(III) adsorption onto chitosan was studied from the thermodynamic viewpoint in order to support the interaction mechanism proposed in the section 4.3. At first, isotherm curves were

experimentally constructed at 298, 308, 318 and 3298 K, using 1.0 g L of chitosan, which was put in contact with LCD leached solutions of different In(III) initial concentrations. The isotherms were extremely favorable and classified as type L [45]. Then, the Langmuir model was fitted in the isotherms [46, 47]. All isotherms were successfully represented by the Langmuir model, with R^2 values higher than 0.96 and *ARE* values lower than 10%. The Langmuir constant (k_L) ranged from 0.237 to 1.706 L mg^{-1}. The thermodynamic equilibrium constant (k_e, dimensionless) was then calculated from k_L using Eq. (8) and finally, the values of standard Gibbs free energy change (ΔG^0, kJ mol^{-1}), enthalpy change (ΔH^0, kJ mol^{-1}) and entropy change (ΔS^0, kJ mol^{-1} K^{-1}) were computed according to the Eqs. (9–11) [48, 49].

$$k_e = \frac{k_L M_W \gamma^{In(III)}}{\gamma} \quad (8)$$

$$\Delta G^0 = -RT\ln(k_e) \quad (9)$$

$$\Delta G^0 = \Delta H^0 - T\Delta S^0 \quad (10)$$

$$\ln(k_e) = \frac{\Delta S^0}{R} - \frac{\Delta H^0}{RT} \quad (11)$$

where M_W is the molecular mass of the In(III) (g mol^{-1}), $\gamma^{In(III)}$ is the activity coefficient of In(III) in solution (dimensionless, assuming $\gamma^{In(III)}$=1), γ is the unitary activity coefficient (1 mol L^{-1}), T is the temperature (K) and R is the universal gas constant (8.31 × 10^{-3} kJ mol^{-1} K^{-1}).

The thermodynamic parameters of In(III) adsorption onto chitosan are depicted in Table 2. The k_e values presented an inversely proportional trend in relation to the temperature. This shows that under ambient conditions (298 K), the formation of the complex In(III)–chitosan is favored. The values of ΔG^0 were negative, confirming the spontaneity and favorability of the In(III) adsorption onto chitosan. The negative value of ΔS^0 revealed that, after the In(III) adsorption, the chitosan surface becomes more ordered. The negative ΔH^0 indicates an

exothermic nature of this adsorption process. The magnitude of ΔH^0 (49.9 kJ mol^{-1}) is in agreement with coordination ligations between metals and adsorbents to form coordination complexes in the surface [50]. This is other indicative that reinforce the adsorption mechanism presented in Figure 10.

Table 2: Thermodynamic parameters of In(III) adsorption onto chitosan.

T(K)	k_e (-)	ΔG^0 (kJ mol^{-1})	ΔH^0 (kJ mol^{-1})	ΔS^0 (kJ mol^{-1} K^{-1})
298.15	195.8761	-13.0819	-49.991	-0.1229
308.15	113.1853	-12.1156		
318.15	86.8274	-11.8075		
328.15	51.803	-9.0120		

4.2.5 Conclusion

Ten adsorbents of different origins were applied to uptake In(III) from a leachate solution of LCD screens, in order to find a solid matrix with high indium concentration. Artificial neural network (ANN) and adaptive neuro–fuzzy interference system (ANIFS) were constructed in order to predict the In(III) adsorption on these different adsorbents, as a function of its characteristics (specific surface area and point of zero charge) and process conditions (time and adsorbent dosage).

The statistical indicators (R^2, *MSE*, *SSE* and *ARE*) and the epochs revealed that the ANN model applied with the Levenberg–Marquardt feed–backward propagation function and the ANFIS model developed using the Hybrid method were able to predict the In(III) adsorption capacity as a function of specific surface area, point of zero charge, time and adsorbent dosage. Low dosages of chitosan and short times were required to maximize the In(III) adsorption capacity. Chitosan was an excellent adsorbent to concentrate indium from the LCD leachates,

attaining adsorption capacity of 1000 mg g^{-1} within only 20 min of operation. Then, adsorption using chitosan was able to concentrate indium from 0.6 mg g^{-1} (original LCD screens) to 1000 mg g^{-1}. The good performance of this material was attributed to a coordination ligation between In(III) and chitosan. Considering the availability and cost benefit of chitosan, and also its high values of adsorption capacity and short times of operation, this biopolymer is promising for different purposes that involves the In(III) removal/recovery from aqueous media, including industrial and environmental applications.

4.2.6 References

[1] F.J. Alguacil, F.A. Lopez, O. Rodriguez, S. Martinez–Ramirez, I. Garcia–Diaz, Ecotoxicology and Environmental Safety Sorption of indium (III) onto carbon nanotubes, Ecotoxicol. Environ. Saf. 130 (2016) 81–86.

[2] A.B. Argenta, C.M. Reis, G.P. Mello, G.L. Dotto, E.H. Tanabe, D.A. Bertuol, Supercritical CO_2 extraction of indium present in liquid crystal displays from discarded cell phones using organic acids, J. Supercritical Fluids 120 (2017) 95–101.

[3] European Commission (2017), Study on the review of the list of Critical Raw Materials. https://doi.org/10.2873/49178.

[4] U.S. Geological Survey (2017), Mineral Commodity Summaries. U.S. Geological Survey (Vol. 1), https://doi.org/http://dx.doi.org/10.3133/70140094.

[5] K. Zhang, Y. Wu, W. Wang, B. Li, Y. Zhang, T. Zuo, Resources, Conservation and Recycling Recycling indium from waste LCDs : A review, Res. Cons. Recycling 104 (2015) 276–290.

[6] A.V.M. Silveira, M.S. Fuchs, D.K. Pinheiro, E.H. Tanabe, D.A. Bertuol, Recovery of indium from LCD screens of discarded cell phones, Waste Manage. 45 (2015) 334–342.

[7] C.H. Lee, M.K. Jeong, M. Fatih Kilicaslan, J.H. Lee, H.S. Hong, S.J. Hong, Recovery of indium from used LCD panel by a time efficient and environmentally sound method assisted HEBM, Waste Manage. 33 (2013) 730–734.

[8] S.M. Grimes, N.G. Yasri, A.J. Chaudhary, Recovery of critical metals from dilute leach solutions – Separation of indium from tin and lead, Inorganic Chim. Acta 461 (2017) 161–166.

[9] S. Lee, U. Lee, Adsorption and desorption property of iminodiacetate resin (Lewatit 1 TP207) for indium recovery, J. Ind. Eng. Chem. 40 (2016) 23–25.

[10] D.S.P. Franco, E.H. Tanabe, D.A. Bertuol, G.S. dos Reis, E.C. Lima, G.L. Dotto, Alternative treatments to improve the potential of rice husk as adsorbent for methylene blue, Water Sci. Technol. 75 (2017) 296–305.

[11] M.A. Zazycki, E.H. Tanabe, D.A. Bertuol, G.L. Dotto, Adsorption of valuable metals from leachates of mobile phone wastes using biopolymers and activated carbon, J. Environ. Manage. 188 (2017) 18–25.

[12] L.N. Côrtes, E.H. Tanabe, D.A. Bertuol, G.L. Dotto, Biosorption of gold from computer microprocessor leachate solutions using chitin, Waste Manage. 45 (2015) 272–279.

[13] A. Bonilla–Petriciolet, D.I. Mendoza–Castillo, G.L. Dotto, C.J. Duran–Valle, Adsorption in Water Treatment, Reference Module in Chemistry, Molecular Sciences and Chemical Engineering, 2019 https://doi.org/10.1016/B978–0–12–409547–2.14390–2

[14] A. Bonilla–Petriciolet, D.I. Mendoza–Castillo, E. Reynel–Avila, Adsorption Processes for Water treatment and Purification, Springer, Basel, 2017.

[15] I. Anastopoulos, A. Robalds, H.N. Tran, D. Mitrogiannis, D.A. Giannakoudakis, A. Hosseini–Bandegharaei, G.L. Dotto, Removal of heavy metals by leaves–derived biosorbents, Environ. Chem. Let. *In press* (2019) 1–12. https://doi.org/10.1007/s10311–018–00829–x

[16] L.B. Escudero, P.Y. Quintas, R.G. Wuilloud, G.L. Dotto, Recent advances on elemental biosorption, Environ. Chem. Let. *In press* (2019) 1–19. https://doi.org/10.1007/s10311–018–0816–6

[17] M.J.C. Calagui, D.B. Senoro, C.C. Kan, J.W.L. Salvacion, C.M. Futalan, M.W. Wan, Adsorption of indium(III) ions from aqueous solution using chitosan–coated bentonite beads, J. Hazard. Mater. 277 (2014) 120–126.

[18] C. Jeon, J.H. Cha, J.Y. Choi, Adsorption and recovery characteristics of phosphorylated sawdust bead for indium(III) in industrial wastewater, J. Ind. Eng. Chem. 27 (2015) 201–206.

[19] N.S. Kwak, Y. Baek, T.S. Hwang, The synthesis of poly(vinylphosphonic acid–co–methacrylic acid) microbeads by suspension polymerization and the characterization of their indium adsorption properties, J. Hazard. Mater. 203–204 (2012) 213–220.

[20] Z. Li, G.L. Dotto, A. Bajahzar, L. Sellaoui, H. Belmabrouk, A. Ben Lamine, A. Bonilla–Petriciolet, Adsorption of indium (III) from aqueous solution on raw, ultrasound and supercritical–modified chitin: Experimental and theoretical analysis, Chem. Eng. J. 373 (2019) 1247–1253.

[21] A.M. Ghaedi, A. Vafaei, Applications of artificial neural networks for adsorption removal of dyes from aqueous solution: A review, Adv. Colloid Interface Sci. 245 (2017) 20–39.

[22] M. Ghaedi, A.M. Ghaedi, F. Abdi, M. Roosta, A. Vafaei, A. Asghari, Principal component analysis–adaptive neuro–fuzzy inference system modeling and genetic algorithm optimization of adsorption of methylene blue by activated carbon derived from *Pistacia khinjuk*, Ecotoxicol. Environ. Saf. 96 (2013) 110–117.

[23] M. Ghaedi, R. Hosaininia, A.M. Ghaedi, A. Vafaei, F. Taghizadeh, Adaptive neuro–fuzzy inference system model for adsorption of 1,3,4–thiadiazole–2,5–dithiol onto gold nanoparticles–activated carbon, Spectrochim. Acta A: Mol. Biomol. Spectroscopy 131 (2014) 606–614.

[24] M. Dolatabadi, M. Mehrabpour, M. Esfandyari, H. Alidadi, M. Davoudi, Modeling of simultaneous adsorption of dye and metal ion by sawdust from aqueous solution using of ANN and ANFIS, Chem. Intelligent Lab. Syst. 181 (2018) 72–78.

[25] P.R. Souza, G.L. Dotto, N.P.G. Salau, Artificial neural network (ANN) and adaptive neuro–fuzzy interference system (ANFIS) modelling for nickel adsorption onto agro–wastes and commercial activated carbon, J. Environ. Chem. Eng. 6 (2018) 7152–7160.

[26] G.L. Dotto, L.A.A. Pinto, Adsorption of Food Dyes onto Chitosan: Optimization Process and Kinetic, Carbohydr. Polym. 84 (2011) 231–238.

[27] D.R. Lima, L. Klein, G.L. Dotto, Application of ultrasound modified corn straw as adsorbent for malachite green removal from synthetic and real effluents, Environ. Sci. Pollut. Res. 24 (2017) 21484–21495.

[28] L.B. Escudero, G. Vanni, F.A. Duarte, T. Segger, G.L. Dotto, Biosorption of silver from aqueous solutions using wine industry wastes, Chem. Eng. Comm. 205 (2018) 325–337.

[29] G.L. Dotto, L. Meili, A.K. de Souza Abud, E.H. Tanabe, D.A. Bertuol, E.L. Foletto, Comparison between Brazilian agro–wastes and activated carbon as adsorbents to remove Ni(II) from aqueous solutions, Water Sci. Technol. 73 (2016) 2713–2721.

[30] D.S.P. Franco, E.H. Tanabe, G.L. Dotto, Continuous Adsorption of a Cationic Dye on Surface Modified Rice Husk: Statistical Optimization and Dynamic Models, Chem. Eng. Comm. 204 (2017) 625–634.

[31] M. Thommes, K. Kaneko, A.V. Neimark, J.P. Olivier, F. Rodriguez–Reinoso, J. Rouquerol, Physisorption of gases, with special reference to the evaluation of surface area and pore size distribution (IUPAC Technical Report), Pure Appl. Chem. 87 (2015) 1051–1069.

[32] M.K. Miyittah, F.W. Tsyawo, K.K. Kumah, C.D. Stanley, J.E. Rechcigl, Suitability of Two Methods for Determination of Point of Zero Charge (PZC) of Adsorbents in Soils, Comm. Soil Sci. Plant Anal. 47 (2016) 101–111.

[33] R.M. Silverstein, F.X. Webster, D.J. Kiemle, Spectrometric identification of organic compounds, Wiley, New York, 2007.

[34] D.S.P. Franco, F.A. Duarte, N.P.G. Salau, G.L. Dotto, Adaptive neuro–fuzzy inference system (ANIFS) and artificial neural network (ANN) applied for indium (III) adsorption on carbonaceous materials, Chem. Eng. Comm. *In press* (2019) 1–12. https://doi.org/10.1080/00986445.2019.1566129

[35] Y. Akama, S. Suzuki, Y. Monobe, Study on the Adsorption and Selective Separation of Indium from Zing with Chelating Cellulose, Cellulose Chem. Technol. 50 (2016) 147–152.

[36] H. Li, J. Liu, X. Gao, C. Liu, L. Guo, S. Zhang, C. Liu, Adsorption behavior of indium(III) on modified solvent impregnated resins (MSIRs) containing sec–octylphenoxy acetic acid, Hydrometallurgy 121–124 (2012) 60–67.

[37] G.L. Dotto, M.L.G. Vieira, L.A.A. Pinto, Kinetics and mechanism of tartrazine adsorption onto chitin and chitosan, Ind. Eng. Chem. Res. 51 (2012) 6862–6868.

[38] M. Rinaudo, Chitin and chitosan: Properties and applications, Prog. Polym. Sci. 31 (2006) 603–632.

[39] Y.M. Fan, T. Saito, A. Isogai, Chitin nanocrystals prepared by TEMPO–mediated oxidation of α–Chitin, Biomacromolecules 9 (2008) 192–198.

[40] F.A. Al–Sagheer, M.A. Al–Sughayer, S. Muslim, M.Z. Elsabee, Extraction and characterization of chitin and chitosan from marine sources in Arabian Gulf, Carbohydr. Polym. 77 (2009) 410–419.

[41] J.F.Q. Rey, T.S. Plivelic, R.A. Rocha, S.K. Tadokoro, I. Torriani, E.N.S. Muccillo, Synthesis of In_2O_3 nanoparticles by Thermal Decomposition of a Citrate Gel Precursor, J. Nanoparticle Res. 7 (2005) 203–208.

[42] A. Yahia, A. Attaf, H. Saidi, M. Dahnoun, C. Khelifi, A. Bouhdjer, A. Saadi, H. Ezzaoui, Structural, optical, morphological and electrical properties of indium oxide thin films prepared by sol gel spin coating process, Surf. Interfaces 14 (2019) 158–165.

[43] R.B. Hernández, A.P. Franco, O.R. Yola, A. López–Delgado, J. Felcman, M.A.L. Recio, A.L.R. Mercê, Coordination study of chitosan and Fe^{3+}, J. Mol. Structure 877 (2008) 89–99.

[44] G.A. Lawrance, Introduction to Coordination Chemistry, Wiley, 2009.

[45] C. H. Giles, D. A. Smith, General Treatment and Classification of the Solute Adsorption Isotherm Part I. Theoretical, J. Colloid Interface Sci. 47 (1974) 755–765.

[46] I. Langmuir, The Adsorption of Gases on Plane Surfaces of Glass, Mica and Platinum, J. Am. Chem. Soc. 40 (1918) 1361–1403.

[47] Y. Peng, Y. Sun, R. Sun, Y. Zhou, D.C.W. Tsang, Q. Chen, Optimizing the synthesis of Fe/Al (Hydr)oxides-Biochars to maximize phosphate removal via response surface model, J. Clean. Prod. 237 (2019) 117770.

[48] E. C. Lima, A. H. Bandegharaei, J. C. Moreno–Piraján, I. Anastopoulos, A critical review of the estimation of the thermodynamic parameters on adsorption equilibria. Wrong use of equilibrium constant in the Van't Hoof equation for calculation of thermodynamic parameters of adsorption, J. Mol. Liq. 273 (2019) 425–434.

[49] I. Ali, O.M.L. Alharbi, Z. Alothman, A.Y. Badjah, A. Alwarthan, A.A. Basheer, Artificial neural network modelling of amido black dye sorption on ironcomposite nano material: Kinetics and thermodynamics studies, J. Mol. Liq. 250 (2018) 1–8.

[50] N.F. Cardoso, E.C. Lima, B. Royer, M.V. Bach, G.L. Dotto, L.A.A. Pinto, T. Calvete, Comparison of *Spirulina platensis* microalgae and commercial activated carbon as adsorbents for the removal of Reactive Red 120 dye from aqueous effluents, J. Hazard. Mater. 241–242 (2012) 146–153.

4.3 ARTIGO III: Interpretations on the mechanism of In(III) adsorption onto chitosan and chitin: a mass transfer model approach

Dison S. P. Franco[1]; Julien Vieillard[2], Nina Paula G. Salau[1] Guilherme Luiz Dotto[1*]

[1]Chemical Engineering Department, Federal University of Santa Maria, 97105–900, Santa Maria, Brazil.

[2]Normandie Université, INSA Rouen, UNIROUEN, CNRS, COBRA, 55 Rue Saint Germain, 27000, Evreux, France.

*Corresponding author: Guilherme L. Dotto, E–mail: guilherme_dotto@yahoo.com.br

List of symbols

ARE	Average relative error, %
B_i	Modified Biot number, dimensionless
$C_{Ax}\|_{x=L/2}$	In(III) concentration at the external surface of the particle, mg L^{-1}
C_0	Initial In(III) concentration in bulk solution, mg L^{-1}
C_A	In(III) concentration in bulk solution, mg L^{-1}
C_{Ax}	In(III) concentration within the adsorbent varying with x and t, mg L^{-1}
C_e	In(III) concentration in bulk solution at equilibrium, mg L^{-1}
C_{exp}	Experimental In(III) concentration in bulk solution at equilibrium, mg L^{-1}
C_{model}	Predicted In(III) concentration, mg L^{-1}
d_A	Average adsorbent diameter, cm
D_{AB}	Indium diffusion coefficient at infinite dilution, cm^2 s^{-1}
D_o	Mass of adsorbent per volume of solution, g L^{-1}
D_p	Effective pore volume diffusion coefficient, cm^2 s^{-1}
D_S	Surface diffusion coefficient, cm^2 s^{-1}
k_e	Equilibrium constant, dimensionless
k_L	External mass transfer coefficient, cm s^{-1}
K_F	Freundlich constant, (mg g^{-1})(mg L^{-1})$^{-1/n}$
K_L	Langmuir constant, L mg^{-1}
q_e	Mass of In(III) adsorbed per gram of adsorbent at equilibrium, mg g^{-1}
q_{exp}	Experimental q_e value, mg g^{-1}
q_{max}	Maximum adsorption capacity from Langmuir model, mg g^{-1}
q_{model}	Predicted q_e value, mg g^{-1}
q_t	Mass of In(III) adsorbed per gram of adsorbent at any t, mg g^{-1}
k	Constant parameter from the most suitable isotherm fit, L mg^{-1}
L	Adsorbent thickness, cm
m	Adsorbent mass, g
M_a	In(III) atomic mass, mg mol^{-1}
n	Number of experimental values, dimensionless
n^{-1}	Heterogeneity factor, dimensionless
P	Number of parameters of the model

par_1	model parameter one
par_2	model parameter two
R	Universal gas Constant, 8.31×10^{-3} kJ mol^{-1} K^{-1}
R^2	Coefficient of determination, dimensionless
S	External surface area per mass of adsorbent, cm^2 g^{-1}
SSE	Sum of squared errors
T	Temperature of the solution, K
V	Solution volume, L
V_p	Pore volume of adsorbent, cm^3 g^{-1}
X	Cartesian coordinate, cm
y_{exp}	Experimental data
y_{pred}	Predicted data

Greek Letters

$\gamma^{In(III)}$	Activity coefficient of In (III) in solution, 1 dimensionless
Γ	Unitary activity coefficient of In (III), 1 L mol^{-1}
ΔG^0	Standard Gibbs free energy, kJ mol^{-1}
ΔH^0	Standard enthalpy change, kJ mol^{-1}
ΔS^0	Standard entropy change, kJ mol^{-1} K^{-1}
ρ_p	Apparent density of the adsorbent, g L^{-1}
ρ_s	Bulk density of the adsorbent, g L^{-1}
ε_p	Void fraction, dimensionless

4.3.1 Abstract

The mass transport mechanism of the In(III) adsorption on chitin and chitosan was elucidated in this research. The chitosan and chitin presented specific surface area values of 3.60 and 4.30 $m^2\ g^{-1}$, with average pore radius of 14.30 and 33.10 Å, respectively. It was identified in chitosan and chitin, typical groups, such as N–H and C–O. It was found that both materials present a rigid surface without the presence of visible pores and cavities, with a geometry that resembles plates. Further analysis indicates the presence of the In(III) on the surface of both materials. The isotherm experiments indicated that the temperature caused an increase in the adsorption capacity for both materials. The Langmuir model was chosen for describing the equilibrium in both cases. The External Mass Transfer Model (EMTM) and Pore Volume and Surface Diffusion Model (PVSDM) were used for describing the indium concentration decay curves for the chitosan and chitin. Nevertheless, the modified Biot number (between 8.82×10^{-4} and 2.71) indicated that, in this case, the external mass transfer was the dominant mechanism. In addition, chitin and chitosan were efficient adsorbents for In(III), since that only 0.35 mg L^{-1} of In(III) remained in solution after adsorption. Chitosan provided faster adsorption kinetics, and this fact was attributed to its higher external surface area. The findings revealed that the overall mass transport mechanism is as follows: the indium species in the bulk solution are transferred to the adsorbent surface and then, adsorbed by surface precipitation and/or coordination bonds.

Keywords: External mass transfer; indium; mass transfer models; Modified Biot number; surface precipitation.

4.3.2 Introduction

The recovery of metals from alternative sources is an important subject in relation to environmental and economic viewpoints. One metal that fits this classification is indium, which in turn, when present on the environment, can further cause human health disorders [1,2]. In addition, the indium is classified as critical raw material indicating a shortfall in the next year [3,4]. One alternative way for indium recovery from secondary sources is liquid screen displays (LCD), which are mainly composed of indium tin oxide. LCD screens can be dismantled and submitted to acid leaching. However, the indium generally ends diluted in the liquid phase, thus a further step for the indium concentration should be explored [5–7].

Different techniques can be employed for the removal/recovery of heavy metals present in the liquid phase, such as adsorption [8], chemical precipitation [9], membrane filtration [10] and coagulation–flocculation [11]. Among these methods, adsorption is the easiest technique to be applied, being economically limited by the adsorbent choice [12–18]. It is reported that different adsorbents can be employed in the adsorption of indium [12–15]. However, the preparation of these materials can lead to major problems from the economic and environmental viewpoints [19]. One solution is the application of more eco–friendly and abundant materials, such as chitin and chitosan. These materials are natural polymers that possess a high affinity to adsorb a wide range of species, from dyes to heavy metals [20–22]. This characteristic is related directly to the presence of amide/amine and hydroxyl groups [23].

Concerning the adsorption of metallic species using chitin and chitosan, the process kinetic is extremely important. Basically, kinetic studies define the operation time and consequently affect operational costs. There are many excellent works in the literature in relation to the application of diffusional models in the liquid phase adsorption [24–27]. However, there is a great deal of work using kinetic reaction models, which are known, not to be suitable for the design of continuous systems [28]. These models consider that adsorption

can be described as a chemical reaction, thus limiting any interpretation in relation to the mass transfer phenomena [29].

On the other hand, the mass transfer models (including external mass transfer model (EMTM) and Pore Volume and Surface Diffusion Model (PVSDM) bring more information in relation to the adsorption, since they are based in mass transfer steps that occur in the adsorbent and its surroundings. It is reported that the EMTM has been used for describing the adsorption of organic compounds (pyridine, phenol, 1–naphthalene sulfonic acid, pentachlorophenol and methylene blue) on the activated carbon [30]. The PVSDM model has been used for describing the adsorption of Zn(II) on the walnut shell [31]. Furthermore, the PVSDM was also used for describing the adsorption of organic micropollutants onto activated carbon [32]. Take into consideration the utility of the mass transfer models, and an efficient and fast In(III) recovery from solutions, using chitin and chitosan, the mass transfer mechanism needs to be carefully investigated by mass transfer model approaches [33].

This work focused, for the first time in literature, the elucidation of the mechanism of In(III) adsorption onto chitosan and chitin based on mass transfer models approaches. At first, the biopolymers chitin and chitosan were produced and characterized in detail by several techniques. Then, adsorption equilibrium and thermodynamics were constructed and analyzed. Finally, the EMTM and PVSDM models were applied to elucidate the mass transfer phenomena considering plate–like geometries for the chitosan and chitin.

4.3.3 Materials and methods

4.3.3.1 . Adsorbate and adsorbents

A stock solution of indium (III) (1.00 g L^{-1}) was prepared using indium (III) nitrate hydrate (Sigma Aldrich) and deionized water [34]. All the experiments were carried out by diluting the stock solution until the desired concentrations. Chitosan and chitin were obtained from shrimp wastes. At first, chitin was obtained by demineralization, deproteinization and deodorization steps. Chitosan paste was obtained by alkaline deacetylation of chitin followed by purification and drying [35–37].

4.3.3.2 Characterization of the adsorbent materials

The chitin and chitosan materials were characterized by adsorption/desorption isotherms of N_2, which were used for the determination of the specific surface area and pore size distribution through Brunauer–Emmett–Teller (BET) and Barret–Joyner–Halenda (BJH) methods, respectively. For this, it was employed a porosity analyzer from Micrometrics, model ASAP 2020 (USA) operating at 94.3 K. The functional groups were determined by Fourier transform infrared spectroscopy (FTIR) using KBr tablets, operating in a range of 4000 to 400 cm^{-1} (Shimadzu, IR–Prestige–21, Japan). The aspects of the surface, before and after adsorption, were identified by scanning electron microscopy (SEM), X–ray mapping and EDS spectra. It was used a Zeiss model Sigma 300 VP (Germany) equipment. Other characteristics of the materials (apparent density, external surface area and void fraction) were estimated according to the literature [25,30,38].

4.3.3.3 . Adsorption essays

The adsorption studies were conducted using a thermostatic agitator (Dubnoff, model SL–157, Brazil). All the experiments were made using 0.05 g of each adsorbent (chitin or chitosan) added in 50 mL of In(III) solution at pH 2.5. First, the equilibrium curves were obtained for 298.15 K, 308.15, 318.15 and 328.15 K, with initial indium concentrations of 0, 5, 12.5, 25, 50, 75, 100 mg L^{-1}, being the samples collected after the equilibrium time (three consecutive equal measurements of In(III) concentration in liquid phase (6 hours)). Second, the kinetic studies were made for the initial In(III) concentrations of 50 and 25 mg L^{-1}. Samples were taken at 2.5, 5, 10, 20, 30, 40, 60, 90 and 120 min. All the assays were conducted in triplicates, being the In(III) concentration in the liquid phase determined by ICP (inductively coupled plasma) in a Ciros CCD equipment (Germany). All the experiments were conducted using an agitation speed of 150 rpm. Determination of the adsorption capacity at the equilibrium was done by Equation (1):

$$q_e = \frac{(C_0 - C_e)}{D_o} \quad (1)$$

4.3.3.4 Equilibrium curves and thermodynamic estimations

For the describing the equilibrium curves, the following models were chosen: Langmuir [39] (Equation (2)), which considerate that the adsorption is homogeneous in all bind sites and Freundlich (Equation (3)), that is an empirical approach for describing the heterogeneous adsorption [40]:

$$q_e = q_{max} \frac{K_L C_e}{1 + K_L C_e} \quad (2)$$

$$q_e = K_F C_e^{1/n} \quad (3)$$

The estimation of the isotherm parameters was made using the Particle swarm optimization Algorithm hybridized with *fmincon*, available inbuilt in Matlab®. For this, it was used the non–linear least squares (Equation (4)) [41,42]:

$$\min\left|f(par_1, par_2)\right| = \sum_{i=1}^{n} \left(q_{exp} - q_{model}\right)^2 \quad (4)$$

The standard Gibbs free energy change (ΔG^0), standard enthalpy change (ΔH^0), and standard entropy change (ΔS^0) were estimated using the constant from the best model fitted to the equilibrium data (Equation (8)) and also the Equations (5–8) [43]:

$$k_e = \frac{k M_a \gamma^{In(III)}}{\gamma} \quad (5)$$

$$\Delta G^0 = -RT\ln(k_e) \quad (6)$$

$$\Delta G^0 = \Delta H^0 - T\Delta S^0 \quad (7)$$

$$\ln(k_e) = \frac{\Delta S^0}{R} - \frac{\Delta H^0}{RT} \quad (8)$$

The solution of the thermodynamics parameters has been done using the *fsolve* routine with the Levenberg–Marquardt algorithm, built–in the Matlab [44–46].

4.3.3.5 Mass transfer models

The mass transfer mechanism of In(III) on chitin and chitosan was elucidated using mass transfer models. To verify if the adsorption is controlled by external mass transfer, the external mass transfer model (EMTM) was used. EMTM assumes that intraparticle diffusion is instantaneous. Therefore, the movement of solute from the liquid phase to the adsorbent is controlled mainly by the external mass transfer [47]. Here the EMTM is represented by Equations (9–12):

$$V\frac{dC_A}{dt} = -mSk_L(C_A - C_{Ax}|_{x=L/2}) \quad (9)$$

$$t=0,\ C_A = C_{A0} \quad (10)$$

$$\frac{m}{\rho_p}\varepsilon_p\frac{dC_{Ax}|_{x=L/2}}{dt} + m\frac{dq_t}{dt} = mSk_L(C_A - C_{Ax}|_{x=L/2}) \quad (11)$$

$$t=0,\ C_{Ax}=0,\ q_t=0 \quad (12)$$

To verify if the In(III) adsorption on chitin and chitosan is controlled by internal mechanisms (pore or surface diffusion), the pore volume and surface diffusion model (PVSDM) was selected. It is one of the most complete diffusional models and considers that the mechanism occurs in three consecutive steps of mass transfer, being: the external mass transfer, intraparticle diffusion and the adsorption on active sites [29,33]. In addition, here the geometry of the adsorbent was considerate plate–like. The PVDSM is presented here by Equations (13–18):

$$V\frac{dC_A}{dt} = -mSk_L(C_A - C_{Ax}|_{x=L/2}) \quad (13)$$

$$t=0,\ C_A=C_{A0} \tag{14}$$

$$\varepsilon_p \frac{\partial C_{Ax}}{\partial t}+\rho_p \frac{\partial q}{\partial t}=\frac{\partial}{\partial x}\left(D_p \frac{\partial C_{Ax}}{\partial x}+\rho_p D_S \frac{\partial q}{\partial x}\right) \tag{15}$$

$$t=0,\ 0\leq x\leq L/2,\ C_{Ax}=0 \tag{16}$$

$$\left.\frac{\partial C_{Ax}}{\partial x}\right|_{x=0}=0 \tag{17}$$

$$D_p \frac{\partial C_{Ax}}{\partial x}+\rho_p D_S \frac{\partial q}{\partial x}=k_L\left(C_A-C_{Ax}|_{x=L/2}\right) \tag{18}$$

Furthermore, the indium adsorption of the active sites was considered instantaneous. In other words, the indium concentration present in the solution and adsorbed on the solid can be related through adsorption isotherm [47] (Equation (19))

$$q=f(C_{Ax}) \tag{19}$$

The solution of both models was done by applying the method of finite–difference approximations, for solving the partial differential equations (PDE). This method consists in turning the PDE onto a set of first–order ordinary differential equations (ODE) [38,48]. The ODE system is solved using the *ode15s* built–in Matlab. This is a variable–step, variable–order (VSVO) solver based on the numerical differentiation formulas (NDFs) [49].

4.3.3.6 Estimation of the mass transfer parameters

The mass transfer parameters namely the external mass transfer coefficient (k_L), effective pore volume diffusion coefficient (D_p) and surface diffusion coefficient (D_S), were

estimated as follows: First, the k_L was estimated from the slope of Equation (20) for the first two points of the adsorption decay curve [50]:

$$\left[\frac{d(C_t/C_0)}{dt}\right] = \frac{-mSk_L}{V} \quad (20)$$

Second, D_p was related to the indium diffusivity (D_{AB}) and the tortuosity factor [51] (Equations (21,22)). In this case, the D_{AB} for the In (III) was obtained from the literature [52].

$$D_p = \frac{D_{AB}\varepsilon_p}{\tau} \quad (21)$$

$$\tau = \frac{(2-\varepsilon_p)^2}{\varepsilon_p} \quad (22)$$

Lastly, the surface diffusion coefficient was obtained by parameter estimation using the Matlab®. For this, the *lsqnonlin* with the Trust–Region–Reflective algorithm was used. The used function is the minimum least–squares (Equation (23)):

$$\min|f(D_S)| = \sum_{i=1}^{n}\left(C_{exp}-C_{model}\right)^2 \quad (23)$$

2.7. Fit evaluation

The fitness between the experimental data and the predicted data was evaluated through average relative error (ARE) (Equation (24), the sum of the squared errors (SSE) (Equation (25)) and coefficient of determination (R^2) (Equation (26)):

$$ARE=\frac{100\%}{n}\sum_{i=1}^{n}\left|\frac{y_{exp}-y_{pred}}{y_{exp}}\right| \quad (24)$$

$$SSE=\sum_{i=1}^{n}\left(y_{exp}-y_{pred}\right)^2 \quad (25)$$

$$R^2=1-\frac{\sum_{i=1}^{n}\left(y_{exp}-y_{pred}\right)^2}{\sum_{i=1}^{n}\left(y_{exp}-\bar{y}_{exp}\right)^2} \quad (26)$$

4.3.4 Results and Discussion

4.3.4.1 Chitin and chitosan characteristics

Some fundamental physical characteristics of the chitosan and chitin particles are presented in Table 1. In general, chitosan particulate material presented better characteristics than chitin for adsorption purposes. The specific surface area of chitosan was 20% higher than for chitin. In the same way, the values of the average pore radius and pore volume were two times higher for chitosan particles. As a consequence, the porosity for chitosan was also higher. The differences in these characteristics can be attributed to the deacetylation reaction that transforms chitin into chitosan [35]. During this reaction, a fraction of acetamide groups of chitin is converted into amino groups. These amino groups, in turn, are lower in size than the acetamide. As a consequence, void spaces are created in the polymer. It is expected that these better characteristics of chitosan make it a better adsorbent in terms of capacity and velocity.

Concerning the functional groups present in chitin and chitosan, the vibrational bands are presented in Table 2. These bands are typical of the chitosan and chitin based materials. For chitosan, amides, amines, and hydroxyl groups were identified. For chitin, amides I and II were observed, and also hydroxyl groups [47,53].

Table 1: Chitin and chitosan physical characteristics

Physical characteristics	Chitosan*	Chitin*
Particle size (mm)	0.072 ± 0.003	0.072 ± 0.003
Specific surface area ($m^2\ g^{-1}$)	4.30 ± 0.12	3.60 ± 0.05
Average pore radius (Å)	33.10 ± 1.62	14.30 ± 0.34
Pore volume ($cm^3\ g^{-1}$)	0.095 ± 0.002	0.049 ± 0.004
Solid specific mass ($kg\ m^{-3}$)	1550 ± 5	1550 ± 5
Bulk specific mass ($kg\ m^{-3}$)	1351 ± 2	1440 ± 3
Porosity (–)	0.128 ± 0.007	0.071 ± 0.005

Table 2: FTIR bands found for chitosan and chitin.

FTIR bands (cm^{-1})	Chitosan	FTIR bands (cm^{-1})	Chitin
3450	N–H stretching	3350	O–H stretching
3250–3100	O–H stretching	3150	N–H vibrations
2850	C–N stretching of amides	1550	C–H stretching
1650	Deformation of C–O–H and H–C–H	1450	Amide I, carbonyl C=O
1550	C–N stretch from the amino groups	1075	Amide II, deformation of N–H
1450	C–O and C–O–C bonds	1250–950	CH_X vibration
1250–950	N–H bending	680	C–O and C–O–C bonds

The SEM images for chitosan (A) and chitin (B) are presented in Figure 1. Both materials presented a rigid surface without visible pores and cavities, with plate–like geometry. From the SEM images, it can be also observed that the thickness of the particles is extremely lower than its length and height. Based on these observations, it is reasonable the assumptions of plate–like geometry and one–dimensional transference for the diffusional models.

Figure 1: SEM images of chitosan (A) and chitin (B) with magnification of × 300 and × 100, respectively.

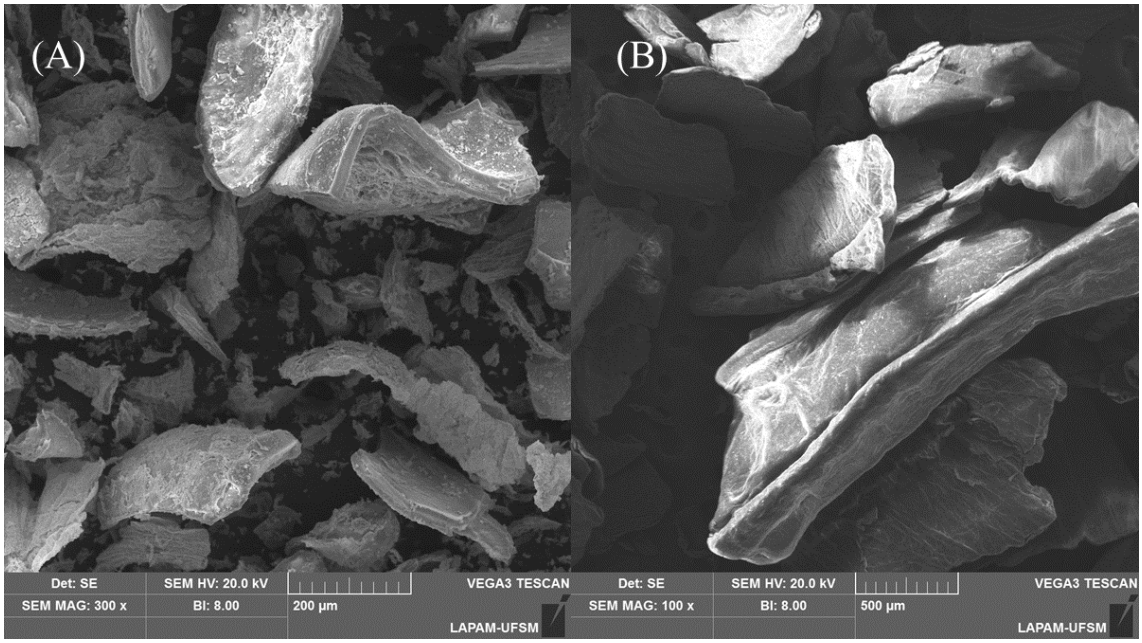

Figure 2 shows SEM images of chitin and chitosan after In(III) adsorption, and also, the In X–ray mappings on the surface of the adsorbent. It is possible to observe in Figures 2 (A) and 2(C) that, the surfaces of chitin and chitosan were modified after In(III) adsorption. In these Figures, it looks like that the surfaces were covered by little precipitates, suggesting that adsorption can be occurred by the surface precipitation phenomenon. Other strong indications of the surface covering and surface precipitation mechanism are the yellow points in Figures 2 (B) and 2 (D), which are relative to the presence of In on the chitin and chitosan surfaces.

Figure 2: SEM images (× 1000) for chitosan (A) and chitin (C) after the In(III) adsorption, coupled with In mapping for chitosan (B) and chitin (D).

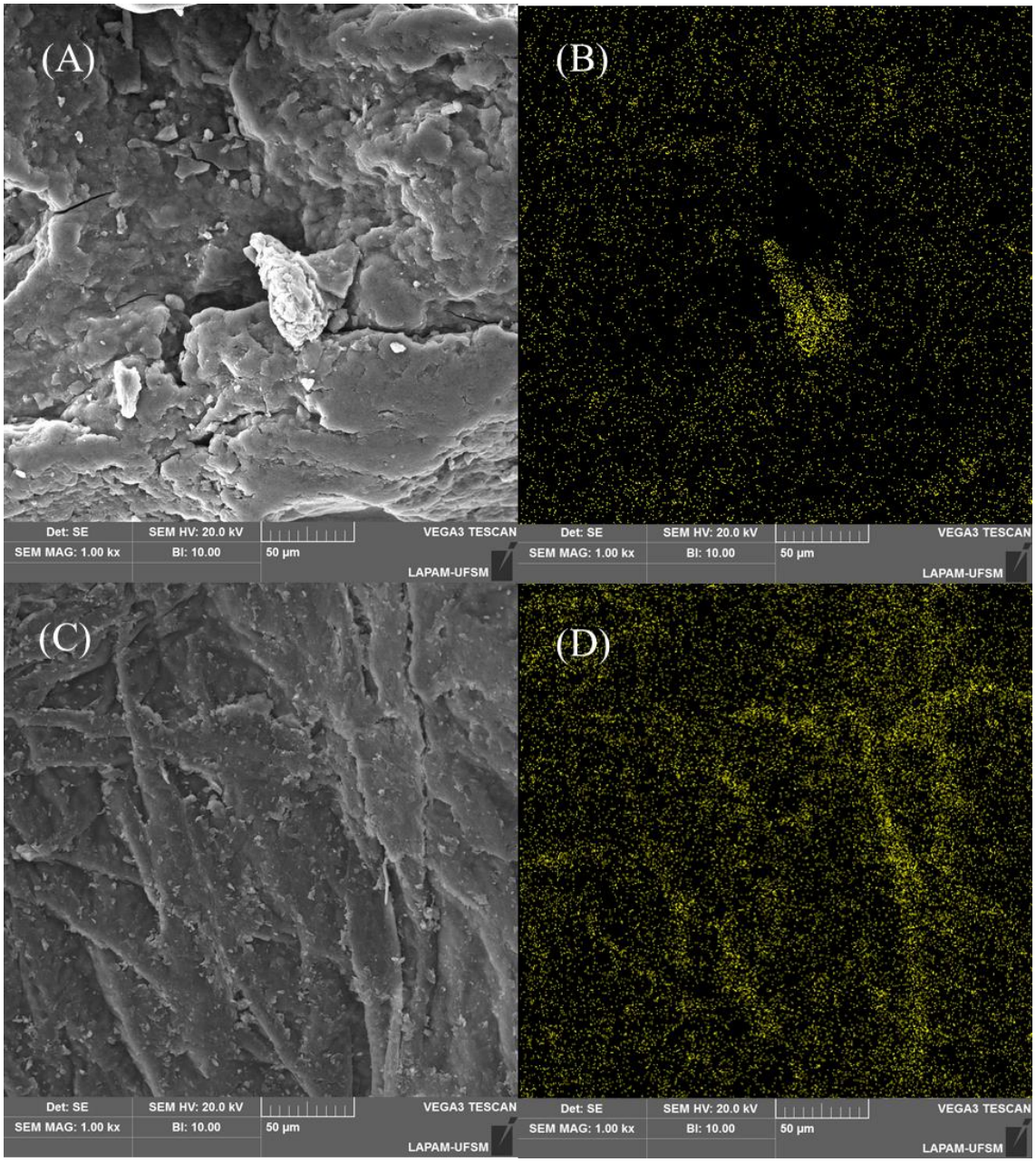

Figure 3: EDS spectra for chitosan (A) and chitin (B) after the In(III) adsorption.

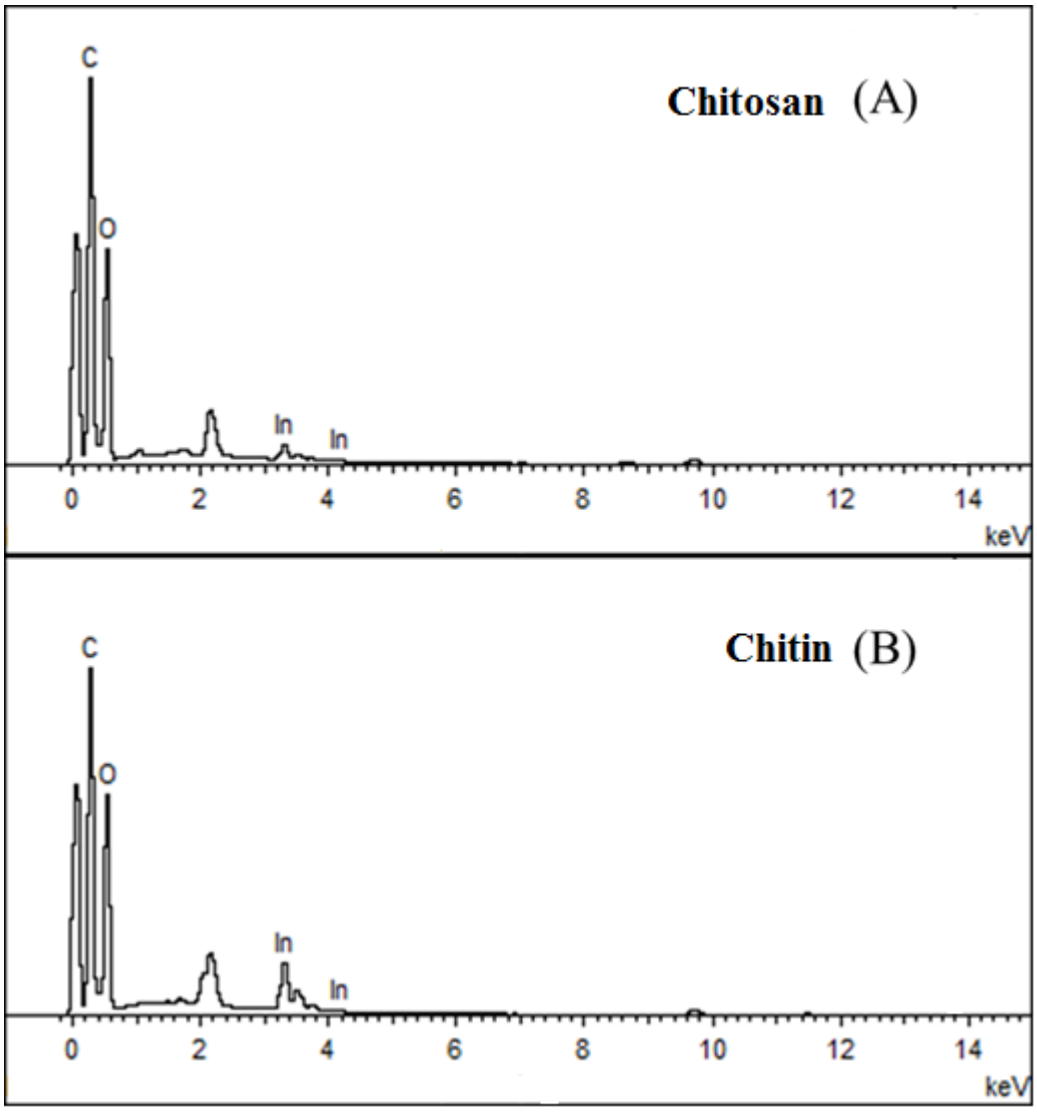

The confirmation of In adsorption on chitosan and chitin is depicted in Figure 3. This Figure shows the EDS spectra for chitosan (A) and chitin (B) after the In(III) adsorption. It can be observed the presence of C and O, typical of chitin and chitosan, and also the presence of In.

4.3.4.2 Adsorption isotherms and thermodynamics

The equilibrium curves for the adsorption of In(III) onto chitosan (A) and chitin (B) are presented in Figure 4. The first aspect is the influence of the temperature on the In(III) adsorption. For both materials, the temperature increase caused a decrease in the adsorption

capacity. This increase indicates exothermic adsorption [25]. A similar trend has also been found by [19] when studying the adsorption of In(III) onto chitin. Another aspect is that the curves were convex, indicating favorable adsorption. The curves were characterized by a strongly inclined portion at lower C_e values. This shows that both adsorbents were efficient, providing high removal percentages coupled with high adsorption capacities.

Figure 4: Equilibrium curves for the adsorption of In(III) onto chitosan (A) and chitin (B), accompanied by the prediction of Langmuir's model.

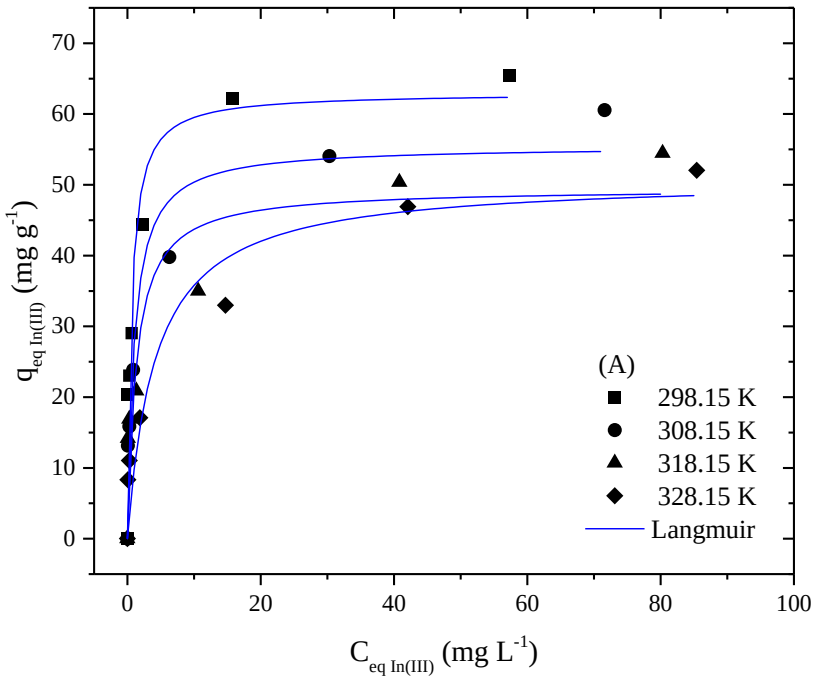

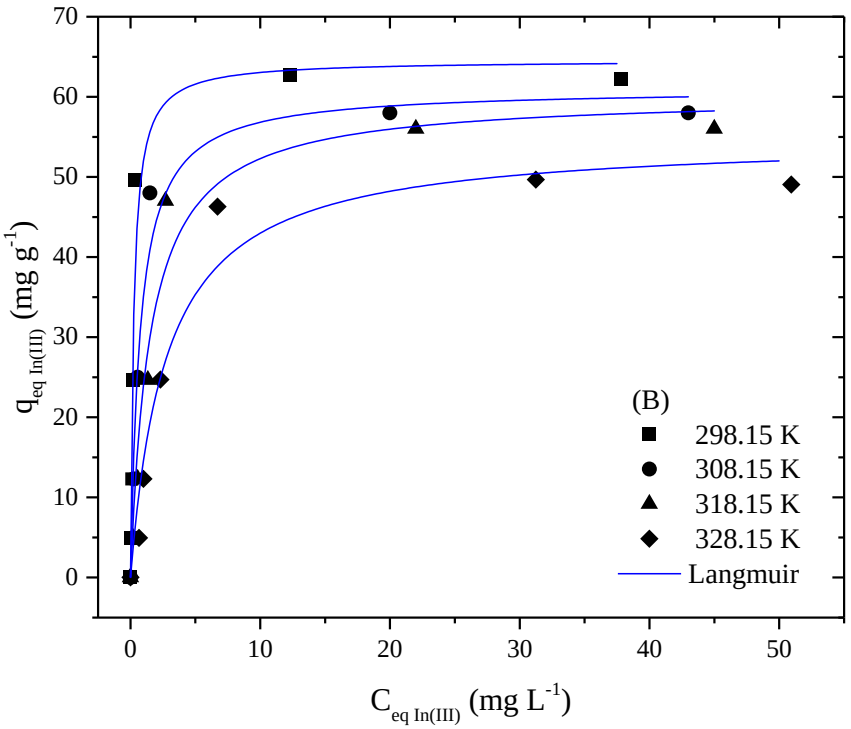

The estimated parameters for the isotherm models are presented in Table 3. From the statistical viewpoint, the Freundlich model is the proper one for representing the In(III) adsorption onto chitosan. However, the Langmuir model also presented good values for SSE, ARE and R^2. Taking into consideration that the Langmuir model presents the theoretical background and it is far more accepted for thermodynamics estimations [35,43], this model was selected to represent the system In(III)/chitosan. In the case of chitin, the Langmuir model is the proper one for representing the equilibrium curves of In(III). Thus, for describing both systems the Langmuir model was chosen. This model was substituted in Equation 19 to solve the PVSDM model. Concerning the temperature effect on the parameters q_{max} and K_L, the behavior was inversely proportional. Both q_{max} and K_L increased with the temperature decrease, reaching maximum values at 298.15 K. This confirms that for chitin and chitosan, the In(III) adsorption capacity and its affinity with the adsorbent, are most pronounced under ambient

conditions. Finally, it can be verified in Table 3 that chitin and chitosan presented similar adsorption capacities for In(III).

Table 3: Isotherm parameters for In(III) adsorption onto chitosan and chitin.

Parameter	Chitosan				Chitin			
	298.15 K	308.15 K	318.15 K	328.15 K	298.15 K	308.15 K	318.15 K	328.15 K
Langmuir								
q_{max} (mg g^{-1})	62.98	55.48	49.48	50.87	64.55	61.03	60.19	54.88
K_L (L mg^{-1})	1.71	0.98	0.76	0.24	4.14	1.35	0.66	0.36
ARE (%)	16.35	19.31	27.56	28.17	22.00	22.31	15.70	22.20
SSE	260.6	209.7	345.2	174.4	215.5	94.4	107.7	100.9
R^2	0.9689	0.9716	0.9441	0.9771	0.976	0.9887	0.9853	0.9833
Freundlich								
K_F (mg g^{-1})(mg L^{-1})$^{-1/n}$	34.1	24.7	21.9	15.71	34.88	27.40	23.30	17.89
n	0.18	0.22	0.21	0.28	0.19	0.23	0.26	0.29
ARE (%)	8.46	5.20	5.32	4.03	60.37	54.78	47.16	46.29
SSE	111.9	25.4	15.4	13.2	825.2	604.4	510.4	432.0
R^2	0.9834	0.9958	0.9967	0.9973	0.9012	0.9169	0.9253	0.9209

The estimated thermodynamic parameters for In(III) adsorption on chitosan and chitin are shown in Table 4. It can be seen that the equilibrium constant increased with the temperature decrease, indicating that the formation of the complex In(III)/adsorbent was favored at 298 K. For both cases, the adsorption presented a spontaneous aspect, with a standard Gibbs free energy (ΔG^0) ranging from –13.1 to –9.0 kJ mol^{-1} for the chitosan and –15.3 to –10.2 kJ mol^{-1} for chitin. In addition, the enthalpy was of –50.0 and –65.6 kJ mol^{-1} for chitosan and chitin, respectively, confirming the exothermic nature of the adsorption. Enthalpy values with this magnitude indicate a possible coordination bond between the In(III) and the adsorbents [12]. Last, the standardentropy change was found –0.12 and –0.17 kJ mol^{-1} for chitosan and chitin respectively, this indicates a minor adjustment of the In(III) on the surface of the materials.

Table 4: Thermodynamic parameters for In(III) adsorption onto chitosan and chitin.

Adsorbent	T (K)	k_e (dimensionless)	ΔG^0 (kJ mol^{-1})	ΔH^0 (kJ mol^{-1})	ΔS^0 (kJ mol^{-1} K^{-1})	R^2
Chitosan	298.15	195.9	–13.1	–50.0	–0.12	0.9093
	308.15	113.2	–12.1			
	318.15	86.8	–11.8			
	328.15	27.2	–9.0			
Chitin	298.15	475.2	–15.3	–65.6	–0.17	0.9859
	308.15	155.0	–12.9			
	318.15	75.8	–11.4			
	328.15	41.4	–10.2			

4.3.4.3 Mass transfer mechanism

The overall mass transfer mechanism in liquid phase adsorption is normally represented by the following consecutive steps: (I) external mass transfer, (II) intraparticle diffusion and (III) adsorption on the active sites. The external mass transfer is relative to the movement of adsorbate species from the bulk solution to the external surface of the adsorbent. The intraparticle diffusion involves all mass transfer mechanisms that occur inside the adsorbent particle, being the most commons, surface diffusion, and effective pore diffusion. Adsorption on the active sites is relative to the specific interaction that occurs between the adsorbate and adsorbent. In this work, step III was considered instantaneous [12,27]. So, it was assumed that the overall mass transfer for the systems studied here can occur by the steps I or II, or even I and II simultaneously. In this way, EMTM and PVSDM were selected to verify these possible mechanisms.

The In(III) concentration decay curves for initial concentrations of 50 and 25 mg L^{-1} adsorbed onto chitosan and chitin are presented in Figures 5 and 6, respectively. It can be seen that all curves were typical, with a decrease in the liquid phase In(III) concentration along the

time, from C_0 to C_e. The effectiveness of both, chitin and chitosan as In(III) adsorbents, can be also verified in Figures 5 and 6, where all the C_e values were lower than 0.35 mg L^{-1} of In(III). For chitosan (Figure 5), the decay curves were dependent on the initial In(III) concentration until 60 min. After 60 min, an overlapping of both curves was observed, is that, at 90 min, both curves attained 1.47 mg L^{-1} of In(III) concentration. In the chitin case (Figure 6), similar behavior can be seen, however, the decay curves were dependent on the initial In(III) concentration until 40 min. All these aspects observed in the curves will be discussed based on the mass transfer parameters, which are depicted in Table 5.

Figure 5: Concentration decay curves for In(III) adsorption onto chitosan, EMTM (A) and PVSDM (B) predictions.

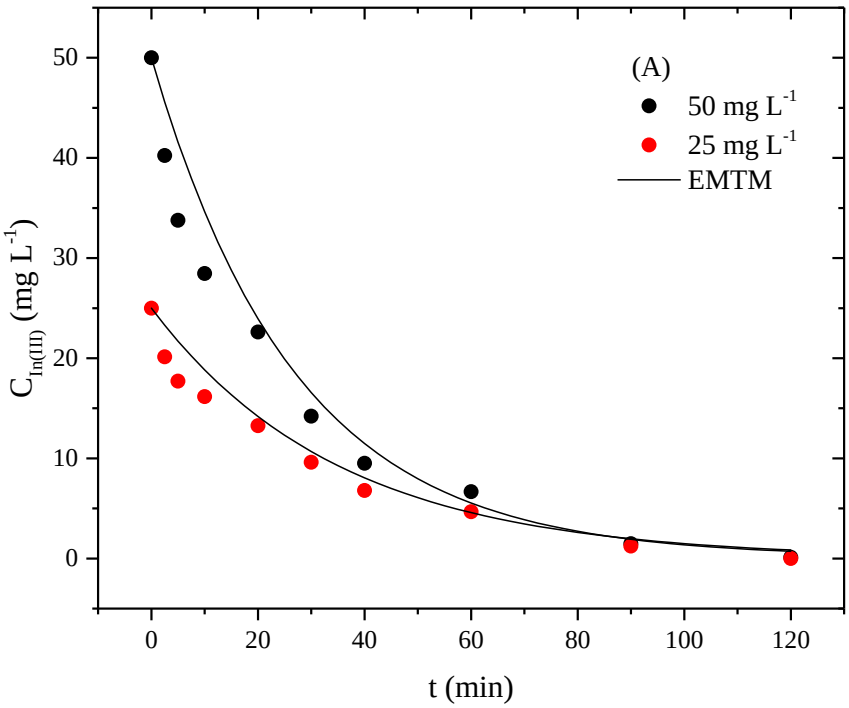

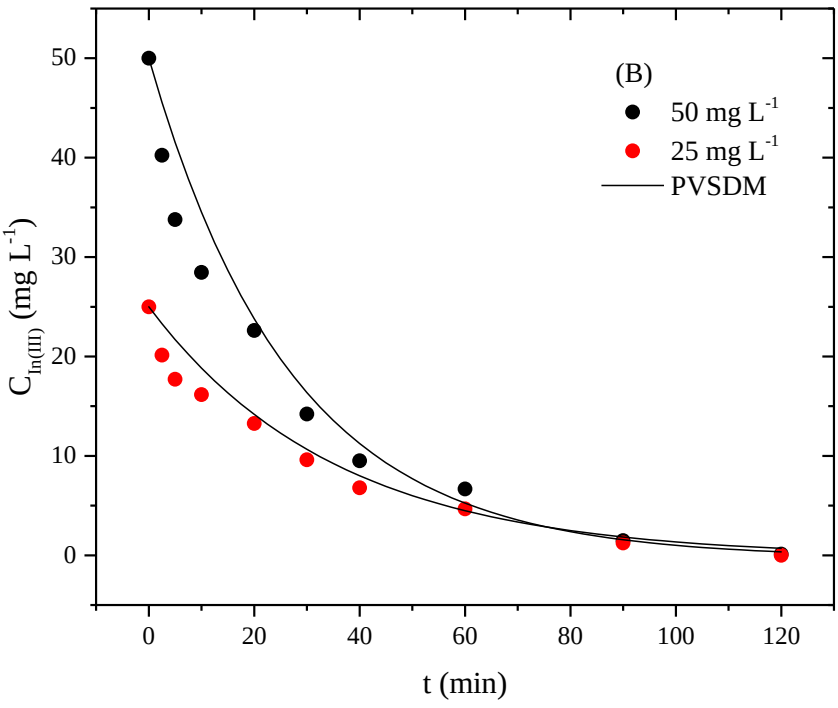

Figure 6: Concentration decay curves for In(III) adsorption onto chitin, EMTM (A) and PVSDM (B) predictions.

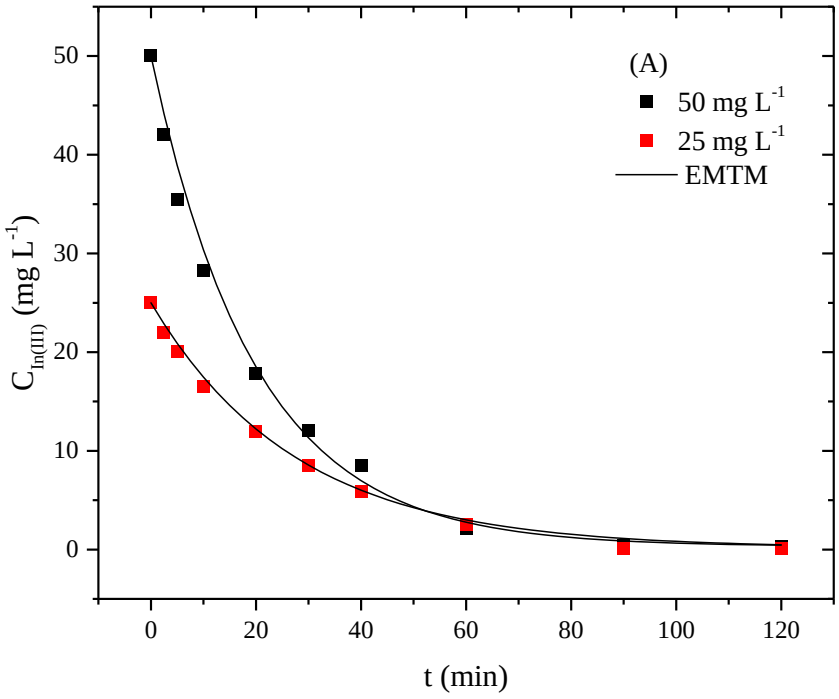

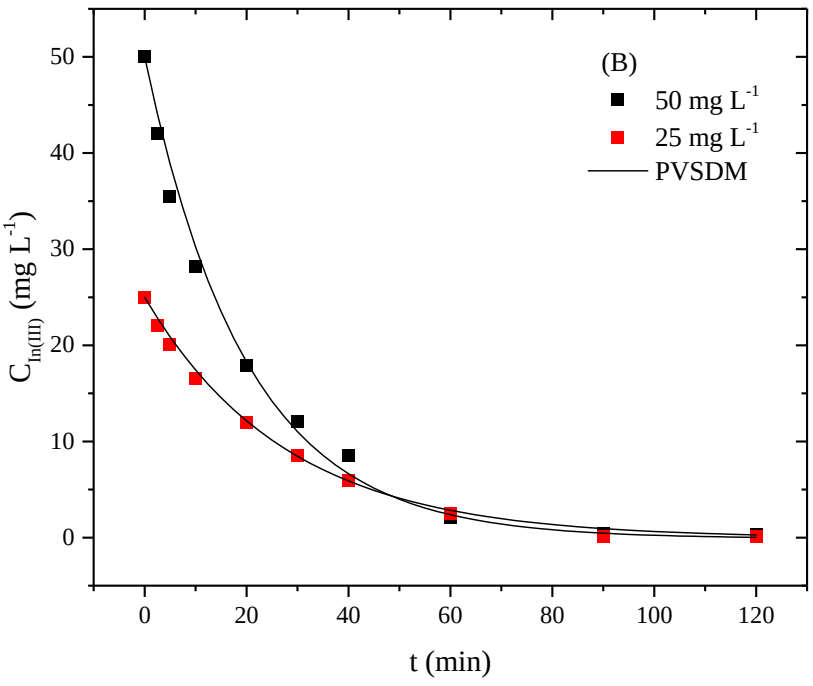

It was verified in Figures 5 and 6 that EMTM and PVSDM models were adequate to predict the adsorption decay curves. So, it is not possible to infer the dominant mechanism on the basis of the model fitting. One way to find the dominant mass transfer mechanism is the dimensionless modified Biot number (Equation (30)) [25,26]. The dominance of the external mass transfer is assumed for $B_i<0.5$, and, internal diffusional mechanisms predominate if $B_i>10$ [38,47,50].

$$B_i=\frac{k_f\bar{d}C_{A0}}{2\rho_p D_S q_e} \tag{30}$$

The estimated B_i number and the other mass transfer parameters are presented in Table 5. The B_i number was found between 8.82×10^{-4} and 2.71, indicating that the external mass transfer is dominant in comparison with the internal diffusion mechanisms. This is corroborated by the D_s values, which were around 4 magnitudes higher than the values reported in the literature [54,55]. So, the surface diffusion mechanism is extremely fast, presenting little effect on the overall adsorption rate. Another indicative that external mass transfer is dominant, is the relation between the average pore size of chitin and chitosan and the diameter of the adsorbed species. Both have the same magnitude [12,27], thus hindering the penetration of the adsorbate inside the adsorbent.

Table 5: Estimated mass transfer parameters for the adsorption of In(III) onto chitosan and chitin.

Material	C_{A0} (mg L^{-1})	C_{Ae} (mg L^{-1})	q_e (mg g^{-1})	$k_L \times 10^3$ (cm s^{-1})	$D_p \times 10^9$ (cm^2 s^{-1})	$D_s \times 10^6$ (cm^2 s^{-1})	B_i
Chitosan	50	0.31	49.67	3.20	4.21	7.60	7.70×10^{-2}
	25	0.14	24.86	2.30	4.21	0.15	2.71
	C_{A0} (mg L^{-1})	C_{Ae} (mg L^{-1})	q_e (mg g^{-1})	$k_L \times 10^4$ (cm s^{-1})	$D_p \times 10^8$ (cm^2 s^{-1})	$D_s \times 10^4$ (cm^2 s^{-1})	Bi
Chitin	50	0.12	49.88	9.52	1.48	7.97	8.82×10^{-4}
	25	4.86×10^{-4}	25.00	7.28	1.48	2.18	2.46×10^{-3}

Assuming that the In(III) adsorption on chitosan and chitin occurred by external mass transfer, it can be seen that, for both adsorbents, the k_L values increased with the initial In(III) concentration (Table 5). Evidently, the mass transport was faster at higher In(III) concentrations. This is due to the higher concentration gradient between the bulk solution and the external surface of the adsorbents.

An interesting fact in Table 5 is that the k_L values were higher for chitosan (10^{-3} cm s^{-1}) in relation to chitin (10^{-4} cm s^{-1}). This shows that the In(III) adsorption on chitosan was a faster process. Considering that k_L was estimated by Equation (20) and that the experiments were carried out in the same conditions, this result can be only justified on the basis in the S value of each adsorbent. The S values for chitosan and chitin were, respectively, 616.8 cm^2 g^{-1} and 578.7 cm^2 g^{-1}. In this way, the In(III) adsorption on chitosan was faster due to the higher value of the external surface area of this adsorbent.

4.3.5 Conclusion

In this work, the mechanism of In(III) adsorption onto chitosan and chitin was investigated based on characterization techniques, isotherms, thermodynamics and mainly in the mass transfer models. It was possible to conclude that chitosan and chitin presented rigid

surfaces with no visible porous, and also that In(III) was adsorbed in the external surface of both biopolymers. SEM and X–ray mappings suggested that surface precipitation of In can occur. Isotherms and thermodynamics indicated favorable and exothermic adsorption, with possible coordination bonds between the In(III) and the adsorbents. The low values of the modified Biot number (between 8.82×10^{-4} and 2.71), and the good fit of the EMTM model with the experimental data, indicated that the overall mass transfer was controlled by the external mass transfer mechanism. The In(III) adsorption on chitosan was a faster process, being that, the external surface area of the adsorbents presented an important role in the adsorption rate. In summary, In(III) species were transferred from the bulk solution to the external surface of the adsorbents and, instantaneously adsorbed by surface precipitation and/or coordination bonds.

4.3.6 Acknowledgments

The authors would like to thanks the EBW+ (Euro Brazillian Windows) granted by the Erasmus Mundus program. The authors would like to thank the financial grant from FAPERGS (Fundação de Amparo à Pesquisa do Estado do Rio Grande do Sul).

4.3.7 References

Adegoke KA, Bello OS (2015) Dye sequestration using agricultural wastes as adsorbents. Water Res Ind 12:8–24.

Alencar WS, Lima EC, Royer B, dos Santos BD, Calvete T, da Silva EA, Alves CN (2012) Application of aqai stalks as biosorbents for the removal of the dye Procion Blue MX–R from aqueous solution. Sep Sci Technol 47:513–526.

Ali I (2010) The Quest for Active Carbon Adsorbent Substitutes: Inexpensive Adsorbents for Toxic Metal Ions Removal from Wastewater. Sep Purif Rev 39:95–171.

Ali I (2012) New generation adsorbents for water treatment. Chem Rev 112:5073–5091.

Ali I (2014) Water treatment by adsorption columns: Evaluation at ground level. Sep Purif Rev 3:175–205.

Ali I, Aboul–Enein HY (2006) Instrumental methods in metal ions speciation: Chromatography, Capillary Electrophoresis and Electrochemistry. Taylor & Francis, New York.

Ali I, Aboul–Enein HY, Gupta VK (2009) Nano Chromatography and Capillary Electrophoresis: Pharmaceutical and Environmental Analyses, Wiley, Hoboken.

Ali I, Al–Othman ZA, Al–Harbi OML (2016d) Uptake of pantoprazole drug residue from water using novel synthesized composite iron nano adsorbent. J. Mol Liq 218: 465–472.

Ali I, Al–Othman ZA, Alwarthan A (2016a) Molecular uptake of congo red dye from water on iron composite nanoparticles, J Mol Liq 224:171–176.

Ali I, Al–Othman ZA, Alwarthan A (2016b) Green synthesis of functionalized iron nano particles and molecular liquid phase adsorption of ametryn from water. J Mol Liq 221:1168–1174.

Ali I, Al–Othman ZA, Alwarthan A (2016c) Synthesis of composite iron nano adsorbent and removal of ibuprofen drug residue from water. J Mol Liq 219:858–864.

Ali I, Al–Othman ZA, Alwarthan A (2017) Uptake of propranolol on ionic liquid iron nanocomposite adsorbent: Kinetic, thermodynamics and mechanism of adsorption. J Mol Liq 236:205–203.

Ali I, Tabrez MA, Khan A (2012) Low cost adsorbents for removal of organic pollutants from wastewater. J Environ Manage 113:170–183.

Ali I, Gupta VK (2006) Advances in Water Treatment by Adsorption Technology. Nature Protocol 1:2661–2667.

Almeida EJR, Corso CR (2014) Comparative study of toxicity of azo dye Procion Red MX–5B following biosorption and biodegradation treatments with the fungi *Aspergillus niger* and *Aspergillus terreus*. Chemosphere 112:317–322.

Anastopoulos I, Kyzas GZ (2014) Agricultural peels for dye adsorption: A review of recent literature. J Mol Liq 200:381−389.

Anastopoulos, I, Kyzas GZ (2016) Are the thermodynamic parameters correctly estimated in liquid–phase adsorption phenomena? J Mol Liq 218:174–185.

Bazzo A, Adebayo MA, Dias SLP, Lima EC, Vaghetti JCP, Oliveira ER (2016) Avocado seed powder: characterization and its application for crystal violet dye removal from aqueous solutions. Desalin Water Treat 57: 15873–15888.

Bharathi KS, Ramesh ST (2013) Removal of dyes using agricultural waste as low–cost adsorbents: a review. Appl Water Sci 3:773–790.

Bonilla–Petriciolet A, Mendoza–Castillo DI, Reynel–Ávila E (2017) Adsorption Processes for Water Treatment and Purification. Springer International Publishing, Cham.

Brazilian Fruit Yearbook (2015). Gazeta, Santa Cruz do Sul. Available at: http://www.grupogaz.com.br/tratadas/eo_edicao/4/2015/03/20150301_106c8c2f1/pdf/4718_2015fruticultura.pdf.

Bretanha MS, Dotto GL, Vaghetti JCP, Dias SLP, Lima EC, Pavan FA (2016) Giombo persimmon seed (GPS) an alternative adsorbent for the removal Toluidine Blue dye from aqueous solutions. Des Water Treat 57:28474–28485.

Brindley GW, Brown G (1980) Crystal Structures of Clay Minerals and Their X−ray Identification. Mineralogical Society, London.

Calvete T, Lima EC, Cardoso NF, Dias SLP, Pavan FA (2009) Application of carbon adsorbents prepared from the Brazilian pine-fruit-shell for the removal of Procion Red MX 3B from

aqueous solution–Kinetic, equilibrium, and thermodynamic studies. Chem Eng J 155:627–636.

Cestari AR, Vieira EFS, Santos AGP, Mota JA, Almeida VP (2004) Adsorption of anionic dyes on chitosan beads. 1. The influence of the chemical structures of dyes and temperature on the adsorption kinetics. J Colloid Interface Sci 280:380–386.

Dotto GL, Salau NPG, Piccin JS, Cadaval TRS, Pinto LAA (2017) Adsorption Kinetics in Liquid Phase: Modeling for Discontinuous and Continuous Systems. Chapter 3, p. 53–76 In: Bonilla–Petriciolet A, Mendoza–Castillo DI, Reynel–Ávila E. Eds. Adsorption Processes for Water Treatment and Purification. Springer International Publishing, Cham.

Foletto VS, Ferreira AB, Severo EC, Colazzo GC, Folletto EL, Dotto GL (2017) Iron–based adsorbent prepared from Litchi peel biomass via pyrolysis process for the removal of pharmaceutical pollutant from synthetic aqueous solution. Environ Sci Pollut Res 24:10547–10556.

Franco DSP, Tanabe EH, Dotto GL (2017) Continuous Adsorption of a Cationic Dye on Surface Modified Rice Husk: Statistical Optimization and Dynamic Models. Chem Eng Commun 204:625–634.

Freundlich H (1906) Over the adsorption in solution. Z Phys Chem 57:358–471.

Goldstein JI, Newbury DE, Echil P, Joy DC, Romig Jr AD, Lyman CE, Fiori C, Lifshin E (1992) Scanning electron microscopy and X–ray microanalysis. Plenum Press, New York.

Ho YS, Mckay G (1998) Kinetic models for the sorption of dye from aqueous solution by wood. Proc Safety Environ Protect 76:183–191.

Khan TA, Sharma S, Ali I (2011) Adsorption of Rhodamine B dye from aqueous solution onto acid activated mango (*Magnifera indica*) leaf powder: equilibrium, kinetic and thermodynamic studies. J Toxicol Environ Health Sci 3:286–297.

Lagergren S (1898) About the theory of so–called adsorption of soluble substances. Kung Svenska Vetenskap 24:1–39.

Langmuir I (1918) The adsorption of gases on plane surfaces of glass, mica and platinum. J Amer Chem Soc 40:1361–1403.

Leite AJB, Carmalin S, Thue PS, dos Reis GS, Dias SLP, Lima EC, Vaghetti JCP, Pavan FA, Alencar WS (2017) Activated carbon from avocado seeds for the removal of phenolic compounds from aqueous solutions. Desalin Water Treat 71:168–181.

Lima DR, Klein L, Dotto GL (2017) Application of ultrasound modified corn straw as adsorbent for malachite green removal from synthetic and real effluents. Environ Sci Pollut Res. 24:21484–21495.

Orts F, del Río AI, Molina J, Bonastre F (2017) Electrochemical treatment of real textile wastewater: Trichromy Procion HEXL® Cases. J Electroanal Chem In press.

Pachhade K, Sandhya S, Swaminathan K (2009) Ozonation of reactive dye, Procion red MX–5B catalyzed by metal ions. J Hazard Mater 167:313–318.

Palas B, Ersöz G, Atalay S (2016) Heterogeneous photo Fenton–like oxidation of Procion Red MX–5B using walnut shell based green catalysts. J Photochem Photobio A: Chem 324:165–174.

Palma C, Lloret L, Puen A, Tobar M, Contreras E (2016) Energy, Resources and Environmental Technology Production of carbonaceous material from avocado peel for its application as alternative adsorbent for dyes removal. Chinese J Chem Eng 24:521–528.

Piccin JS, Cadaval TRS, Pinto LAA, Dotto GL (2017) Adsorption Isotherms in Liquid Phase: Experimental, Modeling, and Interpretations. Chapter 2, p. 31–52 In: Bonilla–Petriciolet A, Mendoza–Castillo DI, Reynel–Ávila E. Eds. Adsorption Processes for Water Treatment and Purification. Springer International Publishing, Cham.

Qiu H, Pan LL, Zhang QJ, Zhang W, Zhang Q (2009) Critical review in adsorption kinetic models. J Zhejiang Univ Sci A10:716–724.

Rahman A, Urabe T, Kishimoto N (2013) Color removal of reactive procion dyes by clay adsorbents. Proc Environ Sci 17:270–278.

Redlich O, Peterson DL (1959) A useful adsorption isotherm. J Phys Chem 63:1024–1024.

Ruthven DM (1984) Principles of Adsorption and Adsorption Processes. John Wiley & Sons, New York.

Saavedra J, Cordova A, Navarro R, Díaz–Calderon P, Fuentealba C, Astudillo–Castro C, Toledo L, Enrione J, Galvez L (2017) Industrial avocado waste: Functional compounds preservation by convective drying process. J Food Eng 198:81–90.

Sahel K, Perol N, Dappozze F, Bouhent M, Derriche Z, Guillard C (2010) Photocatalytic degradation of a mixture of two anionic dyes: Procion Red MX–5B and Remazol Black 5 (RB5). J Photochem Photobio A: Chem 212:107–112.

Silverstein RM, Webster FX, Kiemle DJ (2007) Spectrometric identification of organic compounds. Wiley, New York.

Sips R (1948) On the structure of a catalyst surface. J Chem Phys 16:490−495.

Thommes M, Kaneko K, Neimark AV, Olivier JP, Rodriguez−Reinoso F, Rouquerol J, Sing KSW (2015) Physisorption of gases, with special reference to the evaluation of surface area and pore size distribution. Pure Appl Chem 87:1051–1069.

Tran HN, You SJ, Bandegharaei AH, Chao HP (2017) Mistakes and inconsistencies regarding adsorption of contaminants from aqueous solutions: A critical review. Water Research 120:88–116.

Umpierres CS, Prola LDT, Adebayo MA, Lima EC, dos Reis GS, Kunzler DD, Benvenutti EV (2017) Mesoporous Nb2O5/SiO2 material obtained by sol–gel method and applied as adsorbent of crystal violet dye. Environ Technol 38:566–578.

Yagub MT, Sen TK, Afroze S, Ang HM (2014) Dye and its removal from aqueous solution by adsorption: a review. Adv Colloid and Interface Sci 209:172–184.

Zazycki MA, Godinho M, Perondi D, Foletto EL, Collazzo GC, Dotto GL (2018) New biochar from pecan nutshells as an alternative adsorbent for removing reactive red 141 from aqueous solutions. J Cleaner Prod 171:57–65.

Zhu Y, Kolar P, Shah SB, Cheng JJ, Lim PK (2016) Avocado seed–derived activated carbon for mitigation of aqueous ammonium. Ind Crop Prod 92:34–41.

5 CONCLUSÕES GERAIS

Considerando os dados obtidos nos três artigos publicados, é possível chegar a diferentes conclusões em relação a aplicação da metodologia matemática escolhida e a adsorção do In(III) por diferentes adsorventes. Primeiramente, considerado as modelagens de rede aplicadas, MLFNN e ANFIS, é possível concluir que ambos métodos são capazes de predizer a capacidade de adsorção do In(III) considerando diferentes aspectos de entrada nas redes. Estes podendo ser parâmetros de operação como a dosagem de adsorvente e o tempo de contanto, incluindo características dos materiais como a área específica superficial ou o ponto de carga zero. Segundo, é possível verificar que a maioria dos adsorventes testados foram capazes de adsorver o In (III), indicando a possibilidade de ser recuperado de maneira fácil e prática através da operação de adsorção. Dentre os materiais testados foi encontrando que os nanotubos de carbono de múltiplas paredes funcionalizado com COOH conseguem adsorver uma maior quantidade de In(III) em comparação com outros materiais carbonáceos testados. Entretanto, quando comparado a todos os adsorventes utilizados, os biopolímeros (quitina e quitosana) conseguem alcançar as mesmas capacidades de adsorção e são materiais mais economicamente viáveis. As caracterizações e estudos conduzidos utilizando a quitina e quitosana, mostraram que ambos materiais possuem uma superfície rígida e sem presença de poros. A adsorção é favorável e possui caráter exotérmico, com a possibilidade de ligações de coordenação acontecendo entre o In (III) e a superfície dos polímeros. Baseado nos valores do número de Biot modificado e do bom ajuste do EMTM, é possível concluir que a transferência de massa é controlada globalmente pela transferência de massa externa. Sendo assim, o In (III) se desloca rapidamente do seio da solução onde é transferido até superfície externa da quitina/quitosana, sendo instantaneamente adsorvido por uma possível precipitação/ligação de coordenação. Por fim, é possível concluir que a quitina e quitosana são promissores adsorventes para a recuperação de In (III) extraído a partir de telas de LCD.

6 REFERÊNCIAS

AGHAJANI, K.; TAYEBI, H. A. Adaptive Neuro-Fuzzy Inference system analysis on adsorption studies of Reactive Red 198 from aqueous solution by SBA-15/CTAB composite. **Spectrochimica Acta - Part A: Molecular and Biomolecular Spectroscopy**, v. 171, p. 439–448, 2017. Elsevier B.V. Disponível em: http://dx.doi.org/10.1016/j.saa.2016.08.025.

AHMED, Md Juned K.; AHMARUZZAMAN, M. A review on potential usage of industrial waste materials for binding heavy metal ions from aqueous solutions. **Journal of Water Process Engineering**, [s. l.], v. 10, p. 39–47, 2016. Disponível em: <http://dx.doi.org/10.1016/j.jwpe.2016.01.014>ALFANTAZI, A. M.; MOSKALYK, R. R. Processing of indium: A review. **Minerals Engineering**, [s. l.], v. 16, n. 8, p. 687–694, 2003. HAMBLIN, MICHAEL R. ELIEH-ALI-KOMI, Daniel. Chitin and Chitosan: Production and Application of Versatile Biomedical Nanomaterials. **International journal of advanced research**, [s. l.], v. 4, n. 3, p. 411–427, 2016. TURAN, Nurdan Gamze; MESCI, Başak. Use of pistachio shells as an adsorbent for the removal of zinc(ii) ion. **Clean - Soil, Air, Water**, [s. l.], v. 39, n. 5, p. 475–481, 2011. SINGH, N. B. et al. Water purification by using Adsorbents: A Review. **Environmental Technology and Innovation**, [s. l.], v. 11, p. 187–240, 2018. Disponível em: <https://doi.org/10.1016/j.eti.2018.05.006>BHATTACHARJEE, Chiranjit; DUTTA, Suman; SAXENA, Vinod K. A review on biosorptive removal of dyes and heavy metals from wastewater using watermelon rind as biosorbent. **Environmental Advances**, [s. l.], v. 2, n. July, p. 100007, 2020. Disponível em: <https://doi.org/10.1016/j.envadv.2020.100007>

ALGUACIL, F. J.; LOPEZ, F. A.; RODRIGUEZ, O.; MARTINEZ-RAMIREZ, S.; GARCIA-DIAZ, I. Ecotoxicology and Environmental Safety Sorption of indium (III) onto carbon nanotubes. **Ecotoxicology and Environmental Safety**, v. 130, p. 81–86, 2016. Elsevier. Disponível em: http://dx.doi.org/10.1016/j.ecoenv.2016.04.008.

ARGENTA, A. B.; REIS, C. M.; MELLO, G. P.; et al. Supercritical CO2 extraction of indium present in liquid crystal displays from discarded cell phones using organic acids. **The Journal of Supercritical Fluids**, v. 120, p. 95–101, 2017. Elsevier B.V. Disponível em: http://dx.doi.org/10.1016/j.supflu.2016.10.014.

BAGHBAN, A.; SASANIPOUR, J.; HARATIPOUR, P.; ALIZAD, M.; VAFAEE AYOURI, M. ANFIS modeling of rhamnolipid breakthrough curves on activated carbon. **Chemical Engineering Research and Design**, v. 126, p. 67–75, 2017. Institution of Chemical Engineers. Disponível em: http://dx.doi.org/10.1016/j.cherd.2017.08.007.

CALAGUI, M. J. C.; SENORO, D. B.; KAN, C. C.; et al. Adsorption of indium(III) ions from aqueous solution using chitosan-coated bentonite beads. **Journal of Hazardous Materials**, v. 277, p. 120–126, 2014. Elsevier B.V. Disponível em: http://dx.doi.org/10.1016/j.jhazmat.2014.04.043.

CALAGUI, M. J. C.; SENORO, D. B.; KAN, C. C.; et al. Adsorption of indium(III) ions from aqueous solution using chitosan-coated bentonite beads. **Journal of Hazardous Materials**, v. 277, p. 120–126, 2014. Elsevier B.V. Disponível em: http://dx.doi.org/10.1016/j.jhazmat.2014.04.043.

CÔRTES, Letícia N. et al. Biosorption of gold from computer microprocessor leachate solutions using chitin. **Waste Management**, [s. l.], v. 45, p. 272–279, 2015. Disponível em: http://dx.doi.org/10.1016/j.wasman.2015.07.016

Disponível em https://link.springer.com/article/10.1007%2Fs11356-017-9802-y.

DOTTO, G. L.; MEILI, L.; DE SOUZA ABUD, A. K.; et al. Comparison between Brazilian agro-wastes and activated carbon as adsorbents to remove Ni(II) from aqueous solutions. **Water Science and Technology**, v. 73, n. 11, p. 2713–2721, 2016. Disponível em: http://wst.iwaponline.com/cgi/doi/10.2166/wst.2016.095.

DOTTO, G. L.; SANTOS, J. M. N.; RODRIGUES, I. L.; et al. Adsorption of Methylene Blue by ultrasonic surface modified chitin. **Journal of colloid and interface science**, v. 446, p. 133–140, 2015. Elsevier Inc. Disponível em: http://dx.doi.org/10.1016/j.jcis.2015.01.046.

DOTTO, G. L.; VIEIRA, M. L. G.; PINTO, L. A. A. Kinetics and mechanism of tartrazine adsorption onto chitin and chitosan. **Industrial and Engineering Chemistry Research**, v. 51, n. 19, p. 6862–6868, 2012. Disponível em: https://pubs.acs.org/doi/abs/10.1021/ie2030757.

EINSTEIN, A. On the Motion of Small Particles Suspended in a Stationary Liquid, as Required by the Molecular Kinetic Theory of Heat. **Annalen der Physik**, v. 322, p. 549–560, 1905. Disponível em: papers3://publication/uuid/3B00FCED-6369-4D10-A7AD-A815B5F0C18D%5Cnhttp://www3.interscience.wiley.com/cgi-bin/abstract/112477420/ABSTRACT.

ESCUDERO, L. B.; VANNI, G.; DUARTE, F. A.; SEGGER, T.; DOTTO, G. L. Biosorption of silver from aqueous solutions using wine industry wastes. **Chemical Engineering Communications**, v. 205, n. 3, p. 325–337, 2018. Taylor & Francis. Disponível em: https://doi.org/10.1080/00986445.2017.1387856.

EUROPEAN COMMISSION. **Study on the review of the list of Critical Raw Materials.** 2017.

FRANCO, D. S. P.; TANABE, E. H.; BERTUOL, D. A.; et al. Alternative treatments to improve the potential of rice husk as adsorbent for methylene blue. **Water Science and Technology**, v. 75, n. 2, p. 296–305, 2017. Disponível em: http://wst.iwaponline.com/lookup/doi/10.2166/wst.2016.504.

FRANCO, D. S. P.; TANABE, E. H.; DOTTO, G. L. Continuous Adsorption of a Cationic Dye on Surface Modified Rice Husk: Statistical Optimization and Dynamic Models. **Chemical Engineering Communications**, v. 204, n. 6, p. 625–634, 2017. Disponível em: https://www.tandfonline.com/doi/full/10.1080/00986445.2017.1300150.

FREUNDLICH, H. Über die Adsorption in Lösungen. **Zeitschrift für Physikalische Chemie**, v. 57U, n. 1, 1907. Disponível em: http://www.degruyter.com/view/j/zpch.1907.57.issue-1/zpch-1907-5723/zpch-1907-5723.xml.

GHAEDI, A. M.; VAFAEI, A. Applications of artificial neural networks for adsorption removal of dyes from aqueous solution: A review. **Advances in Colloid and Interface Science**, v. 245, n. April, p. 20–39, 2017. Elsevier. Disponível em: http://dx.doi.org/10.1016/j.cis.2017.04.015.

GHAEDI, M.; HOSAININIA, R.; GHAEDI, A. M.; VAFAEI, A.; TAGHIZADEH, F. Adaptive neuro-fuzzy inference system model for adsorption of 1,3,4-thiadiazole-2,5-dithiol onto gold nanoparticales-activated carbon. **Spectrochimica Acta - Part A: Molecular and Biomolecular Spectroscopy**, v. 131, p. 606–614, 2014. Elsevier B.V. Disponível em: http://dx.doi.org/10.1016/j.saa.2014.03.055.

GRIMES, S. M.; YASRI, N. G.; CHAUDHARY, A. J. Inorganica Chimica Acta Recovery of critical metals from dilute leach solutions – Separation of indium from tin and lead. **Inorganica Chimica Acta**, v. 461, p. 161–166, 2017. Elsevier B.V. Disponível em: http://dx.doi.org/10.1016/j.ica.2017.02.002.

GUPTA, B.; DEEP, A.; MALIK, P. Liquid-liquid extraction and recovery of indium using Cyanex 923. **Analytica Chimica Acta**, v. 513, n. 2, p. 463–471, 2004. Disponível em: https://doi.org/10.1016/j.aca.2004.02.036.

HIMANSHU VIJAY, D. K. C. Parameters Estimation of an Electric Fan Using ANN. **Journal of Intelligent Learning Systems and Applications**, v. 02, n. 01, p. 39–44, 2010. Disponível em: https://pdfs.semanticscholar.org/ba02/9c1b6281966e80319c081201bc68357bf763.pdf.

KALOGIROU, S. A. Artificial neural networks in renewable energy systems applications: a review. **Renewable & Sustainable Energy Reviews**, v. 5, n. 4, p. 373–401, 2001. Disponível em: http://dx.doi.org/10.1016/j.ijthermalsci.2014.11.030.

KARGE, H. G.; WEITKAMP, J. **Adsorption and diffusion**. 2008.

LANGMUIR, I. The Adsorption of Gases on Plane Surfaces of Glass, Mica and Platinum. **Journal of the American Chemical Society**, v. 40, n. 9, p. 1361–1403, 1918. Disponível em: citeulike-article-id:3880396%5Cnhttp://dx.doi.org/10.1021/ja02242a004.

LEE, S.; LEE, U. Journal of Industrial and Engineering Chemistry Adsorption and desorption property of iminodiacetate resin (Lewatit 1 TP207) for indium recovery. **Journal of Industrial and Engineering Chemistry**, v. 40, p. 23–25, 2016. The Korean Society of Industrial and Engineering Chemistry. Disponível em: http://dx.doi.org/10.1016/j.jiec.2016.05.016.

LEYVA-RAMOS, R.; GEANKOPLIS, C. J. Diffusion in liquid-filled pores of activated carbon. I. Pore volume diffusion. **The Canadian Journal of Chemical Engineering**, v. 72, n. 2, p. 262–271, 1994. Disponivel em https://onlinelibrary.wiley.com/doi/abs/10.1002/cjce.5450720213.

LI, H.; LIU, J.; GAO, X.; et al. Adsorption behavior of indium(III) on modified solvent impregnated resins (MSIRs) containing sec-octylphenoxy acetic acid. **Hydrometallurgy**, v. 121–124, p. 60–67, 2012. Elsevier B.V. Disponível em: http://dx.doi.org/10.1016/j.hydromet.2012.04.005.

LIMA, D. R.; KLEIN, L.; DOTTO, G. L. Application of ultrasound modified corn straw as adsorbent for malachite green removal from synthetic and real effluents. **Environmental Science and Pollution Research**, v. 24, n. 26, p. 21484–21495, 2017.

MCCABE, W. L.; SMITH, J. C.; HARRIOTT, P. Unit Operations of Chemical Engineering., 1993. Disponível em: http://books.google.com/books?id=sa-cQgAACAAJ&pgis=1.

MCCULLOCH, W. S.; PITTS, W. A logical calculus of the ideas immanent in nervous activity. **The Bulletin of Mathematical Biophysics**, v. 5, n. 4, p. 115–133, 1943. Disponivel em: http://dx.doi.org/ 10.1007/BF02478259.

MOHANRAJ, M.; JAYARAJ, S.; MURALEEDHARAN, C. Applications of artificial neural networks for thermal analysis of heat exchangers - A review. **International Journal of Thermal Sciences**, v. 90, p. 150–172, 2015. Elsevier Masson SAS. Disponível em: http://dx.doi.org/10.1016/j.ijthermalsci.2014.11.030.

NAG, S.; MONDAL, A.; ROY, D. N.; BAR, N.; DAS, S. K. Sustainable bioremediation of Cd(II) from aqueous solution using natural waste materials: Kinetics, equilibrium, thermodynamics, toxicity studies and GA-ANN hybrid modelling. **Environmental Technology and Innovation**, v. 11, p. 83–104, 2018. Disponível em: http://dx.doi.org/ 10.1016/j.eti.2018.04.009.

PEREIRA, Estela Bresolin et al. Recovery of indium from liquid crystal displays of discarded mobile phones using solvent extraction. **Minerals Engineering**, [s. l.], v. 119, n. January, p. 67–72, 2018. Disponível em: https://doi.org/10.1016/j.mineng.2018.01.022

REIS, Ricardo Pippi. **Gestão dos resíduos eletrônicos no município de Santa Maria-RS: Proposta de política pública**. 2013. Universidade Federal de Santa Maria-UFSM, [s. l.], 2013.Disponível em: https://repositorio.ufsm.br/handle/1/7840

RONDA, A.; MARTÍN-LARA, M. A.; ALMENDROS, A. I.; PÉREZ, A.; BLÁZQUEZ, G. Comparison of two models for the biosorption of Pb(II) using untreated and chemically treated olive stone: Experimental design methodology and adaptive neural fuzzy inference system (ANFIS). **Journal of the Taiwan Institute of Chemical Engineers**, v. 54, p. 45–56, 2015. Disponível em: http://dx.doi.org/10.1016/j.jtice.2015.03.004.

ROQUE-MALHERBE, R. M. A. **Adsorption and Diffusion in Nanoporous Materials.** 2018.

ROUQUEROL, F.; ROUQUEROL, J.; SING, K. S. W.; LLEWELLYN, P.; MAURIN, G. **Adsorption by powders and porous solids**. 2014.

RUTHVEN M. DOUGLAS. **Principles of Adsorption and Adsorption Processes**. John Wiley & Sons, 1984.

SAUCEDO-DELGADO, B. G.; RIO, D. A. D. H.; GONZÁLEZ-RODRÍGUEZ, L. M.; REYNEL-ÁVILA, H. E. Fluoride adsorption from aqueous solution using a protonated clinoptilolite and its modeling with arti fi cial neural network-based equations. **Journal of Fluorine Chemistry**, v. 204, n. November, p. 98–106, 2017. Elsevier. Disponível em: https://doi.org/10.1016/j.jfluchem.2017.11.002.

SHAMSHIRBAND, S.; PETKOVIĆ, D.; ANUAR, N. B.; GANI, A. Adaptive neuro-fuzzy generalization of wind turbine wake added turbulence models. **Renewable and Sustainable Energy Reviews**, v. 36, p. 270–276, 2014. Disponível em: http://dx.doi.org/10.1016/j.ijthermalsci.2014.11.030.

SILVEIRA, A. V. M.; FUCHS, M. S.; PINHEIRO, D. K.; TANABE, E. H.; BERTUOL, D. A. Recovery of indium from LCD screens of discarded cell phones. **Waste Management**, v. 45, n. April, p. 334–342, 2015. Elsevier Ltd. Disponível em: http://dx.doi.org/10.1016/j.wasman.2015.04.007.

SINGHA, B.; BAR, N.; DAS, S. K. The use of artificial neural network (ANN) for modeling of Pb(II) adsorption in batch process. **Journal of Molecular Liquids**, v. 211, p. 228–232, 2015. Elsevier B.V. Disponível em: http://dx.doi.org/10.1016/j.molliq.2015.07.002.

SOUZA, P. R. **SOLUÇÃO NUMÉRICA DE MODELOS DE TRANSFERÊNCIA DE MASSA DIFUSIVOS EM SISTEMAS DE ADSORÇÃO**, 2017. Dissertação (Mestrado em Engenharia Química) - Universidade Federal de Santa Maria (UFSM), Santa Maria, RS,2017.

SUZUKL, M. **Adsorption engineering**. KODANSHA LTD., Tokyo and ELSEVIER SCIENCE PUBLISHERS B. V., Amsterdam exchive, 1990.

SWAIN, B.; MISHRA, C.; HONG, H. S.; CHO, S. S. Treatment of indium-tin-oxide etching wastewater and recovery of In, Mo, Sn and Cu by liquid-liquid extraction and wet chemical reduction: a laboratory scale sustainable commercial green process. **Green Chemistry**, v. 17, n. 8, p. 4418–4431, 2015. Disponível em: http://dx.doi.org/10.1039/C5GC01244A.

TURAN, N. G.; MESCI, B.; OZGONENEL, O. Artificial neural network (ANN) approach for modeling Zn(II) adsorption from leachate using a new biosorbent. **Chemical Engineering Journal**, v. 173, n. 1, p. 98–105, 2011. Disponível em: http://dx.doi.org/ 10.1016/j.cej.2011.07.042.

U.S. GEOLOGICAL SURVEY. Mineral Commodities Summaries. **Mineral Commodity Summaries**, p. 202, 2016.

U.S. GEOLOGICAL SURVEY. **Mineral Commodity Summaries 2017**. 2017.

WILKE, C.R. ; CHANG, P. Correlation of Diffusion Coefficients in Dilute Solutions. **A.I.Ch.E Journal**, p. 264–270, 1955. Disponível em: http://dns2.asia.edu.tw/~ysho/YSHO-English/2000 Engineering/PDF/AIChE J1, 264.pdf.

YUAN, Y.; LIU, J.; ZHOU, B.; et al. Hydrometallurgy Synthesis of coated solvent impregnated resin for the adsorption of indium (III). **Hydrometallurgy**, v. 101, n. 3–4, p. 148–155, 2010. Elsevier B.V. Disponível em: http://dx.doi.org/10.1016/j.hydromet.2009.12.010.

ZAZYCKI, Maria A. et al. Adsorption of valuable metals from leachates of mobile phone wastes using biopolymers and activated carbon. **Journal of Environmental Management**, [s. l.], v. 188, p. 18–25, 2017. Disponível em: http://dx.doi.org/10.1016/j.jenvman.2016.11.078

APÊNDICE A TRABALHOS CIENTÍFICOS EXCUTADOS ALÉM DA TESE

Neste apêndice são citados os trabalhos científicos que tive a oportunidade de trabalhar e que foram publicados/aceitos além dos trabalhos executados na tese:

1. DE O. SALOMÓN, Y. L.; GEORGIN, J.; DOS REIS, G. S.; et al. Utilization of Pacara Earpod tree (Enterolobium contortisilquum) and Ironwood (Caesalpinia leiostachya) seeds as low-cost biosorbents for removal of basic fuchsin. **Environmental Science and Pollution Research**, v. 27, n. 26, p. 33307–33320, 2020. Environmental Science and Pollution Research. Disponível em: <http://link.springer.com/10.1007/s11356-020-09471-z>. .
2. DE SALOMÓN, Y. L. DE O.; GEORGIN, J.; FRANCO, D. S. P.; et al. Powdered biosorbent from pecan pericarp (Carya illinoensis) as an efficient material to uptake methyl violet 2B from effluents in batch and column operations. **Advanced Powder Technology**, v. 31, n. 7, p. 2843–2852, 2020. Disponível em: <https://linkinghub.elsevier.com/retrieve/pii/S0921883120301965>.
3. DE SALOMÓN, Y. L. O.; GEORGIN, J.; FRANCO, D. S. P.; et al. Application of seed residues from Anadenanthera macrocarpa and Cedrela fissilis as alternative adsorbents for remarkable removal of methylene blue dye in aqueous solutions. **Environmental Science and Pollution Research**, 2020. Environmental Science and Pollution Research. Disponível em: <http://link.springer.com/10.1007/s11356-020-10635-0>.
4. DRUMM, F. C.; et al. Powdered biosorbent from the mandacaru cactus (cereus jamacaru) for discontinuous and continuous removal of Basic Fuchsin from aqueous solutions. **Powder Technology**, v. 364, p. 584–592, 2020. Elsevier B.V. Disponível em: <https://doi.org/10.1016/j.powtec.2020.01.064>.
5. DRUMM, F. C.; FRANCO, D. S. P.; GEORGIN, J.; et al. Macro-fungal (Agaricus bisporus) wastes as an adsorbent in the removal of the acid red 97 and crystal violet dyes from ideal colored effluents. **Environmental Science and Pollution Research**, 2020. Environmental Science and Pollution Research. Disponível em: <http://link.springer.com/10.1007/s11356-020-10521-9>. .
6. DRUMM, F. C.; GRASSI, P.; GEORGIN, J.; et al. Potentiality of the Phoma sp. inactive fungal biomass, a waste from the bioherbicide production, for the treatment of colored effluents. **Chemosphere**, v. 235, p. 596–605, 2019.

7. DRUMM, F. C.; GRASSI, P.; SULKOVSKI, A. A.; et al. Applicability of Coal Bottom Ash from Thermoelectric Power Plant as an Alternative Heterogeneous Catalyst in Photo-Fenton Reaction. **Water, Air, & Soil Pollution**, v. 230, n. 12, p. 274, 2019. Water, Air, & Soil Pollution. Disponível em: <http://link.springer.com/10.1007/s11270-019-4327-2>. .

8. FRANCO, D. S. P.; DOTTO, G. L. A Short Analysis of Biosorbents and its Potential Removal Contaminants from Aqueous Media. , p. 614–616, 2020. Disponível em: <https://irispublishers.com/gjes/fulltext/a-short-analysis-of-biosorbents-and-its-potential-removal-contaminants-from-aqueous-media.ID.000610.php>.

9. FRANCO, D. S. P.; FAGUNDES, J. L. S.; GEORGIN, J.; SALAU, N. P. G.; DOTTO, G. L. A mass transfer study considering intraparticle diffusion and axial dispersion for fixed-bed adsorption of crystal violet on pecan pericarp (Carya illinoensis). **Chemical Engineering Journal**, v. 397, n. May, p. 125423, 2020. Elsevier. Disponível em: <https://doi.org/10.1016/j.cej.2020.125423>. .

10. FRANCO, D. S. P.; GEORGIN, J.; DRUMM, F. C.; et al. Araticum (Annona crassiflora) seed powder (ASP) for the treatment of colored effluents by biosorption. **Environmental Science and Pollution Research**, v. 27, n. 10, p. 11184–11194, 2020. Environmental Science and Pollution Research. Disponível em: <http://link.springer.com/10.1007/s11356-019-07490-z>. .LI, Z.; SELLAOUI, L.;

11. FRANCO, D. S. P.; GEORGIN, J.; NETTO, M. S.; et al. Conversion of the forest species Inga marginata and Tipuana tipu wastes into biosorbents: Dye biosorption study from isotherm to mass transfer. **Environmental Technology & Innovation**, v. 22, p. 101521, 2021. Elsevier B.V. Disponível em: <https://doi.org/10.1016/j.eti.2021.101521>. .

12. FRANCO, D. S. P.; NUNES, I. D. S.; et al. Carbon nanotubes impregnated with metallic nanoparticles and their application as an adsorbent for the glyphosate removal in an aqueous matrix. **Journal of Environmental Chemical Engineering**, v. 9, n. 2, 2021.

13. FRANCO, D.; et al. Adsorption of hazardous dyes on functionalized multiwalled carbon nanotubes in single and binary systems: Experimental study and physicochemical interpretation of the adsorption mechanism. **Chemical Engineering Journal**, v. 389, p. 124467, 2020. Elsevier B.V. Disponível em: <https://doi.org/10.1016/j.cej.2020.124467>. .

14. GEORGIN J. FRANDO D. S. P., NETTO M. S., DE SALOMÓN Y. L. O., PICCILLI, D. A., FOLETTO, E. L., DOTTO G. L. Adsorption and mass transfer studies

of methylene blue onto comminuted seedpods from Luehea divaricate and Inga laurina. **Environmental Science and Pollution and Research**, v.28, p.20854-20868,2021. Environmental Science and Pollution Research. Disponível em: https://link.springer.com/article/10.1007%2Fs11356-020-11957-9

15. GEORGIN, J.; DRUMM, F. C.; GRASSI, P.; et al. Potential of Araucaria angustifolia bark as adsorbent to remove Gentian Violet dye from aqueous effluents. **Water Science and Technology**, v. 78, n. 8, p. 1693–1703, 2018.

16. GEORGIN, J.; FRANCO, D. S. P.; DRUMM, F. C.; et al. Paddle cactus (Tacinga palmadora) as potential low-cost adsorbent to treat textile effluents containing crystal violet. **Chemical Engineering Communications**, v. 207, n. 10, p. 1368–1379, 2020. Taylor & Francis. Disponível em: <https://doi.org/10.1080/00986445.2019.1650033>.

17. GEORGIN, J.; FRANCO, D. S. P.; GRASSI, P.; et al. Potential of Cedrella fissilis bark as an adsorbent for the removal of red 97 dye from aqueous effluents. **Environmental Science and Pollution Research**, v. 26, n. 19, p. 19207–19219, 2019. Environmental Science and Pollution Research.

18. GEORGIN, J.; FRANCO, D. S. P.; NETTO, M. S.; et al. Adsorption investigation of 2,4-D herbicide on acid-treated peanut (Arachis hypogaea) skins. **Environmental Science and Pollution Research**, 2021. Environmental Science and Pollution Research.DIEL, J. C.;

19. GEORGIN, J.; FRANCO, D. S. P.; NETTO, M. S.; et al. Evaluation of Ocotea puberula bark powder (OPBP) as an effective adsorbent to uptake crystal violet from colored effluents: alternative kinetic approaches. **Environmental Science and Pollution Research**, v. 27, n. 20, p. 25727–25739, 2020. Environmental Science and Pollution Research. Disponível em: <http://link.springer.com/10.1007/s11356-020-08854-6>.

20. GEORGIN, J.; FRANCO, D. S. P.; NETTO, M. S.; et al. Treatment of water containing methylene by biosorption using Brazilian berry seeds (Eugenia uniflora). **Environmental Science and Pollution Research**, v. 27, n. 17, p. 20831–20843, 2020. Environmental Science and Pollution Research. Disponível em: <http://link.springer.com/10.1007/s11356-020-08496-8>. .GEORGIN, J.; FRANCO, D.;

21. GEORGIN, J.; FRANCO, D. S. P.; SCHADECK NETTO, M.; et al. Transforming shrub waste into a high-efficiency adsorbent: application of Physalis peruvian chalice treated with strong acid to remove the 2,4-dichlorophenoxyacetic acid herbicide. **Journal of Environmental Chemical Engineering**, , n. September, p.

104574, 2020. Elsevier B.V. Disponível em: <https://doi.org/10.1016/j.jece.2020.104574>.

22. GRASSI, P.; DRUMM, F. C.; GEORGIN, J.; et al. Application of Cordia trichotoma sawdust as an effective biosorbent for removal of crystal violet from aqueous solution in batch system and fixed-bed column. **Environmental Science and Pollution Research**, 2020. Environmental Science and Pollution Research. Disponível em: <http://link.springer.com/10.1007/s11356-020-11005-6>. .

23. GRASSI, P.; DRUMM, F. C.; GEORGIN, J.; et al. Water treatment plant sludge as iron source to catalyze a heterogeneous photo-Fenton reaction. **Environmental Technology & Innovation**, v. 17, p. 100544, 2020. Elsevier B.V. Disponível em: <https://doi.org/10.1016/j.eti.2019.100544>. .

24. HERNANDES, P. T.; OLIVEIRA, M. L. S.; GEORGIN, J.; et al. Adsorptive decontamination of wastewater containing methylene blue dye using golden trumpet tree bark (Handroanthus albus). **Environmental Science and Pollution Research**, v. 26, n. 31, p. 31924–31933, 2019. Environmental Science and Pollution Research. Disponível em: <http://link.springer.com/10.1007/s11356-019-06353-x>.

25. HUA, P.; SELLAOUI, L.; FRANCO, D.; et al. Adsorption of acid green and procion red on a magnetic geopolymer based adsorbent: Experiments, characterization and theoretical treatment. **Chemical Engineering Journal**, v. 383, n. October, p. 123113, 2020. Disponível em: <https://linkinghub.elsevier.com/retrieve/pii/S1385894719325252>. .

26. LÚCIA, A.; AZEVEDO, A.; GRAZIELLI, C.; BARROS, D. Removal of rhodamine B cationic dye using activated carbon. , 2020.MECHI, N.; BEN KHEMIS, I.; DOTTO, G. L.; et al. Investigation of the adsorption mechanism of methylene blue (MB) on Cortaderia selloana flower spikes (FSs) and on Cortaderia selloana flower spikes derived carbon fibers (CFs). **Journal of Molecular Liquids**, v. 280, p. 268–273, 2019.

27. PANG, X.; SELLAOUI, L.; FRANCO, D.; et al. Adsorption of crystal violet on biomasses from pecan nutshell, para chestnut husk, araucaria bark and palm cactus: Experimental study and theoretical modeling via monolayer and double layer statistical physics models. **Chemical Engineering Journal**, v. 378, n. June, p. 122101, 2019. Disponível em: <https://linkinghub.elsevier.com/retrieve/pii/S1385894719314950>. .

28. PANG, X.; SELLAOUI, L.; FRANCO, D.; et al. Preparation and characterization of a novel mountain soursop seeds powder adsorbent and its application for the removal of crystal violet and methylene blue from aqueous solutions. **Chemical**

Engineering Journal, v. 391, n. November 2019, p. 123617, 2020. Elsevier. Disponível em: <https://doi.org/10.1016/j.cej.2019.123617>.

29. PIGATTO, R. S.; FRANCO, D. S. P.; NETTO, M. S.; et al. An eco-friendly and low-cost strategy for groundwater defluorination: Adsorption of fluoride onto calcinated sludge. **Journal of Environmental Chemical Engineering**, , n. August 2020, p. 104546, 2020. Disponível em: <https://linkinghub.elsevier.com/retrieve/pii/S0370157320303434>. .

30. SELLAOUI, L.; FRANCO, D.; GHALLA, H.; et al. Insights of the adsorption mechanism of methylene blue on brazilian berries seeds: Experiments, phenomenological modelling and DFT calculations. **Chemical Engineering Journal**, v. 394, p. 125011, 2020. Elsevier B.V. Disponível em: <https://doi.org/10.1016/j.cej.2020.125011>. .

31. ZHANG, L.; SELLAOUI, L.; FRANCO, D.; et al. Adsorption of dyes brilliant blue, sunset yellow and tartrazine from aqueous solution on chitosan: Analytical interpretation via multilayer statistical physics model. **Chemical Engineering Journal**, v. 382, p. 122952, 2020. Elsevier B.V. Disponível em: <https://doi.org/10.1016/j.cej.2019.122952>.